East European

Journal of Physics

East European Journal of Physics

East European Journal of Physics

The editorial policy is to maintain the quality of published papers at the highest level by strict peer review.
Approved for publication by the Academic Council of the Karazin Kharkiv National University (December 26, 2016) EEJP registered by the order of Ministry of Education of Ukraine № 747 of 07.13.2015, and is included in the list of scientific specialized editions of Ukraine, which can be published results of dissertations for the degree of doctor and candidate of physical and mathematical sciences.

East European Journal of Physics

ORIGINAL PAPERS

HISTORY OF SCIENCE

THERMODYNAMICS OF THE FERMI GAS IN A QUANTUM WELL

Yu.M. Poluektov, A.A. Soroka
National Science Center "Kharkov Institute of Physics and Technology"
1, Akademicheskaya Str.,61108 Kharkov, Ukraine
E-mail: yuripoluektov@kipt.kharkov.ua
Received November 2, 2016

For the ideal Fermi gas that fills a quantum well confined by two parallel planes, there are calculated the thermodynamic characteristics in general form for arbitrary temperatures, namely: the thermodynamic potential, energy, entropy, equations of state, heat capacities and compressibilities. The distance between planes is considered as an additional thermodynamic variable. Owing to the anisotropy, the pressure of the Fermi gas along and transverse to the planes is different, so that the system is characterized by two equations of state and a set of different heat capacities. Limiting cases of low and high temperatures are considered. The temperature dependencies of the entropy and heat capacities at low temperatures remain linear, just as in the volume case, and their dependencies on the chemical potential and density undergo jumps at the beginning of the filling of new discrete levels. It is shown that the behavior of thermodynamic quantities with the distance between plates can be either oscillating or monotonic, depending on what quantity is assumed to be fixed: the volume or surface density. For high temperatures the corrections to thermodynamic quantities are obtained, which are proportional to the ratio of the thermal de Broglie wavelength to the distance between planes.
KEY WORDS: Fermi particle, quantum well, thermodynamic functions, low-dimensional systems, equation of state, heat capacity, compressibility

ТЕРМОДИНАМІКА ФЕРМІ-ГАЗУ У КВАНТОВІЙ ЯМІ
Ю.М. Полуектов, О.О. Сорока
Національний науковий центр "Харківський фізико-технічний інститут"
61108, вул. Академічна, 1, Харків, Україна
Для ідеального фермі-газу, що заповнює квантову яму обмежену двома паралельними площинами, у загальному вигляді для довільних температур обчислені термодинамічні характеристики, а саме: термодинамічний потенціал, енергія, ентропія, рівняння стану, теплоємності та стисливості. Відстань між площинами розглядається як додаткова термодинамічна змінна. Через анізотропію тиск фермі-газу уздовж і перпендикулярно площинам відмінний, так що система характеризується двома рівняннями стану і набором різних теплоємностей. Розглянуті граничні випадки низьких і високих температур. Температурні залежності ентропії і теплоємностей при низьких температурах залишаються лінійними, як і в об'ємному випадку, а їх залежності від хімічного потенціалу і густини зазнають стрибки при початку заповнення нового дискретного рівня. Показано, що зміна термодинамічних величин з відстанню між пластинами може мати або осциляційний, або монотонний характер залежно від того, що передбачається фіксованим, об'ємна або поверхнева густина. В області високих температур знайдені поправки до термодинамічних величин, пропорційні відношенню теплової хвилі де Бройля до відстані між площинами.
КЛЮЧОВІ СЛОВА: фермі-частинка, квантова яма, термодинамічні функції, низькорозмірні системи, рівняння стану, теплоємність, стисливість

ТЕРМОДИНАМИКА ФЕРМИ-ГАЗА В КВАНТОВОЙ ЯМЕ
Ю.М. Полуэктов, А.А. Сорока
Национальный научный центр "Харьковский физико-технический институт"
61108, Академическая,1, Харьков, Украина
Для идеального ферми-газа, заполняющего квантовую яму ограниченную двумя параллельными плоскостями, в общем виде для произвольных температур вычислены термодинамические характеристики, а именно: термодинамический потенциал, энергия, энтропия, уравнения состояния, теплоемкости и сжимаемости. Расстояние между плоскостями рассматривается как дополнительная термодинамическая переменная. В силу анизотропии давление ферми-газа вдоль и перпендикулярно плоскостям различно, так что система характеризуется двумя уравнениями состояния и набором различных теплоемкостей. Рассмотрены предельные случаи низких и высоких температур. Температурные зависимости энтропии и теплоемкостей при низких температурах остаются линейными, как и в объемном случае, а их зависимости от химического потенциала и плотности испытывают скачки при начале заполнения нового дискретного уровня. Показано, что изменение термодинамических величин с расстоянием между пластинами может иметь либо осцилляционный, либо монотонный характер в зависимости от того, что предполагается фиксированным, объемная или поверхностная плотность. В области высоких температур найдены поправки к термодинамическим величинам, пропорциональные отношению тепловой волны де Бройля к расстоянию между плоскостями.
КЛЮЧЕВЫЕ СЛОВА: ферми-частица, квантовая яма, термодинамические функции, низкоразмерные системы, уравнение состояния, теплоемкость, сжимаемость

The model of the ideal Fermi gas is the basis for understanding the properties of electron and other many-fermion systems. In many cases it is also possible to describe with reasonable accuracy the behavior of systems of interacting fermi-particles within the approximation of an ideal gas of quasiparticles whose dispersion law differs from the dispersion law of free particles. It is essential that thermodynamic characteristics of the ideal Fermi gas at arbitrary

temperatures in the volume case can be expressed through the special Fermi functions and, therefore, it is possible to obtain and verify all relations of the phenomenological thermodynamics on the basis of the quantum microscopic model.

In recent time, much attention has been paid to investigation of low-dimensional systems, in particular to properties of the two-dimensional Fermi gas in quantum wells, because apart from purely scientific interest the study of such objects is rather promising for the solid-state electronics [1-5]. Thermodynamics relations for the Fermi gas in the confined geometry have been studied much less than in the volume case [6] and require further investigation. A detailed understanding of the properties of such systems must serve as a basis for the study of low-dimensional systems of interacting particles.

It is usual to consider that strongly correlated Fermi systems, to which also two-dimensional Fermi liquids are attributed, in many respects essentially differ from the usual Fermi systems and often show "non-Fermi-liquid" behavior [7]. At that the properties of quasi-two-dimensional and quasi-one-dimensional systems are compared with the theory of bulk Fermi liquid [8,9]. However, as seen even on the example of the quasi-two-dimensional system of noninteracting particles which is considered in detail in the present work, its properties can substantially differ, especially at low temperatures, from the properties of the bulk system owing to the quantum size effect. Therefore, the theory of Fermi liquid itself in conditions of the confined geometry must, generally speaking, be formulated differently than in the volume case. Note that the Migdal's theory of finite Fermi systems [10] does not essentially differ in this respect from the Fermi liquid theory of uniform systems.

The consideration of low-dimensional models of interacting Fermi particles leads to a conclusion about, in many cases, unique properties of such systems [11,12]. It should be kept in mind, however, that real systems are always three-dimensional and their low dimensionality manifests itself only in the boundedness of motion of particles in one, two or three coordinates. In considering statistical properties of the three-dimensional many-particle systems one usually passes to the thermodynamic limit, setting in final formulas the volume and number of particles to infinity at a fixed density. It is of general theoretical interest to study the statistical properties of many-particle systems occupying a volume, one or two dimensions of which remain fixed, and the thermodynamic limiting transition is carried out only over remaining coordinates. In this case the coordinates, over which the thermodynamic limiting transition is not performed, should be considered as additional thermodynamic variables. The model of the ideal Fermi gas allows to build the thermodynamics of such systems on the basis of the statistical treatment.

The idea of taking account of the spatial quantization when calculating the electron heat capacity of small particles was for the first time used by Fröhlich [13]. Thermodynamic properties of the Fermi gas at low temperatures in the confined geometry within the quasiclassical approach were considered in the works of I.M. Lifshits and A.M. Kosevich [14,15]. Since the fermions possess a quasidiscrete spectrum in the confined geometry, in a similar way as it takes place for electrons in the magnetic field [6], the authors of these works showed that the thermodynamic potential contains under such conditions a component that oscillates with varying the chemical potential. However, as seen from the results of the given work, the presence of the oscillating component in the thermodynamic potential does not yet guarantee that the full thermodynamic potential and thermodynamic quantities are oscillating.

It should be noted that in experiments the quantum oscillation phenomena in thin metallic, semimetallic, semiconducting films and nanostructures were observed for the kinetic coefficients such as the conductivity, the mobility, the Hall coefficient and others [2,5], but not for the thermodynamic quantities.

The aim of the proposed work is obtaining general thermodynamic relations for the Fermi gas in conditions of the confined geometry on the basis of a microscopic treatment. In the work there are derived exact formulas for the thermodynamic potential, energy, entropy, pressures, heat capacities and compressibilities which allow to analyze the equilibrium properties of the Fermi system at arbitrary temperatures and geometric dimensions. Any thermodynamic quantity proves to be expressed through some standard functions and their derivatives that depend only on the dimensionless temperature and the dimensionless chemical potential. It is shown that, owing to the anisotropy of the system under consideration, the pressure of the Fermi gas along and transverse to planes is different, so that the system is characterized by two equations of state and a set of different heat capacities. The cases of low and high temperatures are studied. At low temperatures the dependencies of the entropy and heat capacities on temperature remain linear, just as in the volume case, and their dependencies on the chemical potential and density undergo jumps at the beginning of the filling of new discrete levels. It is shown that the behavior of thermodynamic quantities with the distance between plates can be qualitatively different, depending on what quantity is assumed to be fixed: the volume or surface density. Thus, at a fixed surface density the chemical potential and pressure vary monotonically with the thickness and at a fixed volume density these dependencies have an oscillating character. In the area of high temperatures the corrections to thermodynamic quantities are obtained, proportional to the ratio of the thermal de Broglie wavelength to the distance between planes.

FERMI GAS IN A VOLUME

Before proceeding to consideration of the Fermi gas of particles with mass m in conditions of the confined geometry, here we give the basic formulas for the three-dimensional Fermi gas enclosed in the rectangular parallelepiped of volume $V = L_x L_y L_z$, lengths of all sides of which are large. In the case when $L_i >> 2\pi/k_i$ ($\mathbf{k}$ is a

wave vector), the wave functions of particles have the form of plane waves $\varphi_{\mathbf{k}}(\mathbf{r}) = V^{-1/2} e^{i\mathbf{kr}}$ and the energy of particles $\varepsilon_k = \hbar^2 k^2 / 2m$. Generally, in books authors restrict themselves to considering the two limiting cases: either the case of high temperatures in which a description of motion of gas particles based on the laws of the classical mechanics is valid, or the case of very low temperatures when the Fermi gas is degenerate [6]. Meanwhile, all thermodynamic functions of the Fermi gas at arbitrary temperature can be exactly expressed through the special functions

$$\Phi_s(t) = \frac{1}{\Gamma(s)} \int_0^\infty \frac{z^{s-1} dz}{e^{z-t} + 1}, \tag{1}$$

where s is an integer or half-integer positive number, $\Gamma(s)$ is the gamma function. For calculation of the bulk properties of the Fermi gas it is sufficient to know the functions (1) with half-integer indices $s = 1/2, 3/2, 5/2$.

The thermodynamic potential Ω, energy E, entropy S, particle number density n and pressure p of the Fermi gas of particles with the spin 1/2 in a volume, expressed through the functions (1), are given by the formulas:

$$\Omega = -\frac{2TV}{\Lambda^3} \Phi_{5/2}(t), \qquad E = \frac{3TV}{\Lambda^3} \Phi_{5/2}(t), \qquad S = \frac{2V}{\Lambda^3} \left[\frac{5}{2} \Phi_{5/2}(t) - t\Phi_{3/2}(t) \right],$$

$$n = \frac{N}{V} = \frac{2}{\Lambda^3} \Phi_{3/2}(t), \qquad p = \frac{2T}{\Lambda^3} \Phi_{5/2}(t). \tag{2}$$

Here $t \equiv \mu/T$, μ is the chemical potential. The thermal de Broglie wavelength enters into the formulas (2):

$$\Lambda \equiv \left(\frac{2\pi\hbar^2}{mT} \right)^{1/2}. \tag{3}$$

In a bulk gas in addition to the thermal wavelength of a particle (3) there exists one more characteristic length $l = n^{-1/3}$ which defines an average distance between particles. The ratio of these lengths

$$q_\Lambda \equiv \frac{\Lambda}{l} = \Lambda n^{1/3} = \left[2\Phi_{3/2}(t) \right]^{1/3} \tag{4}$$

characterizes the extent of proximity of the gas to the degenerate state, so to say the measure of its "quantumness". Depending on the density of number of particles and temperature the quantum mechanical properties of the gas will manifest themselves to a greater or lesser extent. If q_Λ is small, the system can be well described by the classical mechanics. With decreasing temperature at a fixed density the thermal wavelength increases and, therefore, the "quantumness" of the gas increases in this case, and besides, as we see, the parameter q_Λ depends on the single parameter t.

Here we also give the formulas for the heat capacities at a constant volume and a constant pressure:

$$C_V = \frac{15}{2} \frac{V}{\Lambda^3} \left[\Phi_{5/2}(t) - \frac{3}{5} \frac{\Phi_{3/2}^2(t)}{\Phi_{1/2}(t)} \right],$$

$$C_p = \frac{25}{2} \frac{V}{\Lambda^3} \Phi_{5/2}(t) \left[\frac{\Phi_{1/2}(t) \Phi_{5/2}(t)}{\Phi_{3/2}^2(t)} - \frac{3}{5} \right]. \tag{5}$$

It should be noted that the heat capacities per one particle C_V/N and C_p/N also depend on the single parameter t. The properties of Fermi systems in the presence of the discrete levels in magnetic field were studied with the help of the functions (1) in work [16].

THERMODYNAMICS OF THE FERMI GAS IN A RECTANGULAR QUANTUM WELL

The model of the ideal Fermi gas is the basis for studying the bulk properties of the Fermi systems for particles of different nature. In the two-dimensional case an analogous role is played by the ideal Fermi gas contained between two parallel planes, therefore a detailed study of such the system is also of general physical interest. In particular, it is important to obtain exact formulas for thermodynamic quantities of the Fermi gas contained between two parallel planes $z = L/2$, $z = -L/2$ and to make analysis of its thermodynamic properties. It is assumed everywhere that the spin of the Fermi particle is equal to 1/2. The lengths L_x, L_y are as before considered to be macroscopic, where $A = L_x L_y$ is the area in the (x, y) plane, but no restrictions are imposed on the length of the third side $L_z = L$ and it can be small, that corresponds to transition to the quasi-two-dimensional case. The total volume occupied by the Fermi gas $V = AL$. The case when $L_x \gg L$, $L_y \gg L$ is of the most interest and the main attention will be paid to it. Note that in work [15] this case was not considered in detail. Let us assume that the potential barrier at the points $z = L/2$ and $z = -L/2$ is infinite, so that the wave function of a particle turns into zero at boundaries. In this case solutions of the Schrödinger equation have the form

$$\varphi_{\mathbf{k},n}^{(+)}(x,y,z) = \sqrt{\frac{2}{AL}} e^{i\mathbf{k}\mathbf{r}} \cos(2n+1)\frac{\pi z}{L}, \qquad (n=0,1,2,\ldots),$$

$$\varphi_{\mathbf{k},n}^{(-)}(x,y,z) = \sqrt{\frac{2}{AL}} e^{i\mathbf{k}\mathbf{r}} \sin 2n\frac{\pi z}{L}, \qquad (n=1,2,\ldots).$$

(6)

The first of these functions is even and the second is odd with respect to the transformation $z \to -z$. Here $\mathbf{k} \equiv (k_x, k_y)$ and $\mathbf{r} \equiv (x,y)$ are two-dimensional vectors. The energy of a particle:

$$\varepsilon_{kn} = \frac{\hbar^2 k^2}{2m} + \varepsilon_L n^2,$$

(7)

$n = 1,2,\ldots$ and $k^2 = k_x^2 + k_y^2$. For odd n the levels correspond to even wave functions, and for even n − to odd wave functions. The energy

$$\varepsilon_L \equiv \frac{\pi^2 \hbar^2}{2mL^2}$$

(8)

is conditioned by localization of a quantum particle between planes and increases with decreasing the distance L between them. This characteristic energy of a problem (we assume the particle is an electron), expressed in Rydbergs, can be written in the form $\tilde{\varepsilon}_L = \pi^2/\tilde{L}^2$, where $\tilde{L} = L/a_0$ is the distance in the Bohr radiuses. Considering that $1\,Ry = 13.6\,eV = 15.8\cdot10^4\,K$, we obtain: 1) at $\tilde{L} = 10^2$ − $\tilde{\varepsilon}_L = 156\,K$; 2) at $\tilde{L} = 10^3$ − $\tilde{\varepsilon}_L = 1.56\,K$; 3) at $\tilde{L} = 10^4$ − $\tilde{\varepsilon}_L = 0.016\,K$; 4) at $\tilde{L} = 10^6$ − $\tilde{\varepsilon}_L = 1.6\cdot10^{-6}\,K$. Thus, quantum effects connected with the presence of the energy (8), as it had to be expected, must manifest themselves essentially at low temperatures and small distances between planes. The distribution function in this case has the form

$$f_{kn} = \left[\exp(\varepsilon_{kn} - \mu)/T + 1\right]^{-1}.$$

(9)

After integration over momenta with the function (9), the thermodynamical potential

$$\Omega = -2T \sum_{k,n} \ln\left[1 + e^{-(\varepsilon_{kn}-\mu)/T}\right]$$

(10)

will be determined by the formula

$$\Omega = -\frac{2TA}{\Lambda^2} \Psi_2(\tau,\eta).$$

(11)

Instead of the parameter $t = \mu/T$, that was used in formulas for the volume case, it is convenient to introduce the dimensionless chemical potential $\eta \equiv \mu/\varepsilon_L$ and the dimensionless temperature $\tau \equiv T/\varepsilon_L$, then $t = \eta/\tau$. We define the function

$$\Psi_s(\tau,\eta) \equiv \sum_{n=1}^{\infty} \Phi_s\left[\tau^{-1}(\eta - n^2)\right].$$

(12)

The details of calculation of such functions are given in Appendix. The thermodynamic potential (11) is a function of the temperature, chemical potential, area and distance between plates: $\Omega = \Omega(T,\mu,A,L)$. In contrast to the volume case when Ω is proportional to the volume V, in this case it is proportional to the area A and depends in a complicated manner on the distance L. This circumstance is conditioned by the evident anisotropy of the system under consideration, since here the motions in the (x,y) plane and in the direction of the z axis are qualitatively different. In statistical mechanics it is customary to pass in the final formulas to the thermodynamic limit $V \to \infty, N \to \infty$ at $n = N/V = \text{const}$. In the present case it is more accurate to write down the thermodynamic limit somewhat differently, namely

$$A \to \infty, \quad N \to \infty \quad \text{at} \quad n_A \equiv N/A = \text{const}.$$

(13)

It is thereby stressed that the transition to infinite volume occurs only owing to increasing the area, at a fixed distance L.

The differential of the thermodynamic potential (11) has the form

$$d\Omega = -\frac{2A}{\Lambda^2}\left(2\Psi_2 + \tau\frac{\partial\Psi_2}{\partial\tau}\right)dT - \frac{2A}{\Lambda^2}\Psi_1 d\mu + \frac{\Omega}{A}dA - \frac{4AT}{\Lambda^2 L}\left(\tau\frac{\partial\Psi_2}{\partial\tau} + \eta\frac{\partial\Psi_2}{\partial\eta}\right)dL.$$

(14)

It was taken into account that $\partial\Psi_2/\partial\eta = \tau^{-1}\Psi_1$ and $d\varepsilon_L = -(2\varepsilon_L/L)dL$. Since $S = -(\partial\Omega/\partial T)_{\mu,A,L}$ and $N = -(\partial\Omega/\partial\mu)_{T,A,L}$, from (14) there follow expressions for the entropy and number of particles:

$$S = \frac{2A}{\Lambda^2}\left(2\Psi_2 + \tau\frac{\partial\Psi_2}{\partial\tau}\right),$$

(15)

$$N = \frac{2A}{\Lambda^2}\Psi_1. \tag{16}$$

The volume and surface densities of number of particles are defined by obvious relations: $n \equiv N/AL$, $n_A \equiv N/A$. The same formulas for the entropy and number of particles can be derived, of course, straight by means of the distribution function (9). The energy is determined by the formula:

$$E = \frac{2AT}{\Lambda^2}\left(\Psi_2 + \frac{\eta}{\tau}\Psi_1 + \tau\frac{\partial\Psi_2}{\partial\tau}\right). \tag{17}$$

Naturally, the relation holds $\Omega = E - TS - \mu N$.

PRESSURES

In a bulk system the pressure is connected with the thermodynamical potential by the known formula $p = -\Omega/V$. In the considered case the system is anisotropic, since the character of motion of particles in the directions parallel and perpendicular to planes is different, and, therefore, the usual formula for the pressure is invalid. The force exerted by the gas on the wall perpendicular to the z axis is different from the force exerted on the side walls perpendicular to the x and y axes. These forces can be calculated in the same way as in the volume case [6]. The pressures in directions parallel to the (x, y) plane and on the planes perpendicular to the z axis are given by the formulas

$$p_{\parallel} = -\frac{1}{L}\left(\frac{\partial E}{\partial A}\right)_{S,L}, \qquad p_{\perp} = -\frac{1}{A}\left(\frac{\partial E}{\partial L}\right)_{S,A}. \tag{18}$$

Since

$$\left(\frac{\partial E}{\partial A}\right)_{S,N,L} = \left(\frac{\partial \Omega}{\partial A}\right)_{T,\mu,L}, \qquad \left(\frac{\partial E}{\partial L}\right)_{S,N,A} = \left(\frac{\partial \Omega}{\partial L}\right)_{T,\mu,A}, \tag{19}$$

it is then more convenient to calculate the pressures (18) using the formulas

$$p_{\parallel} = -\frac{1}{L}\left(\frac{\partial \Omega}{\partial A}\right)_{T,\mu,L}, \qquad p_{\perp} = -\frac{1}{A}\left(\frac{\partial \Omega}{\partial L}\right)_{T,\mu,A}. \tag{20}$$

The differential of the thermodynamic potential (14) can be represented in the form

$$d\Omega = -SdT - Nd\mu - p_{\parallel}LdA - p_{\perp}AdL. \tag{21}$$

Considering the form of the thermodynamic potential (11), we obtain the formulas determining the pressures through the functions (12):

$$p_{\parallel} = \frac{2T}{\Lambda^2 L}\Psi_2, \qquad p_{\perp} = \frac{4T}{\Lambda^2 L}\left(\tau\frac{\partial\Psi_2}{\partial\tau} + \frac{\eta}{\tau}\Psi_1\right). \tag{22}$$

The quantity $-p_{\parallel}L$ is an analog of the surface tension in the theory of surfaces [6]. The energy (17) is connected with the pressures (22) by the relation

$$E = AL\left(p_{\parallel} + \frac{1}{2}p_{\perp}\right), \tag{23}$$

which in the volume limit $p_{\parallel} = p_{\perp} = p$ turns into the known relation $pV = (2/3)E$ for the Fermi gas [6].

REDUCED FORM OF THERMODYNAMIC QUANTITIES

It is convenient to introduce dimensionless quantities, which we will call "reduced" and designate them by a tilde on top, for the entropy, energy, pressures, volume and surface densities:

$$\tilde{S} \equiv \frac{2L^2}{\pi A}S, \quad \tilde{E} \equiv \frac{2mL^4}{\pi^3\hbar^2 A}E, \quad \tilde{p}_{\parallel} \equiv \frac{2mL^5}{\pi^3\hbar^2}p_{\parallel}, \quad \tilde{p}_{\perp} \equiv \frac{2mL^5}{\pi^3\hbar^2}p_{\perp},$$

$$\tilde{n} \equiv \frac{2L^3}{\pi}n, \quad \tilde{n}_A \equiv \frac{2L^2}{\pi}n_A. \tag{24}$$

The reduced quantities are functions of only two independent dimensionless variables — the temperature τ and chemical potential η:

$$\tilde{S} = \tau\left[2\Psi_2 + \tau\frac{\partial\Psi_2}{\partial\tau}\right], \quad \tilde{E} = \frac{\tau^2}{2}\left(\Psi_2 + \frac{\eta}{\tau}\Psi_1 + \tau\frac{\partial\Psi_2}{\partial\tau}\right), \quad \tilde{n} = \tilde{n}_A = \tau\Psi_1,$$

$$\tilde{p}_{\parallel} = \frac{\tau^2}{2}\Psi_2, \quad \tilde{p}_{\perp} = \tau^2\left(\frac{\eta}{\tau}\Psi_1 + \tau\frac{\partial\Psi_2}{\partial\tau}\right). \tag{25}$$

The use of the reduces quantities is convenient owing to the fact that they do not contain explicitly geometric dimensions of the system.

HEAT CAPACITIES

An important directly observable thermodynamic quantity is the heat capacity. In the geometry under consideration heat capacities can be defined under various conditions different from that which take place in the volume case. In order to determine heat capacities, it is necessary to calculate the quantity $C = T\left(dS/dT\right)$. For this purpose, it is convenient to express the differential of the entropy through the reduced quantities:

$$dS = \frac{\pi A}{2L^2}\left(-\frac{\tilde{S}}{\tilde{n}_A}d\tilde{n}_A + d\tilde{S}\right) = \frac{\pi A}{2L^2}\left[\left(\frac{\partial \tilde{S}}{\partial \eta} - \frac{\tilde{S}}{\tilde{n}_A}\frac{\partial \tilde{n}_A}{\partial \eta}\right)d\eta + \left(\frac{\partial \tilde{S}}{\partial \tau} - \frac{\tilde{S}}{\tilde{n}_A}\frac{\partial \tilde{n}_A}{\partial \tau}\right)d\tau\right]. \tag{26}$$

In the volume case at a fixed number of particles, which is assumed here, the equation of state is: $p = p(T,V)$. If the chemical potential is used as an independent variable, then the equation of state is defined parametrically by the equations $p = p(T,V,\mu)$ and $N = N(T,V,\mu)$. To obtain the heat capacity as a function of only temperature, one constraint should be imposed between the pressure and the volume. In the simplest case, it its possible to fix either the volume or the pressure, thus determining the heat capacities C_V and C_p.

Under given conditions, owing to anisotropy of the system, there are two equations of state (22) for two pressures $p_\parallel = p_\parallel(T,A,L,\mu)$ and $p_\perp = p_\perp(T,A,L,\mu)$, which at a fixed number of particles should be considered together with the equation (16) $N = N(T,A,L,\mu)$. To obtain the heat capacity as a function of only temperature, two additional constraints should be set between the pressures $p_\parallel, p_\perp$ and the dimensions of the system A, L, namely $F_1(p_\parallel, p_\perp, A, L) = 0$ and $F_2(p_\parallel, p_\perp, A, L) = 0$. In the simplest case, two of four quantities $p_\parallel, p_\perp, A, L$ can be fixed. Then the heat capacity as a function of temperature can be considered under fixation of one of the following pairs of quantities: (A, L), $(p_\parallel, p_\perp)$, $(A, p_\parallel)$, $(A, p_\perp)$, $(L, p_\parallel)$, $(L, p_\perp)$. Fixation of the first of pairs (A, L) corresponds to the volume case of the heat capacity at a constant volume, and of the second $(p_\parallel, p_\perp)$ − at a constant pressure.

With account of the fixation of a number of particles, we have

$$d\tilde{n}_A = \tilde{n}_A\left(2\frac{dL}{L} - \frac{dA}{A}\right). \tag{27}$$

Also it should be taken into account that

$$\frac{d\tau}{dT} = \frac{1}{\varepsilon_L} + \frac{2\tau}{L}\frac{dL}{dT}. \tag{28}$$

Finally, we obtain formulas for the reduced heat capacities $\tilde{C} \equiv \frac{2L^2}{\pi A}C$ under different conditions for arbitrary temperatures:

$$\tilde{C}_{AL} = \tau\left[\frac{\partial \tilde{S}}{\partial \tau} - \frac{\partial \tilde{S}}{\partial \eta}\frac{(\partial \tilde{n}_A/\partial \tau)}{(\partial \tilde{n}_A/\partial \eta)}\right], \tag{29}$$

$$\tilde{C}_{p_\parallel p_\perp} = \tau\frac{\left\{\left(\frac{\partial \tilde{S}}{\partial \eta} - \frac{\tilde{S}}{\tilde{n}_A}\frac{\partial \tilde{n}_A}{\partial \eta}\right)\left(\tilde{p}_\perp\frac{\partial \tilde{p}_\parallel}{\partial \tau} - \tilde{p}_\parallel\frac{\partial \tilde{p}_\perp}{\partial \tau}\right) + \left(\frac{\partial \tilde{S}}{\partial \tau} - \frac{\tilde{S}}{\tilde{n}_A}\frac{\partial \tilde{n}_A}{\partial \tau}\right)\left(\tilde{p}_\parallel\frac{\partial \tilde{p}_\perp}{\partial \eta} - \tilde{p}_\perp\frac{\partial \tilde{p}_\parallel}{\partial \eta}\right)\right\}}{\left[\tilde{p}_\parallel\frac{\partial \tilde{p}_\perp}{\partial \eta} - \tilde{p}_\perp\frac{\partial \tilde{p}_\parallel}{\partial \eta} + \frac{2}{5}\tau\left(\frac{\partial \tilde{p}_\parallel}{\partial \eta}\frac{\partial \tilde{p}_\perp}{\partial \tau} - \frac{\partial \tilde{p}_\parallel}{\partial \tau}\frac{\partial \tilde{p}_\perp}{\partial \eta}\right)\right]}, \tag{30}$$

$$\tilde{C}_{Lp_\parallel} = \tau\left\{\left(\frac{\partial \tilde{S}}{\partial \tau} - \frac{\tilde{S}}{\tilde{n}_A}\frac{\partial \tilde{n}_A}{\partial \tau}\right) - \left(\frac{\partial \tilde{S}}{\partial \eta} - \frac{\tilde{S}}{\tilde{n}_A}\frac{\partial \tilde{n}_A}{\partial \eta}\right)\frac{(\partial \tilde{p}_\parallel/\partial \tau)}{(\partial \tilde{p}_\parallel/\partial \eta)}\right\}, \tag{31}$$

$$\tilde{C}_{Ap_\parallel} = \tau\frac{\left\{\tilde{n}_A\frac{\partial \tilde{p}_\parallel}{\partial \eta}\left(\frac{\partial \tilde{S}}{\partial \tau} - \frac{\tilde{S}}{\tilde{n}_A}\frac{\partial \tilde{n}_A}{\partial \tau}\right) - \tilde{n}_A\frac{\partial \tilde{p}_\parallel}{\partial \tau}\left(\frac{\partial \tilde{S}}{\partial \eta} - \frac{\tilde{S}}{\tilde{n}_A}\frac{\partial \tilde{n}_A}{\partial \eta}\right) + \frac{5}{2}\tilde{p}_\parallel\left(\frac{\partial \tilde{S}}{\partial \eta}\frac{\partial \tilde{n}_A}{\partial \tau} - \frac{\partial \tilde{S}}{\partial \tau}\frac{\partial \tilde{n}_A}{\partial \eta}\right)\right\}}{\tilde{n}_A\frac{\partial \tilde{p}_\parallel}{\partial \eta} - \frac{5}{2}\tilde{p}_\parallel\frac{\partial \tilde{n}_A}{\partial \eta} + \tau\left(\frac{\partial \tilde{n}_A}{\partial \eta}\frac{\partial \tilde{p}_\parallel}{\partial \tau} - \frac{\partial \tilde{n}_A}{\partial \tau}\frac{\partial \tilde{p}_\parallel}{\partial \eta}\right)}. \tag{32}$$

The heat capacities $\tilde{C}_{Lp_\perp}$ and $\tilde{C}_{Ap_\perp}$ are determined by the formulas (31),(32) with account of the replacement $p_\parallel \to p_\perp$.

COMPRESSIBILITIES

Another directly observable quantities are compressibilities. We define "parallel" and "perpendicular" compressibilities by the relations

$$\gamma_{\parallel} = \frac{1}{n}\left(\frac{\partial n}{\partial p_{\parallel}}\right)_{L}, \qquad \gamma_{\perp} = \frac{1}{n}\left(\frac{\partial n}{\partial p_{\perp}}\right)_{A}. \tag{33}$$

Compressibilities can be calculated under condition of constant temperature (isothermal) and constant entropy (adiabatic). For compressibilities in isothermal conditions, defined by the relations (33), we obtain:

$$\tilde{\gamma}_{\parallel T} \equiv \frac{\pi^3\hbar^2}{4mL^5}\gamma_{\parallel T} = \frac{(\partial\tilde{n}/\partial\eta)}{2\tilde{n}(\partial\tilde{p}_{\parallel}/\partial\eta)}, \tag{34}$$

$$\tilde{\gamma}_{\perp T} \equiv \frac{\pi^3\hbar^2}{4mL^5}\gamma_{\perp T} = \frac{(\partial\tilde{n}/\partial\eta)}{4\left[\left(\frac{5}{2}\tilde{p}_{\perp} - \tau\frac{\partial\tilde{p}_{\perp}}{\partial\tau}\right)\frac{\partial\tilde{n}}{\partial\eta} - \left(\tilde{n} - \tau\frac{\partial\tilde{n}}{\partial\tau}\right)\frac{\partial\tilde{p}_{\perp}}{\partial\eta}\right]}. \tag{35}$$

The adiabaticity condition consists in the invariance of the entropy per one particle (and therefore of the total entropy in the system with a fixed number of particles). In the volume case in adiabatic processes the parameter $t = \mu/T$ is constant. It is easy to verify, using the formulas (2), that this condition leads to the known equations of the adiabat: $n/T^{3/2} = C_1$, $p/n^{5/3} = C_2$, $p/T^{5/2} = C_3$, where C_i are constants.

In the considered case the adiabaticity condition has the form:

$$\sigma \equiv \frac{S}{N} = \frac{1}{\Psi_1}\left(2\Psi_2 + \tau\frac{\partial\Psi_2}{\partial\tau}\right) \equiv \Theta(\tau,\eta) = \text{const.} \tag{36}$$

Together with the equation for the number of particles (16) the equation (36) determines relationships between the density, temperature and pressures in adiabatic processes. The adiabatic compressibilities are given by the formulas:

$$\tilde{\gamma}_{\parallel\sigma} = \frac{\dfrac{\partial\Theta}{\partial\eta}\dfrac{\partial\tilde{n}}{\partial\tau} - \dfrac{\partial\Theta}{\partial\tau}\dfrac{\partial\tilde{n}}{\partial\eta}}{2\tilde{n}\left[\dfrac{\partial\Theta}{\partial\eta}\dfrac{\partial\tilde{p}_{\parallel}}{\partial\tau} - \dfrac{\partial\Theta}{\partial\tau}\dfrac{\partial\tilde{p}_{\parallel}}{\partial\eta}\right]}, \tag{37}$$

$$\tilde{\gamma}_{\perp\sigma} = \frac{\dfrac{\partial\Theta}{\partial\eta}\dfrac{\partial\tilde{n}}{\partial\tau} - \dfrac{\partial\Theta}{\partial\tau}\dfrac{\partial\tilde{n}}{\partial\eta}}{4\left[\dfrac{5}{2}\tilde{p}_{\perp}\left(\dfrac{\partial\Theta}{\partial\eta}\dfrac{\partial\tilde{n}}{\partial\tau} - \dfrac{\partial\Theta}{\partial\tau}\dfrac{\partial\tilde{n}}{\partial\eta}\right) - \tilde{n}\left(\dfrac{\partial\Theta}{\partial\eta}\dfrac{\partial\tilde{p}_{\perp}}{\partial\tau} - \dfrac{\partial\Theta}{\partial\tau}\dfrac{\partial\tilde{p}_{\perp}}{\partial\eta}\right)\right]}. \tag{38}$$

Certainly, at zero temperature the isothermal and adiabatic compressibilities coincide.

ANALYSIS OF FUNCTIONS $\Psi_1(\tau,\eta)$ AND $\Psi_2(\tau,\eta)$

As shown above, all thermodynamic quantities are expressed through the functions $\Psi_1(\tau,\eta)$, $\Psi_2(\tau,\eta)$ and their derivatives. In this section we study the properties of these functions. The details of calculations are given in Appendix. Note that when studying oscillations in the Fermi gas with quantized levels, usually the Poisson formula is used for the extraction of an oscillating part [6,14,15]. But a detailed analysis undertaken by the authors shows that it is more convenient to calculate the standard functions (12), by which thermodynamic quantities are expressed, without use of the Poisson formula. This, in particular, is connected with the fact that the possibility of extraction of an oscillating part in some function does not at all mean that the total function is oscillating, and the contribution of non-oscillating part should be analyzed as well. As a simples example let us consider the function $f(x,a) = (a/2)x^2 + \sin 2x$. Despite this function contains an oscillating term, its behavior depends on the value of its non-oscillating part, that is, the value of the parameter a. The form of this function and its derivative at some values of a is shown in Fig. 1. At $a = 0.1$ both the function and its derivative oscillate (curves *1*). At $a = 2$ the function itself already proves to be monotonically increasing, while its derivative remains oscillating (curves *2*). And at $a = 4$ both the function and its derivative monotonically increase (curves *3*). As it will be seen, a similar situation takes place as well for the functions considered in the present work. Also it should be noted that for establishing correct thermodynamic relations, the total thermodynamic potential should be considered, with account of contributions of both oscillating and non-oscillating parts.

At fixed particle number density and at high temperatures, the same as in the volume case, the chemical potential is negative. With decreasing temperature it increases and at some temperature T_0 turns into zero $(\eta = 0)$, becoming further positive. There is one more characteristic temperature T_L, at which $\mu = \varepsilon_L$ $(\eta = 1)$. The dependencies of the

dimensionless chemical potential η on the dimensionless temperature τ are shown in Fig. 2. The characteristic temperatures $\tau_0 = T_0/\varepsilon_L$ and $\tau_L = T_L/\varepsilon_L$ are determined from the equations:

$$\tilde{n}_A = \tau_0\, \Psi_1\left(\tau_0, 0\right), \qquad \tilde{n}_A = \tau_L\, \Psi_1\left(\tau_L, 1\right). \tag{39}$$
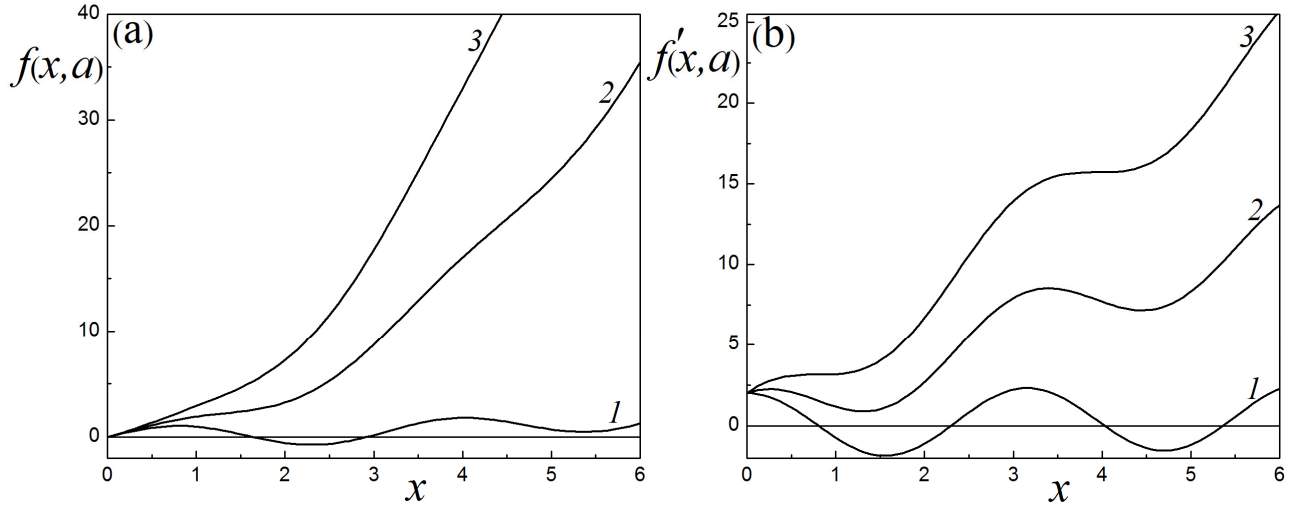
Fig. 1. Graphs of the functions $f(x,a)$, $f'(x,a)$ for some values of the parameter a.

(a) The function $f(x,a) = \dfrac{a}{2}x^2 + \sin 2x$ for the values of the parameter a: (1) 0.1; (2) 2.0; (3) 4.0.

(b) The derivative $f'(x,a) = ax + 2\cos 2x$ for the same values of the parameter a: (1) 0.1; (2) 2.0; (3) 4.0.

The region where $\mu \le \varepsilon_L$ ($\eta \le 1$) will be for convenience called the high temperature region, and the region $\mu > \varepsilon_L$ ($\eta > 1$) − the low temperature region. The functions $\Psi_s(\tau, \eta)$ are calculated differently in these regions. At $\eta \le 1$ they can be calculated by the formula

$$\Psi_s\left(\tau, \eta\right) = \frac{1}{2}\sum_{l=1}^{\infty} \frac{(-1)^{l+1}\, e^{\frac{l\eta}{\tau}}}{l^s}\, \theta_3\left(0, \frac{l}{\pi^2\tau}\right) - \frac{1}{2}\Phi_s\left(\frac{\eta}{\tau}\right), \tag{40}$$

where $\theta_3\left(v, x\right) \equiv 1 + 2\sum_{k=1}^{\infty} e^{-k^2\pi^2 x}\cos 2\pi v x$ is the theta-function.
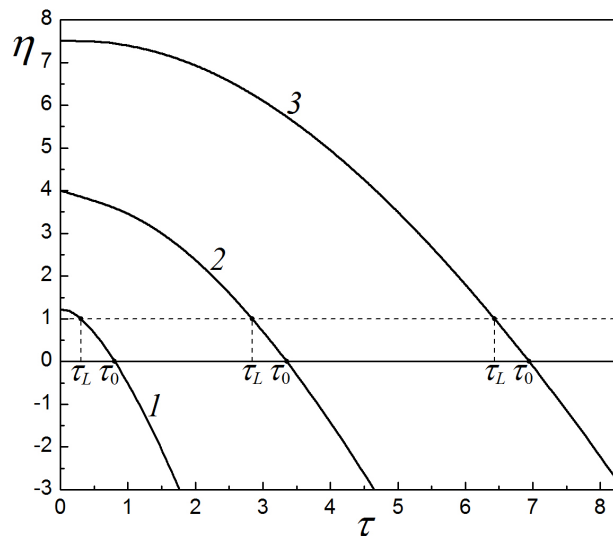
Fig. 2. The dependencies of the chemical potential on temperature $\eta(\tau)$ at different values of the reduced density:

(1) $\tilde{n}_A = 0.21$, $\tau_L = 0.30$, $\tau_0 = 0.81$; (2) $\tilde{n}_A = 3.0$, $\tau_L = 2.84$, $\tau_0 = 3.35$; (3) $\tilde{n}_A = 10.0$, $\tau_L = 6.43$, $\tau_0 = 6.95$.

More interesting is the case $\eta > 1$, which is realized at low temperatures. Then the considered functions can be represented in the form

$$\Psi_1(\tau,\eta) = \frac{\eta}{\tau}\Psi_1'(\eta) + \Psi_1''(\tau,\eta), \tag{41}$$

$$\Psi_2(\tau,\eta) = \frac{\eta^2}{2\tau^2}\Psi_2'(\eta) + \Psi_2''(\tau,\eta). \tag{42}$$

Here the functions

$$\Psi_1'(\eta) = [x_0]\left\{1 - \frac{1}{6\eta}([x_0]+1)(2[x_0]+1)\right\}, \tag{43}$$

$$\Psi_2'(\eta) = [x_0]\left\{1 - \frac{1}{3\eta}([x_0]+1)(2[x_0]+1) + \frac{1}{30\eta^2}([x_0]+1)(2[x_0]+1)(3[x_0]^2 + 3[x_0]-1)\right\} \tag{44}$$

determine the state of the system at zero temperature. For brevity here and in the following it is used the designation $x_0 \equiv \sqrt{\eta}$, $x_0 > 1$ at that, and $[x_0]$ designates the whole part of a number x_0. Graphs of the functions (43), (44) and their derivatives are shown in Fig. 3a and 3b. The function $\Psi_1'(\eta)$ is continuous and monotonically increasing, and its derivative at the specific points $x_0 = [x_0]$ undergoes jumps $\Delta(d\Psi'(\eta)/d\eta)\big|_{[x_0]} = 1/[x_0]^2$ (Fig. 3a). At $\eta \gg 1$ it has the asymptote $\Psi_1'(\eta) \approx 2\sqrt{\eta}/3$. The function $\Psi_2'(\eta)$ is also continuous and monotonically increasing, with the asymptote $\Psi_2'(\eta) \approx 8\sqrt{\eta}/15$ at $\eta \gg 1$. The derivative of the function $\Psi_2'(\eta)$ is an oscillating function with a varying amplitude (Fig. 3b).
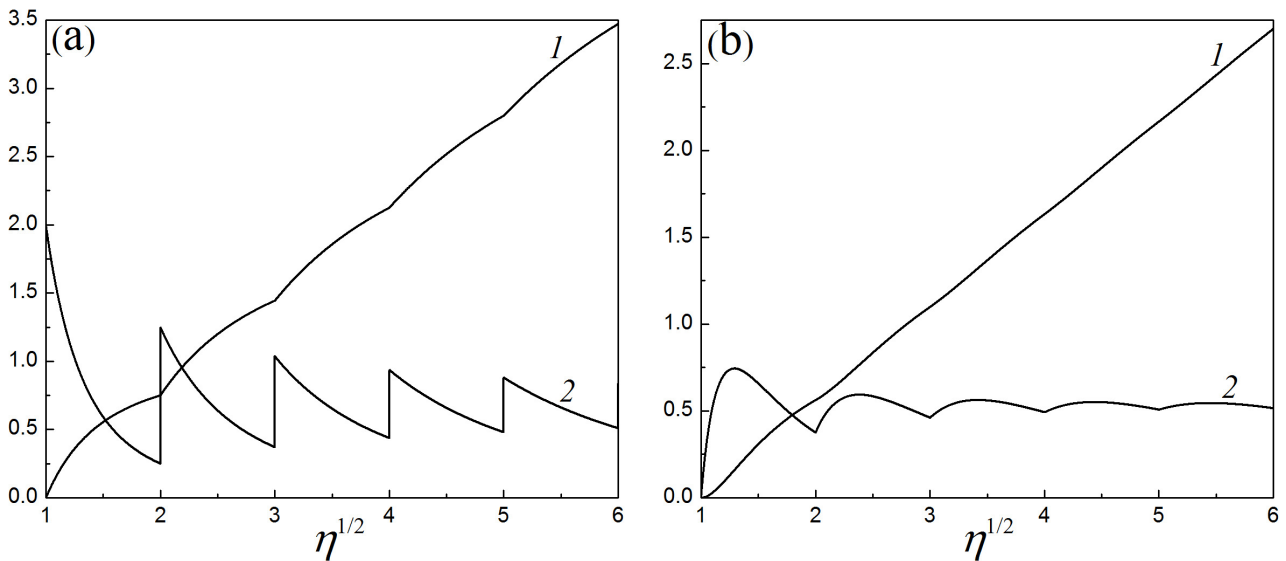
Fig. 3. Graphs of the functions $\Psi_1'(\eta)$, $\Psi_2'(\eta)$ and their derivatives.

(a) The functions $\Psi_1'(\eta)$ (*1*) and $d\Psi_1'(\eta)/d\sqrt{\eta}$ (*2*); (b) The functions $\Psi_2'(\eta)$ (*1*) and $d\Psi_2'(\eta)/d\sqrt{\eta}$ (*2*).

The functions

$$\Psi_1''(\tau,\eta) = \Phi_1\left[\tau^{-1}\left([x_0]^2 - \eta\right)\right] + \Phi_1\left[\tau^{-1}\left(\eta - ([x_0]+1)^2\right)\right] + \overline{\Psi}_1^{\exp}(\tau,\eta), \tag{45}$$

$$\Psi_2''(\tau,\eta) = \frac{\pi^2}{6}[x_0] - \Phi_2\left[\tau^{-1}\left([x_0]^2 - \eta\right)\right] + \Phi_2\left[\tau^{-1}\left(\eta - ([x_0]+1)^2\right)\right] + \overline{\Psi}_2^{\exp}(\tau,\eta) \tag{46}$$

describe the temperature dependencies of thermodynamic quantities at low temperatures. The form of the exponentially small at $\tau \ll 1$ functions $\overline{\Psi}_s^{\exp}(\tau,\eta)$ is given in Appendix (the formula (11)). The dependencies of the functions (45), (46) and their derivatives on the chemical potential are shown in Fig. 4a and 4b. The function $\Psi_1''(\tau,\eta)$ has an oscillating character and its derivative undergoes jumps at $x_0 = [x_0]$ (Fig. 4a). The function $\Psi_2''(\tau,\eta)$ is monotonically increasing and its derivative has oscillations (Fig. 4b). The dependencies of the total functions (41), (42) and their derivatives on the chemical potential are shown in Fig. 5a and 5b.
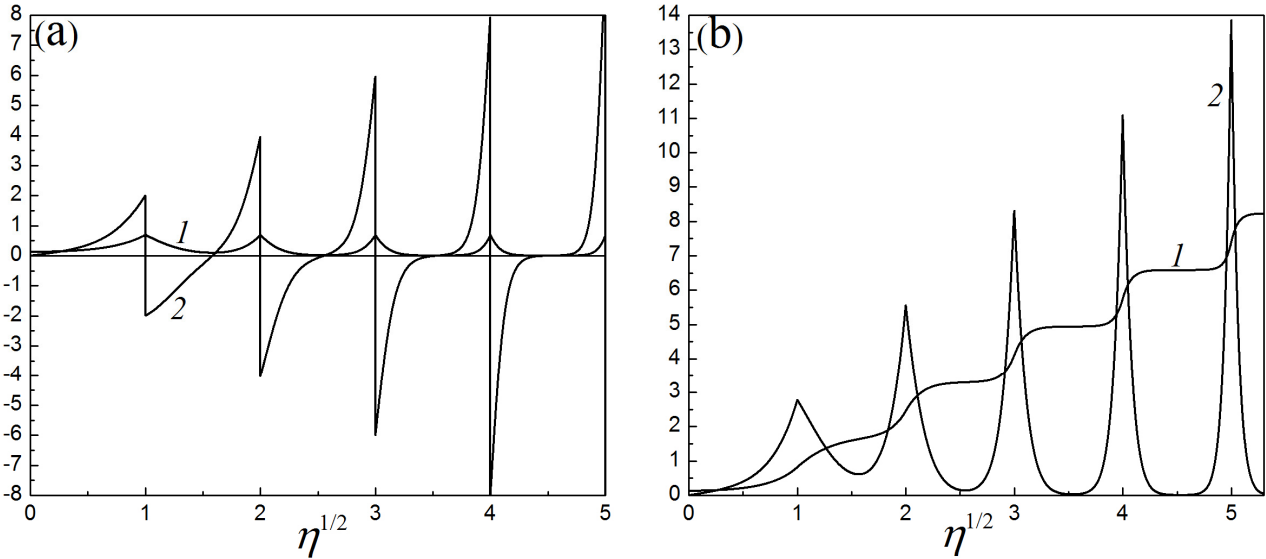
Fig. 4. Graphs of the functions $\Psi_1''(\tau,\eta)$, $\Psi_2''(\tau,\eta)$ and their derivatives at $\tau = 0.5$.

(a) The functions $\Psi_1''(\tau,\eta)$ (*1*) and $d\Psi_1''(\tau,\eta)/d\sqrt{\eta}$ (*2*); (b) The functions $\Psi_2''(\tau,\eta)$ (*1*) and $d\Psi_2''(\tau,\eta)/d\sqrt{\eta}$ (*2*).
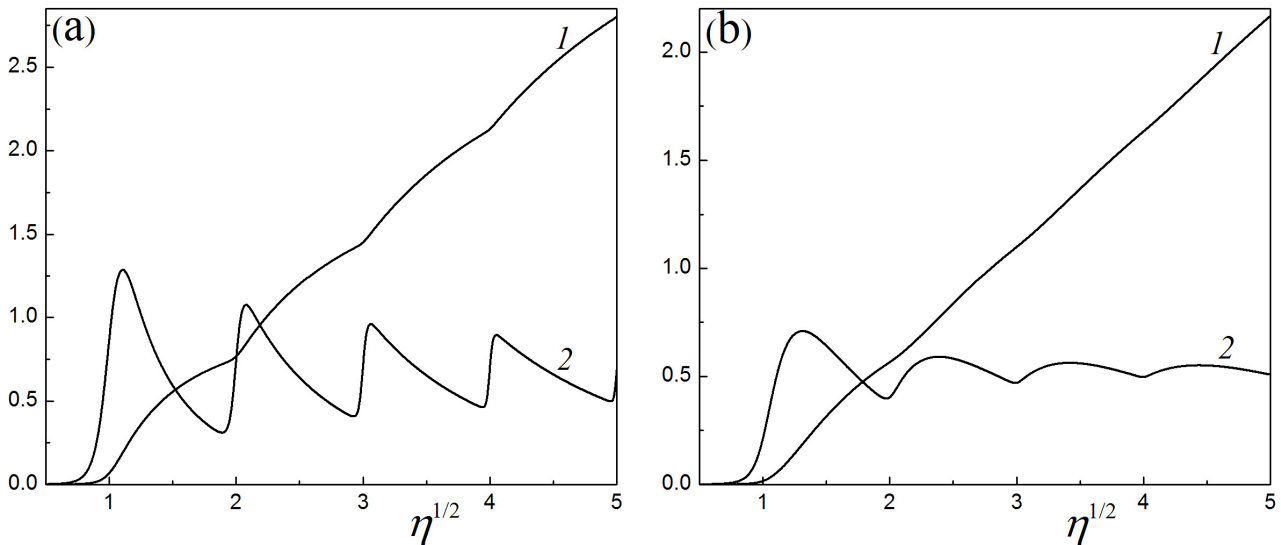
Fig. 5. Graphs of the functions $(\tau/\eta)\Psi_1(\tau,\eta)$, $2(\tau/\eta)^2\Psi_2(\tau,\eta)$ and their derivatives at $\tau = 0.1$.

(a) The functions $(\tau/\eta)\Psi_1(\tau,\eta)$ (*1*) and $d\left[(\tau/\eta)\Psi_1(\tau,\eta)\right]/d\sqrt{\eta}$ (*2*);

(b) The functions $2(\tau/\eta)^2\Psi_2(\tau,\eta)$ (*1*) and $d\left[2(\tau/\eta)^2\Psi_2(\tau,\eta)\right]/d\sqrt{\eta}$ (*2*).

Although, as it was noted, the function $\Psi_1''(\tau,\eta)$ has an oscillation form, the total function $\Psi_1(\tau,\eta)$ proves to be monotonically increasing (Fig. 5a, curve *1*). Also monotonically increasing is the function $\Psi_2(\tau,\eta)$ (Fig. 5b, curve *1*). The derivatives of both of these functions have an oscillating character at not large values of the chemical potential (Fig. 5, curves *2*).

Thus, the functions $\Psi_1(\tau,\eta)$, $\Psi_2(\tau,\eta)$ themselves through which the thermodynamic quantities are expressed are not oscillating, in particular there are absent oscillations of the thermodynamic potential (11) on the chemical potential η. However, as we will see, dependencies of some quantities on the chemical potential that include the derivatives of these functions, such as for example compressibilities, can have a nonmonotonic character.

THERMODYNAMIC QUANTITIES AT LOW TEMPERATURES

The most interesting region where quantum effects can manifest themselves on the macroscopic level is the region of low temperatures. Let us consider the behavior of the observable characteristics at low temperatures, such that $\tau \ll 1$. In this limit, with account of the main exponential corrections

$$\Psi_1(\tau,\eta) = \frac{\eta}{\tau}\Psi_1'(\eta) + \exp\left[\tau^{-1}\left([x_0]^2 - \eta\right)\right] + \exp\left[\tau^{-1}\left(\eta - ([x_0]+1)^2\right)\right], \tag{47}$$

$$\Psi_2(\tau,\eta) = \frac{\eta^2}{2\tau^2}\Psi_2'(\eta) + \frac{\pi^2}{6}[x_0] - \exp\left[\tau^{-1}\left([x_0]^2 - \eta\right)\right] + \exp\left[\tau^{-1}\left(\eta - ([x_0]+1)^2\right)\right]. \tag{48}$$

For the reduced entropy, we obtain in this approximation:

$$\tilde{S} = \frac{\pi^2}{3}[x_0]\tau - (2\tau - a_1)e^{\frac{a_1}{\tau}} + (2\tau - a_2)e^{\frac{a_2}{\tau}}. \tag{49}$$

Here and below for brevity the designations are used $a_1 \equiv [x_0]^2 - \eta$, $a_2 \equiv \eta - ([x_0]+1)^2$. The dependencies of the entropy on temperature and density are shown in Figs. 6, 7. The dependence on temperature proves to be linear as in the volume case, but its slope changes by jumps as the energetic levels are being filled up (Fig. 6). The correction to the linear law, in contrast to the volume case where it is proportional to T^3, in this case is exponentially small.
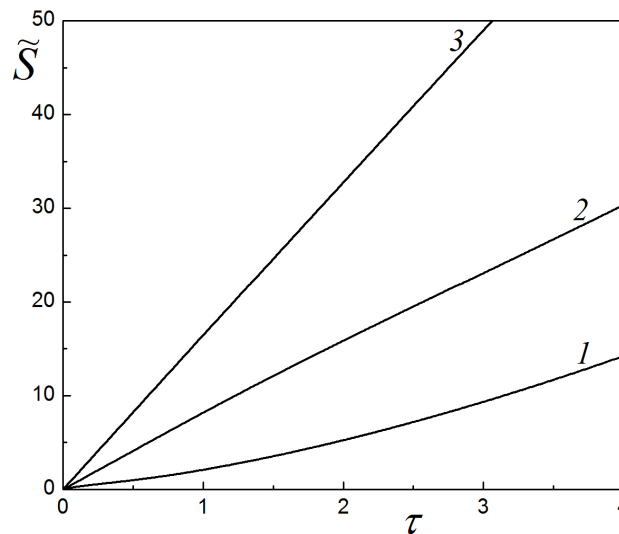
Fig. 6. The temperature dependencies of the reduced entropy $\tilde{S}(\tau;x_0)$ at a fixed value of the chemical potential $x_0 \equiv \sqrt{\eta}$:
(1) $x_0 = 1.1$;   (2) $x_0 = 3.0$;   (3) $x_0 = 5.5$.

With varying the chemical potential or the density at low temperatures the entropy undergoes jumps, which are becoming more indistinct as temperature increases and entirely disappear at rather high temperatures (Fig. 7).
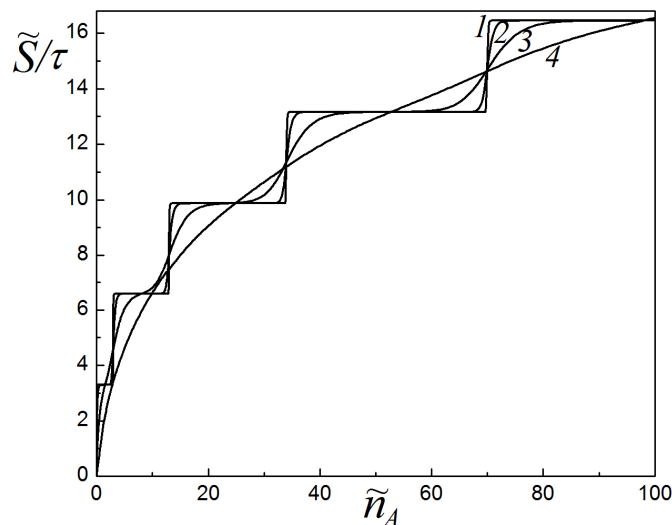
Fig. 7. The dependencies of the quantity $\tilde{S}(\tilde{n}_A;\tau)/\tau$ on the reduced density at fixed temperature:
(1) $\tau = 0.01$;   (2) $\tau = 0.1$;   (3) $\tau = 0.5$;   (4) $\tau = 2.0$.

The value of the entropy jump per unit of area depends only on temperature and is determined by the formula

$$\frac{\Delta S}{A} = \frac{\pi m}{3\hbar^2}T. \tag{50}$$

Pay attention that this quantity does not explicitly depend on the distance L, though certainly this parameter enters into the condition of applicability of the formula (50) $T \ll \pi^2\hbar^2/2mL^2$. The entropy jumps are accompanied by the absorption of heat $\Delta Q = T\Delta S$. For electrons the heat absorbed at the jump of the entropy per unit of area $\Delta Q / A \approx 1.6 \cdot 10^{-5} T^2 \, erg/(cm^2 K^2)$ (temperature in Kelvins). For ^{3}He atoms this quantity is by three orders greater.

The density at low temperatures has only the exponentially small, depending on temperature, correction

$$\tilde{n} = \tilde{n}_A = \eta \Psi_1'(\eta) + \tau \left(e^{\frac{a_1}{\tau}} + e^{\frac{a_2}{\tau}} \right). \tag{51}$$

Neglecting the exponential corrections, the chemical potential in the expression for the entropy (49) and in other thermodynamic quantities can be taken with a good accuracy at zero temperature. In this approximation the chemical potential is connected with the reduced densities by the relation

$$\tilde{n} = \tilde{n}_A = [x_0]\left\{ \eta - \frac{1}{6}([x_0]+1)(2[x_0]+1) \right\}. \tag{52}$$

The density monotonically increases with increasing the chemical potential, undergoing breaks (discontinuities in the derivative) at the specific points $x_0 = [x_0]$. In the limit of rather high density when $x_0 \gg 1$, we can set $[x_0] \approx x_0$ and from (52) there follows the usual formula that relates the density of the bulk Fermi gas with the chemical potential at zero temperature: $n = (2m\mu)^{3/2}/3\pi^2\hbar^3$. The thermodynamical potential in this limit also acquires the usual form $\Omega = -AL(4\sqrt{2}/15\pi^2)(m^{3/2}\mu^{5/2}/\hbar^3)$. The condition $x_0 \gg 1$ is equivalent to the condition $N^{1/3} \gg (A/L^2)^{1/3}$. In the volume case $A \approx L^2$ it is equivalent to the condition $N^{1/3} \gg 1$, which is always true in a system of large number of particles. The exact formulas should be used under fulfilment of the condition $N \sim A/L^2$.

If thermodynamic quantities are taken in the reduced form (24), and the dimensionless chemical potential η and the dimensionless temperature τ are used as independent variables, then as it was shown the geometrical dimensions fall out of the thermodynamic relations, in particular the distance between plates L falls out (or the thickness of a film, from experimentalist's point of view). Meanwhile, exactly the dependencies of the observable quantities on the thickness of a film are of interest in experiment. To obtain such dependencies, the relations derived above should be presented in the dimensional form. At that, the form of dependence of the thermodynamic quantities on the thickness of a film will essentially depend on what quantity is being fixed when studying such dependencies: the total density n or the surface density n_A. Let us show it on the example of dependence of the chemical potential on the thickness of a film.

The formula (52) can be written in the form

$$\frac{2n}{\pi}L^3 = \frac{2n_A}{\pi}L^2 = [x_0]\left\{ x_0^2 - \frac{1}{6}([x_0]+1)(2[x_0]+1) \right\}. \tag{53}$$

As we see, the dependence of the distance L on the parameter x_0 will be different depending on what is fixed − the volume or the surface density. The chemical potential is expressed through L and the parameter x_0 by the formula

$$\mu = \frac{\pi^2\hbar^2}{2mL^2} x_0^2. \tag{54}$$

The formulas (53) and (54) define parametrically (parameter x_0) the dependence of the chemical potential on the thickness of a film at fixed n or n_A. It is easy to check that at a fixed surface density $(d\mu/dL)_{n_A} < 0$ and, therefore, the chemical potential monotonically decreases with increasing L. At a fixed volume density the derivative $(d\mu/dL)_n$ turns into zero at the minimum points determined by the equation $x_0^2 - (1/2)([x_0]+1)(2[x_0]+1) = 0$. The distance between planes at the minimum points of the chemical potential is determined by the formula

$$\frac{2n}{\pi}L_{\min}^3 = \frac{1}{3}[x_0]([x_0]+1)(2[x_0]+1). \tag{55}$$

At the points $x_0 = [x_0] \geq 2$ the sign of the derivative $(d\mu/dL)_n$ changes by a jump. These points correspond to the local maximums of the chemical potential, so that

$$\frac{2n}{\pi}L_{\max}^3 = \frac{1}{6}[x_0]([x_0]-1)(4[x_0]+1). \tag{56}$$

Thus, the dependence of the chemical potential on L at a fixed volume density has an oscillating character. The dependencies $\mu = \mu(L)$ at fixed surface (curve 1) and volume (curve 2) densities are shown in Fig. 8.
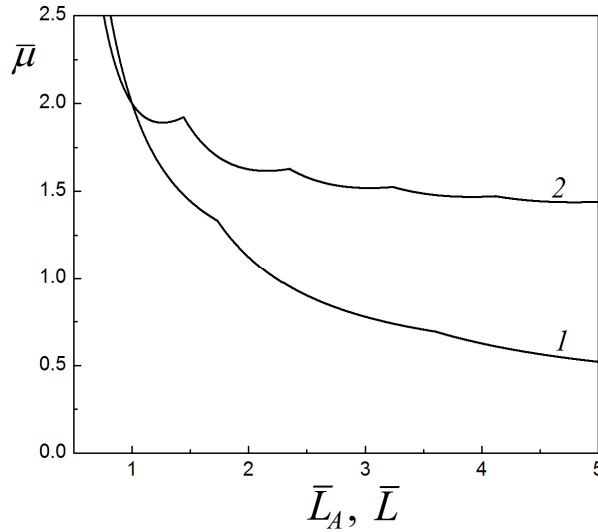
Fig. 8. The dependencies of the chemical potential on the distance between planes:

(1) $\bar{\mu} = \bar{\mu}(\bar{L}_A)$ at a fixed surface density n_A, here $\bar{\mu} \equiv (m/\pi\hbar^2 n_A)\mu$, $\bar{L}_A \equiv (2n_A/\pi)^{1/2} L$;

(2) $\bar{\mu} = \bar{\mu}(\bar{L})$ at a fixed volume density n, here $\bar{\mu} \equiv (2/\pi^4)^{1/3}(m/\hbar^2 n^{2/3})\mu$, $\bar{L} \equiv (2n/\pi)^{1/3} L$.

The pressures at low temperatures are determined by the formulas:

$$\tilde{p}_{\parallel} = \frac{\eta^2}{4}\Psi'_2(\eta) + \frac{\pi^2}{12}[x_0]\tau^2 + \frac{\tau^2}{2}\left(-e^{\frac{a_1}{\tau}} + e^{\frac{a_2}{\tau}}\right),\tag{57}$$

$$\tilde{p}_{\perp} = \eta^2\left[\Psi'_1(\eta) - \Psi'_2(\eta)\right] + \tau\left([x_0]^2 e^{\frac{a_1}{\tau}} + ([x_0]+1)^2 e^{\frac{a_2}{\tau}}\right).\tag{58}$$

As seen, the parallel pressure, in addition to the exponential temperature correction, also contains the power correction proportional to the square of temperature, and the perpendicular pressure contains only the exponential temperature correction. The dependencies of the reduced energy and pressures on the reduced density at zero temperature are shown in Fig. 9. Both the energy and the pressures monotonically increase with increasing the chemical potential or the density. At the points where the filling of discrete levels begins the dependence $\tilde{p}_{\perp} = \tilde{p}_{\perp}(\tilde{n}_A)$ undergoes breaks. In the limit $x_0 \gg 1$ at zero temperature the both pressures $p_{\parallel}$, $p_{\perp}$ prove to be equal to the pressure of the bulk degenerate Fermi gas.
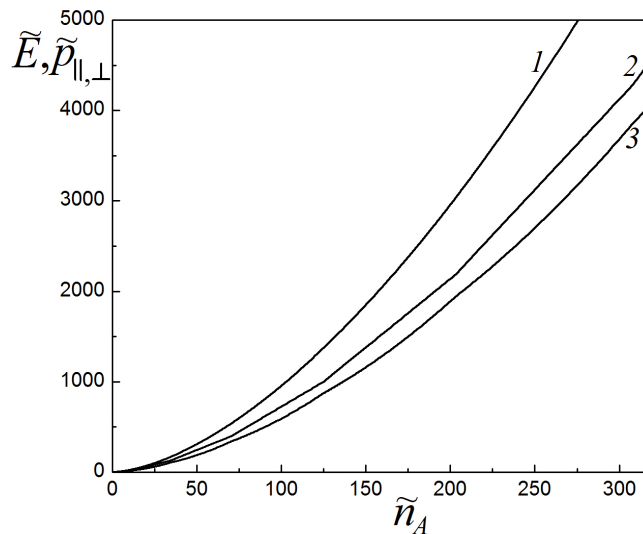
Fig. 9. The dependencies of the reduced energy and pressures on the reduced density at zero temperature:
(1) $\tilde{E}(\tilde{n}_A)$; *(2)* $\tilde{p}_{\perp}(\tilde{n}_A)$; *(3)* $\tilde{p}_{\parallel}(\tilde{n}_A)$.

There are of interest the dependencies of the perpendicular pressure on the distance between planes, presented in Fig. 10. The pressure at fixed n_A decreases with increasing L (curve *1*). At one point, corresponding to $x_0 = 2$, this curve undergoes

a break: the derivative $dp_\perp/dL$ on the left at this point is negative and on the right it equals to zero. At a fixed n the dependence $p_\perp = p_\perp(L)$ has an oscillating form (curve 2). The extremum points of this function can be found in the same way as for the dependence $\mu(L)$ at fixed n and are given by the expressions:

$$\frac{2n}{\pi} L_{\min}^3 = \frac{1}{6}[x_0]([x_0]-1)(4[x_0]+1),$$

$$\frac{2n}{\pi} L_{\max}^3 = \frac{1}{12}[x_0]([x_0]-1)(8[x_0]+11). \tag{59}$$

On the basis of the performed analysis, seemingly, a general conclusion can be made that the oscillating dependencies of thermodynamic quantities on the width L take place for the case of the fixed total density and they are absent when the surface density is fixed.
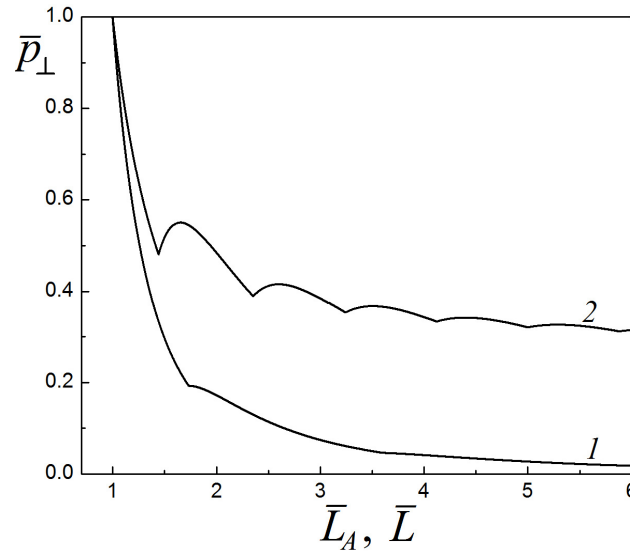
Fig. 10. The dependencies of the perpendicular pressure on the distance between planes:

(1) $\bar{p}_\perp = \bar{p}_\perp(\bar{L}_A)$ at a fixed surface density n_A, here $\bar{p}_\perp \equiv (2m/\pi^3\hbar^2)(\pi/2n_A)^{5/2} p_\perp$, $\bar{L}_A \equiv (2n_A/\pi)^{1/2} L$;

(2) $\bar{p}_\perp = \bar{p}_\perp(\bar{L})$ at a fixed volume density n, here $\bar{p}_\perp = (2m/\pi^3\hbar^2)(\pi/2n)^{5/3} p_\perp$, $\bar{L} \equiv (2n/\pi)^{1/3} L$.

He we give also the formulas, following from the general relations (34) − (38), for the compressibilities at zero temperature:

$$\tilde{\gamma}_\parallel = \frac{[x_0]}{\{\eta \Psi_1'(\eta)\}^2} = \frac{1}{[x_0]\left\{x_0^2 - \frac{1}{6}([x_0]+1)(2[x_0]+1)\right\}^2}, \tag{60}$$

$$\tilde{\gamma}_\perp = \frac{[x_0]}{2\eta^2\left\{(3\Psi_1'(\eta)-5\Psi_2'(\eta))[x_0]+2(\Psi_1'(\eta))^2\right\}} = \frac{1}{[x_0]([x_0]+1)(2[x_0]+1)\left\{x_0^2 - \frac{7}{9}[x_0]^2 - \frac{2}{3}[x_0] + \frac{4}{9}\right\}}. \tag{61}$$

The dependencies of compressibilities on the volume density at zero temperature are shown in Fig. 11. As seen, at some values of density, at which the filling of levels begins, the compressibilities undergo jumps. On approaching to the point that corresponds to $x_0 = 2$ from the side of large densities, the perpendicular compressibility tends to infinity. The nature of this divergence is similar to the nature of the break at this point in the dependence of the perpendicular pressure $p_\perp = p_\perp(L)$ (Fig. 10, curve 1). In the limit $x_0 \gg 1$ we have $\gamma_\parallel = \gamma_\perp = 3^{1/3}/\pi^{4/3} \; m/\hbar^2 n^{5/3}$. The quantity $u^2 = 1/mn\gamma_\parallel = \left(\pi^{4/3}/3^{1/3}\right) \hbar^2 n^{2/3}/m^2$ determines in this case the square of the speed of sound in the bulk Fermi gas.

In conclusion of this section, we proceed to the analysis of the low temperature behavior of heat capacities. For the first time, the calculation of the electron heat capacity for particles of small size with account of the discreteness of the energy levels was made by Fröhlich [13]. He showed that, in contrast to the bulk Fermi gas which has the linear temperature dependence of the heat capacity, in the case of small in all coordinates particles the heat capacity decreases exponentially with decreasing temperature. In the case considered in the present paper, in addition to the discrete levels there is possible a free motion of particles along planes, that leads to the maintenance of the linear law in the temperature dependence in given conditions.
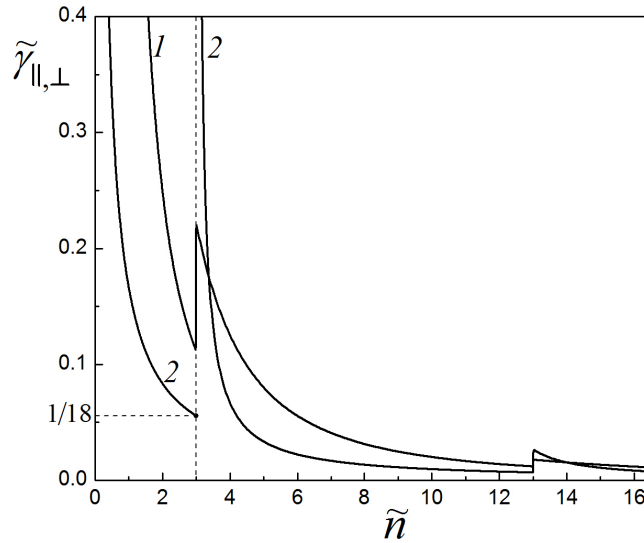
Fig. 11. The dependencies of compressibilities on the reduced density at zero temperature: (*1*) $\tilde{\gamma}_{\|} = \tilde{\gamma}_{\|}(\tilde{n})$; (*2*) $\tilde{\gamma}_{\perp} = \tilde{\gamma}_{\perp}(\tilde{n})$.

In the main approximation all introduced above heat capacities (29) – (32), as it had to be expected, prove to be identical and proportional to temperature

$$\tilde{C} \approx \frac{\pi^2}{3}[x_0]\,\tau. \tag{62}$$

Under fulfilment of the condition $x_0 \gg 1$ the formula (62), naturally, turns into the expression for the low temperature heat capacity of the bulk Fermi gas $C = (\pi/3)^{2/3}(mT/\hbar^2)n^{1/3}LA$. The heat capacity as a function of the chemical potential and density undergoes jumps at the points, in which the filling of new discrete levels begins (Fig. 12). The account for the corrections to the formula (62) smoothes out the steps. The value of the jump of the heat capacity is the same as that of the entropy (50): $\Delta C/A = \pi m T/3\hbar^2$.
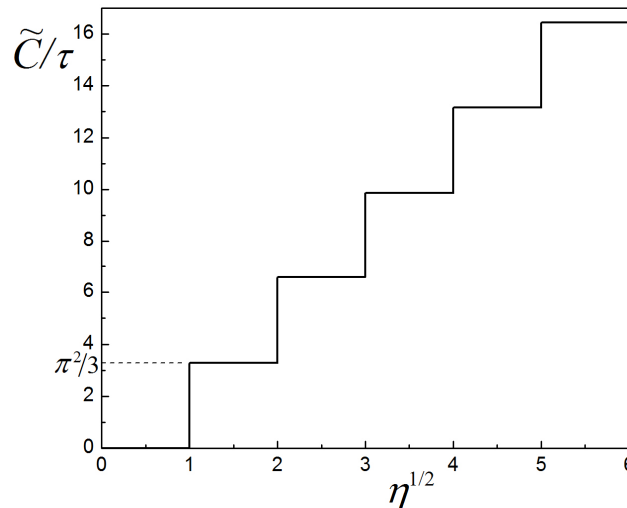
Fig. 12. The dependence of the ratio of the reduced heat capacity to the dimensionless temperature

$$\tilde{C}/\tau = \frac{\pi^2}{3}[x_0] \text{ at } \tau \ll 1 \text{ on the chemical potential } \eta^{1/2}.$$

For the heat capacities $\tilde{C}_{AL}, \tilde{C}_{Ap_{\|}}, \tilde{C}_{Lp_{\perp}}, \tilde{C}_{Ap_{\perp}}$ the corrections to the linear law (62) have the exponential character, and for two heat capacities these corrections are proportional to τ^3:

$$\tilde{C}_{p_{\|}p_{\perp}} \approx \frac{\pi^2}{3}[x_0]\tau\left\{1 + \frac{2\pi^2}{15}\frac{[x_0]}{\eta^2}\frac{\left(5[x_0]\Psi_2' - 3[x_0]\Psi_1' - 2\Psi_1'^2\right)}{\Psi_1'\left([x_0]\Psi_2' + \Psi_1'\Psi_2' - 2\Psi_1'^2\right)}\tau^2\right\}, \tag{63}$$

$$\tilde{C}_{Lp_{\parallel}} \approx \frac{\pi^2}{3}[x_0]\tau\left\{1 + \frac{\pi^2}{3}[x_0]\frac{\tau^2}{(\eta\Psi_1')^2}\right\}. \tag{64}$$

The differences between the heat capacities $\tilde{C}_{p_{\parallel}p_{\perp}}$, $\tilde{C}_{Lp_{\parallel}}$ and other heat capacities are proportional to τ^3.

THERMODYNAMIC QUANTITIES AT HIGH TEMPERATURES

Let us consider the area of high temperatures, where the de Broglie wavelength is much less than the average distance between particles: $\Lambda/l = \Lambda n^{1/3} \ll 1$. This condition is fulfilled if the parameter $t = \eta/\tau$ is negative and large by absolute value $|t| \gg 1$. At high temperatures and macroscopic distances between planes, such that $\Lambda/L = 2/\sqrt{\pi\tau} \ll 1$, also the condition $\sqrt{\tau} \gg 1$ holds. In this approximation, in the sum of the formula (40) it is sufficient to account for the main term with $l = 1$. Taking into account the relation $\theta_3(0,q) = \left[2K(m)/\pi\right]^{1/2}$, we obtain

$$\Psi_s(\tau,\eta) = \frac{1}{2}\left[\sqrt{\frac{2K(m)}{\pi}} - 1\right]e^{\frac{\eta}{\tau}}. \tag{65}$$

Here $K(m)$ is the full elliptic integral of the first kind, and $q \equiv q(m) = \exp\left[-\pi K(1-m)/K(m)\right]$ is the Jacobi parameter [17]. Considering the definition of the theta-function in (40), we find that the parameter m and the dimensionless temperature are connected by the relation

$$\frac{1}{\tau} = \pi\frac{K(1-m)}{K(m)}. \tag{66}$$

For considered large values of τ, the parameter m is close to unity. Using expansions in the small parameter $m_1 = 1 - m$ and taking into account that $K(m) \approx \frac{1}{2}\ln\frac{16}{m_1}$, from (66) we have: $m_1 = 16e^{-\pi^2\tau}$. For $\sqrt{\tau} \gg 1$, taking account of the main terms, we obtain

$$\Psi_s(\tau,\eta) = \frac{1}{2}\left[\sqrt{\pi\tau} - 1\right]e^{\frac{\eta}{\tau}}. \tag{67}$$

Taking account of only the first term in square brackets in (67) leads to the relations for the classical ideal gas, and accounting for the second term in brackets gives the correction on the finite width L proportional to the ratio Λ/L. The thermodynamic potential in the classical limit with account of such correction acquires the form

$$\Omega = -\frac{2TAL}{\Lambda^3}\left(1 - \frac{\Lambda}{2L}\right)e^{\frac{\mu}{T}}. \tag{68}$$

From the formula for the number of particles

$$N = -\left(\frac{\partial\Omega}{\partial\mu}\right)_{T,A,L} = \frac{2AL}{\Lambda^3}\left(1 - \frac{\Lambda}{2L}\right)e^{\frac{\mu}{T}} \tag{69}$$

there follows the dependence of the chemical potential on the density and temperature:

$$\frac{\mu}{T} = \ln\left(\frac{n\Lambda^3}{2}\right) + \frac{\Lambda}{2L}. \tag{70}$$

For the entropy we have the expression that generalizes the Sackur-Tetrode formula [6] to account for the quantum size effect:

$$S = N\ln\frac{2e^{5/2}}{n\Lambda^3} - N\frac{\Lambda}{4L}. \tag{71}$$

In the parallel pressure the linear with respect to Λ/L correction is absent, and it is present in the perpendicular pressure:

$$p_{\parallel} = nT, \qquad p_{\perp} = nT\left(1 + \frac{\Lambda}{2L}\right). \tag{72}$$

Here is also the formula for the energy with account of such correction:

$$E = \frac{3}{2}NT\left(1 + \frac{\Lambda}{6L}\right). \tag{73}$$

Let us write down in the high temperature limit the expressions for all heat capacities, which were defined above, with account of the quantum size correction:

$$C_{AL} = N\left(\frac{3}{2} + \frac{\Lambda}{8L}\right), \qquad C_{p_\parallel p_\perp} = \frac{5}{2}N,$$

$$C_{Lp_\parallel} = N\left(\frac{5}{2} + \frac{\Lambda}{8L}\right), \qquad C_{Ap_\parallel} = N\left(\frac{5}{2} + \frac{3\Lambda}{8L}\right), \tag{74}$$

$$C_{Lp_\perp} = N\left(\frac{5}{2} - \frac{\Lambda}{8L}\right), \qquad C_{Ap_\perp} = N\left(\frac{5}{2} - \frac{3\Lambda}{8L}\right).$$

As seen, in the volume limit C_{AL} turns into the heat capacity at a constant volume of the classical ideal gas $C_V = (3/2)N$, and the other five heat capacities turn into the heat capacity of the classical gas at a constant pressure $C_p = (5/2)N$. It should be also noted that the heat capacity $C_{p_\parallel p_\perp}$ does not contain the linear in the parameter Λ/L correction.

CONCLUSION

In the paper there have been derived the exact formulas for calculation of the thermodynamic functions of the ideal Fermi gas in the quantum well formed by two parallel walls. It is shown that all thermodynamic quantities, written in the dimensionless reduced form not containing the geometric dimensions, can be expressed through some standard functions of the dimensionless temperature and the dimensionless chemical potential and their derivatives. These functions themselves do not oscillate with varying the chemical potential or density, but the derivatives of these functions have oscillations (Fig. 5). Through the introduced standard functions there are calculated the thermodynamic potential, energy, density, entropy, equations of state, heat capacities and compressibilities of the Fermi gas at arbitrary temperatures in the considered conditions of the confined geometry. It is shown that owing to the anisotropy the Fermi gas in this case has two equations of state since the pressures perpendicular and parallel to planes are different, and also is characterized by a set of several heat capacities. At low temperatures the entropy and all heat capacities depend on temperature in the same linear way and undergo jumps at the beginning of the filling of new discrete energy levels. It is shown that the character of dependence of thermodynamic quantities on the distance between planes essentially depends on whether this dependence is considered at a fixed surface or at a fixed volume density. At a fixed surface density the thermodynamic quantities vary monotonically with the distance between planes, and at a fixed volume density they undergo oscillations. In the area of high temperatures the quantum corrections to thermodynamic quantities are obtained, which are proportional to the ratio of the thermal de Broglie wavelength to the distance between planes.

REFERENCES

1. Ando T., Fowler A.B., Stern F. Electronic properties of two-dimensional systems // Rev. Mod. Phys. – 1982. – Vol. 54. – P. 437-672.
2. Komnik Y.F. Physics of metal films. – Moscow: Atomizdat, 1979. – 264 p. (in Russian)
3. Dragunov V.P., Neizvestnyj I.G., Gridchin V.A. Fundamentals of nanoelectronics. – Moscow: Fizmatkniga, 2006. – 496 p. (in Russian)
4. Vagner I.D. Thermodynamics of two-dimensional electrons on Landau levels // HIT J. of Science and Engineering A. – 2006. – Vol. 3. – P. 102-152.
5. Freik D.M., Kharun L.T., Dobrovolska A.M. Quantum-size effects in condensed systems. Scientific and historical aspects // Phys. and Chem. of Solid State. – 2011. – Vol. 12. – P. 9-26.
6. Landau L.D., Lifshitz E.M. Statistical physics, Vol. 5. – Oxford: Butterworth-Heinemann, 1980. – 544 p.
7. Shaginyan V.R., Popov K.G. Strongly correlated Fermi-systems: theory versus experiment // Nanostuctures. Mathematical physics and modeling. – 2010. – Vol. 3. – P. 5-92.
8. Landau L.D. The theory of a Fermi liquid // Sov. Phys. JETP. – 1957. – Vol. 3. – P. 920-925.
9. Pines D., Nozières P. The theory of quantum liquids, Vol. I. – New York: Benjamin, 1966. – 149 p.
10. Migdal A.B. Theory of finite Fermi systems and applications to atomic nuclei. – Moscow: Nauka, 1983. – 432 p. (in Russian).
11. Tomonaga S. Remarks on Bloch's method of sound waves applied to many-fermion problems // Progr. Theor. Phys. – 1950. – Vol. 5. – P. 544-569.
12. Luttinger J.M. An exactly soluble model of a many-fermion fystem // J. Math. Phys. – 1963.– Vol. 4. – P. 1154-1162.
13. Fröhlich H. Die spezifische wärme der elektronen kleiner metallteilchen bei tiefen temperaturen // Physica. – 1937. – Vol. 4. – 406-412. (in German)
14. Lifshits I.M., Kosevich A.M. On the theory of magnetic susceptibility of thin metal layers at low temperatures // DAN SSSR. – 1953. – Vol. XCI (4). – P. 795-798.
15. Lifshits I.M., Kosevich A.M. On oscillations of thermodynamic quantities for degenerate Fermi gas at low temperatures // Izv. AN SSSR, Ser. Fiz. – 1955. – Vol. 19 (4). – P. 395-403.
16. Poluektov Yu.M. Conditions of existence of oscillatory phenomena in an electron gas // Russ. Phys. J. – 2008. – Vol. 51. – P. 568-577.
17. Abramowitz M., Stegun I. (Editors), Handbook of mathematical functions. – Moscow: Nauka, 1979. – 832 p.

APPENDIX

CALCULATION OF FUNCTIONS $\Psi_s(\tau,\eta)$

First, let us consider the case when $\eta < 1$. Using the formula at $t < 0$ that is correct in this case

$$\Phi_s(t) = \sum_{l=1}^{\infty} (-1)^{l+1} \frac{e^{lt}}{l^s}, \tag{A1}$$

we obtain

$$\Psi_s(\tau,\eta) = \frac{1}{2} \sum_{l=1}^{\infty} \frac{(-1)^{l+1} e^{\frac{l\eta}{\tau}}}{l^s} \theta_3\left(0, \frac{l}{\pi^2 \tau}\right) - \frac{1}{2} \Phi_s\left(\frac{\eta}{\tau}\right), \tag{A2}$$

where $\theta_3(v,x) \equiv 1 + 2\sum_{k=1}^{\infty} e^{-k^2\pi^2 x} \cos 2\pi v x$ is the theta-function, so that

$$\theta_3\left(0, \frac{l}{\pi^2 \tau}\right) \equiv 1 + 2\sum_{n=1}^{\infty} e^{-\frac{ln^2}{\tau}}. \tag{A3}$$

Note the useful relations:

$$\Phi_1(t) = \ln(1 + e^t), \quad \frac{d\Phi_1(t)}{dt} = \frac{e^t}{1 + e^t}, \quad \Phi_2(t) = \frac{t^2}{2}\left(1 + \frac{\pi^2}{3t^2}\right) - \Phi_2(-t). \tag{A4}$$

Somewhat more complex is the case $\eta > 1$, realized at low temperatures. We consider that for $t > 0$ and $s \geq 1$:

$$\Phi_s(t) = \frac{t^s}{\Gamma(s+1)}\left[1 + \chi_s(t)\right] + (-1)^{s-1} \Phi_s(-t), \tag{A5}$$

where

$$\chi_s(t) \equiv s(s-1)! \sum_{l=1}^{s-1} \frac{\left[(-1)^l - 1\right]\left(2^{-l} - 1\right)\zeta(l+1)}{(s-1-l)! t^{l+1}}, \tag{A6}$$

$\Gamma(s)$ is the gamma function, $\zeta(l)$ is the Riemann zeta function.

The functions (12) can be written in the form

$$\Psi_s(\tau,\eta) \equiv \sum_{n=1}^{\infty} \Phi_s\left[\tau^{-1}(\eta - n^2)\right] = \sum_{n=1}^{[x_0]} \Phi_s\left[\tau^{-1}(\eta - n^2)\right] + \sum_{n=[x_0]+1}^{\infty} \Phi_s\left[\tau^{-1}(\eta - n^2)\right], \tag{A7}$$

where the designation is used $x_0 \equiv \sqrt{\eta} = \sqrt{\mu/\varepsilon_L}$. In the first term the argument $\tau^{-1}(\eta - n^2) > 0$ and the formula (A5) can be used, and in the second term $\tau^{-1}(\eta - n^2) < 0$ and the expansion (A1) is valid, so that

$$\Psi_s(\tau,\eta) = \frac{1}{\Gamma(s+1)} \sum_{n=1}^{[x_0]} \tau^{-s}(\eta - n^2)^s \left\{1 + \chi_s\left[\tau^{-1}(\eta - n^2)\right]\right\} + \Psi_s^{\exp}(\tau,\eta), \tag{A8}$$

where the function

$$\Psi_s^{\exp}(\tau,\eta) \equiv (-1)^{s+1} \sum_{n=1}^{[x_0]} \Phi_s\left[\tau^{-1}(n^2 - \eta)\right] + \sum_{n=[x_0]+1}^{\infty} \Phi_s\left[\tau^{-1}(\eta - n^2)\right] \tag{A9}$$

contains the exponential terms, which are small for $\tau \ll 1$ but, however, they can be considerable near the specific points at $\eta = n^2$. In (A9) the main contribution is given by the terms with $n = [x_0]$ and $n = [x_0]+1$, and other terms give the exponentially small contribution of higher order. Therefore, after having extracted the main contribution, the formula (A9) can be written in the form

$$\Psi_s^{\exp}(\tau,\eta) = (-1)^{s+1} \Phi_s\left[\tau^{-1}\left([x_0]^2 - \eta\right)\right] + \Phi_s\left[\tau^{-1}\left(\eta - ([x_0]+1)^2\right)\right] + \bar{\Psi}_s^{\exp}(\tau,\eta), \tag{A10}$$

where

$$\bar{\Psi}_s^{\exp}(\tau,\eta) \equiv (-1)^{s+1} \sum_{n=1}^{[x_0]-1} \Phi_s\left[\tau^{-1}(n^2 - \eta)\right] + \sum_{n=[x_0]+2}^{\infty} \Phi_s\left[\tau^{-1}(\eta - n^2)\right]. \tag{A11}$$

In the considered problem we need the functions at $s = 1$ and $s = 2$, which for $\eta > 1$ can be represented in the form (41), (42).

CLASSIFICATION OF PARTICLES AT ARBITRARY QUANTITY OF GENERATIONS. I. HADRONS

Yu.V. Kulish

Ukrainian State University of Railway Transport
Sq. Feuerbach 7, Kharkiv region, 61000, Ukraine
Yu.V.Kulish@gmail.com
Received October 14, 2016

New classification of particles is proposed. This classification is based on $U(N_f, g) \times SU(3, c) \times SU(4, fs) \times O(3)$ -group, where $U(N_f, g)$ corresponds to the particle generations, $SU(3, c)$ - to the color, $SU(4, fs)$ - to the flavor and the spin (instead of known $SU(6, fs)$ -group), and $O(3)$ - to the orbital excitation with the L -momentum. The N_f -number equals the quantity of fermion generations. From the convergence of the integrals corresponding to the Green functions for generalized Dirac equations and the continuity of these functions it follows that the minimal quantity of the N_f -number equals six. The homogeneous solutions of derived equations are sums of fields, corresponding to particles with the same values of the spin, the electric charge, the parities, but with different masses. Such particles are grouped into the kinds (families, dynasties) with members which are the particle generations. For example, the electronic kind ($e_1 = e$, $e_2 = \mu$, $e_3 = \tau$, e_4, e_5, e_6,), the kind of up-quarks ($U_1 = u, U_2 = c, U_3 = t$, U_4, U_5, $U_6, \cdots$), and the kind of down-quarks ($D_1 = d, D_2 = s, D_3 = b$, D_4, D_5, $D_6, \cdots$) can exist. Massless neutrino can be one only. The photonic and the gluonic kinds must include massive particles in addition to usual the photon and the gluon. At $N_f = 6$ the nucleons and $\Delta(1232)$ belong to the $56 \times 1 \times 20 \times 1$ -representation. Lagrangians for the generalized Dirac equations of arbitrary order are derived.

KEY WORDS: generations of particles, symmetry properties, quark models, new particles, Lagrangians

КЛАСИФІКАЦІЯ ЧАСТИНОК ПРИ ДОВІЛЬНІЙ КІЛЬКОСТІ ПОКОЛІНЬ. І. АДРОНИ
Ю.В. Куліш
Український державний університет залізничного транспорту
м. Фейєрбаха 7, Харків, 61000, Україна

Запропоновано нову класифікацію частинок. Ця класифікація основана на групі $U(N_f, g) \times SU(3, c) \times SU(4, fs) \times O(3)$, де $U(N_f, g)$ відповідає поколінням частинок, $SU(3, c)$ - кольору, $SU(4, fs)$ - аромату та спіну (замість відомої групи $SU(6, fs)$), та $O(3)$ - орбітальному збудженню з моментом L. Число N_f дорівнює кількості поколінь ферміонів. Із збіжності інтегралів відповідних функціям Гріна для узагальненого рівняння Дірака та неперервності цих функцій випливає, що мінімальне значення N_f дорівнює 6. Однорідні розв'язки одержаних рівнянь представляють собою суми полів відповідних частинкам з однаковими значеннями спіну, електричного заряду, парності, але з різними масами. Такі частинки групуються у роди (сім'ї, династії) з номерами, які відповідають поколінням частинок. Наприклад, можуть існувати електронний рід ($e_1 = e$, $e_2 = \mu$, $e_3 = \tau$, e_4, e_5, e_6,), рід верхніх кварків ($U_1 = u, U_2 = c, U_3 = t$, U_4, U_5, $U_6, \cdots$), та рід нижніх кварків ($D_1 = d, D_2 = s, D_3 = b$, D_4, D_5, $D_6, \cdots$). Безмасове нейтрино може бути тільки одне. Фотонний та глюонний роди повинні містити масивні частинки в доповнення до звичайних фотона та глюона. При N_f =6 нуклони та $\Delta(1232)$ належать до подання $56 \times 1 \times 20 \times 1$. Одержано лагранжиани узагальнених рівнянь Дірака довільного порядку.

КЛЮЧОВІ СЛОВА: покоління частинок, симетрійні властивості, кваркові моделі, нові частинки, лагранжиани

КЛАССИФИКАЦИЯ ЧАСТИЦ ПРИ ПРОИЗВОЛЬНОМ КОЛИЧЕСТВЕ ПОКОЛЕНИЙ. І. АДРОНЫ
Ю.В. Кулиш
Украинский государственный университет железнодорожного транспорта
пл. Фейербаха 7, Харьков, 61000, Украина

Предложена новая классификация частиц. Эта классификация основана на группе $U(N_f, g) \times SU(3, c) \times SU(4, fs) \times O(3)$, где $U(N_f, g)$ соответствует поколениям частиц, $SU(3, c)$ - цвету, $SU(4, fs)$ - аромату и спину (вместо известной группы $SU(6, fs)$), и $O(3)$ - орбитальному возбуждению с моментом L. Число N_f равно количеству поколений фермионов. Из сходимости интегралов соответствующих функциям Грина для обобщенного уравнения Дирака и непрерывности этих функций следует, что минимальное значение N_f равно 6. Однородные решения полученных уравнений представляют собой суммы полей соответствующих частицам с одинаковыми значениями спина, электрического заряда, четности, но с разными массами. Такие частицы группируются в роды (семьи, династии) с номерами, соответствующими поколениям частиц. Например, могут существовать электронный род ($e_1 = e$, $e_2 = \mu$, $e_3 = \tau$, e_4, e_5, e_6,), род верхних кварков

23

Classification of Particles at Arbitrary Quantity of Generations. I. Hadrons   EEJP Vol.3 No.4 2016

($U_1 = u$, $U_2 = c$, $U_3 = t$, U_4, U_5, U_6, $\cdots$), и род нижних кварков ($D_1 = d$, $D_2 = s$, $D_3 = b$, D_4, D_5, D_6, $\cdots$). Безмассовое нейтрино может быть только одно. Фотонный и глюонный рода должны содержать массивные частицы в дополнение к обычным фотону и глюону. При $N_f = 6$ нуклоны и $\Delta(1232)$ принадлежат представлению $56 \times 1 \times 20 \times 1$.

Получены лагранжианы обобщенных уравнений Дирака любого порядка.

КЛЮЧЕВЫЕ СЛОВА: поколения частиц, свойства симметрий, кварковые модели, новые частицы, лагранжианы

Known particles are separated on hadrons and leptons. Properties of hadrons and leptons are different. Now it is known greater than 300 hadrons and twelve leptons together with antileptons. Mainly hadrons can be classified in quark models as $q\bar{q}-$ and q^3-systems for mesons and baryons, respectively. From usual point of view there are not any relations between the hadrons and the leptons. Investigations of the Adler – Bell – Jackiw axial anomaly in the electroweak theory showed that a contribution of one spin-$\frac{1}{2}$ particle (a quark or a lepton) leads to the linear divergence [1]. But taking into account of some sets of the leptons and the quark such as e, ν_e, u, d (first generation of the particles) or μ, ν_μ, c, s (second generation) or τ, ν_τ, t, b (third generation) allow to eliminate this divergence. Thus the convergence of the axial anomaly gives some relations between the quarks and the leptons.

In connection with this the next questions arise:

1. Why do the particle generations exist?

2. How many of the particle generations must exist?

3. What can hadrons and leptons have got common?

In relation with these questions the divergent integrals for the Green functions of the Klein-Gordon and Dirac equations are studied in Refs. [2, 3]. To avoid these divergences the generalizations of the Klein-Gordon and the Dirac equation is proposed in Refs. [2, 3]. In these papers next generalization of the Klein-Gordon equation has been proposed

$$\left(\Box + m_1^2\right)\left(\Box + m_2^2\right)........\left(\Box + m_{N_b}^2\right)\Phi(x) = \eta(x), \tag{1}$$

where $\Phi(x)$ is the field and $\eta(x)$ is the current (the field source). In momentum space the differential operator in (1) is the polynomial of the N_b-degree. We consider the case of the polynomial with real non-negative different zeros at $m_1 < m_2 < m_3 < .... < m_{N_b}$.

The general classical solution $\Phi_{cl}(x)$ of the linear equation (1) is the sum of the general solution of the corresponding homogeneous equation $\Phi(x)_{free}$ and partial solution $\Phi(x)_{nh}$ of non-homogeneous equation:

$$\Phi(x)_{free} = \int d^4 q \sum_{k=1}^{N_b} \delta\left(q^2 - m_k^2\right)\left[c_k e^{-iqx} + \tilde{c}_k e^{iqx}\right] \tag{2}$$

$$\Phi(x)_{nh} = \int \bar{G}(x - y)\eta(y)d^4 y, \tag{3}$$

where c_k and $\tilde{c}_k$ are the arbitrary constants. Thus $\Phi(x)_{free}$ is the sum on the terms corresponding to particles with the same charges, parity, spin but with different masses. Each term in (2) corresponding to number k is the solution of the homogeneous Klein – Gordon equation as $\left(\Box + m_k^2\right)\left(c_k e^{-iqx} + \tilde{c}_k e^{-iqx}\right) \delta\left(q^2 - m_k^2\right) = 0$. In Ref. [3] it is shown that the case of equal masses in Eq. (1) must be excluded. It was shown that the functions $\Phi(x)_{free}$ can include non- normalizable terms if at least two masses are equal. Thus the masses in the generalized Klein Gordon equation must be different. The N_b-number equals to the quantity of generations for spinless bosons and order of the equation (1) equals $2 N_b$.

The Green functions for the generalized Klein-Gordon equations (1) are given by

$$\bar{G}(x) = \frac{1}{(2\pi)^4} \int \frac{e^{-iqx} d^4 q}{\left(-q^2 + m_1^2\right)\left(-q^2 + m_2^2\right)....\left(-q^2 + m_{N_b}^2\right)} \tag{4}$$

It is clear that the integrals in (4) can converge at $N_b \geq 3$, i. e., when the order of the equation (1) is equal or greater than six.

For the spin-$\frac{1}{2}$ particles the next generalization of the non-homogeneous Dirac equation is proposed in Refs. [2,3]

$$\left(-i\hat{\partial}+m_1\right)\left(-i\hat{\partial}+m_2\right).....\left(-i\hat{\partial}+m_{N_f}\right)\Psi\left(x\right)=\chi\left(x\right). \tag{5}$$

The classical solution of the homogeneous equation (5) is given by analogy with (2)

$$\Psi^{\alpha}\left(x\right)_{free}=\sum_s\sum_{k=1}^{N_f}\int d^4p\,\delta\left(q^2-m_k^2\right)\left[C_k u^{\alpha}_{k,s}\left(q\right)e^{-iqx}+\tilde{C}_k v^{\alpha}_{k,s}\left(q\right)e^{iqx}\right], \tag{6}$$

where α is the bispinor index, s corresponds to spin projection, $u^{\alpha}_{k,s}\left(q\right)$ and $v^{\alpha}_{k,s}\left(q\right)$ are the bispinors, C_k and $\tilde{C}_k$ are arbitrary constants. The Green functions (which are 4×4-matrixes) for this equation may be written as

$$\bar{S}\left(x\right)=\frac{1}{\left(2\pi\right)^4}\int\frac{\left(\hat{q}+m_1\right)\left(\hat{q}+m_2\right)....\left(\left(\hat{q}+m_{N_f}\right)\right)}{\left(-q^2+m_1^2\right)\left(-q^2+m_2^2\right)...\left(-q^2+m_{N_f}^2\right)}d^4q \tag{7}$$

The N_f-number equals to the quantity of generations for the spin-$\frac{1}{2}$ fermions and order of the equation (5). The integrals in (7) can converge at $N_f \geq 5$. Note that for the advanced, retarded and causal Green functions we must write the corresponding imaginary infinitesimal term to each m_k^2 in (4), (7).

In Ref. [4] a continuity of the causal Green functions (4) and (7) has been investigated. It has been shown that these functions can be the continuous functions at $N_b \geq 3$, and $N_f \geq 6$, respectively. For these N_b and N_f the causal Green functions (4) and (7) have no any singularities in all the space-time. Thus, each particle must correspond to some generation. The minimal quantities of the generations for the spinless bosons and for the spin-$\frac{1}{2}$ fermions equal three and six, respectively.

Usually classification of hadrons in quark models is related to some unitary symmetries. These symmetries are valid for some particles with equal masses. In reality these symmetries are broken, as the particle masses are different. If the particles masses are nearly equal then results derived in unitary groups are approximately valid. Such situation is for the $SU(3,f)$-group related to the hadrons consisting of the $u,d,s-$ quarks and the $SU(6,fs)-$ group, which is the union of the $SU(3,f)$-flavor group and the $SU(2,s)-$ spin group [5-7]. Some predictions of these groups are in satisfactory agreement with experimental data. However, the agreement of predictions of the $SU(4,f)$- flavor group for the hadrons consisting of the $u,d,s,c-$ quarks with experimental data is worse (and similarly for the $SU(8,fs)-$ group). Such agreement is not surprise as $m_u \approx m_d \approx 0.36$ GeV, $m_s \approx 0.5$ GeV, $m_c \approx 1.5$ GeV .(in non-relativistic quark models). But the states of hadrons derived in these unitary groups can be used in quark models. In relation with possible existence of the hadrons consisting of the quarks from all the generations (from the first to the N_f-number generations) the question on the classifications of all the hadrons arises.

KINDS OF ELEMENTARY PARTICLES

Consider the distribution of the elementary particles in kinds (dynasties or families). Integrals corresponding to Green functions for the 1-spin diverge too. In Refs. [2, 3] the differential equations similar to Eqs. (1) and (5) for higher spin bosons and fermions have been proposed. Then for the photon and the gluon it can be put $m_1 = 0$. Therefore we can propose that two (or greater) massive members of the photon kind must exist. They must have zero electric charge and $J^P = 1^-$, $C = -1$. These particles must contribute to amplitudes of $e^+e^- \rightarrow e^+e^-$, $e^+e^- \rightarrow \mu^+\mu^-$, $e^+e^- \rightarrow$ hadrons at high energies and give the resonance behavior. We can expect that the coupling constants for the interactions of these members of the photonic kind with the leptons and the hadrons of the same electric charges must be equal. Similarly in the gluonic kind two (or greater) massive colored particles must exist. Besides two (or greater) massive members must exist in the Z^0 - and $W^\pm$ - kinds. In relations with the necessary existence of massive photons and

gluons such questions arise: 1) Is the gauge invariance for massive photons and gluons possible or not?; 2) Does the scaling in deep inelastic lepton – hadron scattering at higher energies exist or not?

It has been shown that for the spin-$\frac{1}{2}$ particles the number of the kind members (i.e. generations) must be equal 6 (or greater). We assume that electronic kind $(e_1 = e, e_2 = \mu, e_3 = \tau, e_4, e_5, e_6, \ldots)$, the neutrino kind $\left(\nu_1 = \nu_e, \nu_2 = \nu_\mu, \nu_3 = \nu_\tau, \nu_4, \nu_5, \nu_6, \ldots\right)$, three kinds of the colored up – quarks, and three kinds of the colored $down$ - quarks exist (for three colors). Note that in our approach only one neutrino may be masses (i. e., m_1 may equal zero and m_k must be positive at $k \geq 2$).

LAGRANGIANS FOR GENERALIZED DIRAC EQUATIONS

Operators of the generalized Dirac equations (5) are polynomials with respect to $-i\hat{\partial}$. They can be written as

$$\prod_{n=1}^{N}(-i\hat{\partial} + m_n) = \sum_{n=1}^{N} S(m_1, m_2, \cdots, m_N)_{N-n}(-i\partial)^n . \tag{8}$$

The S_k values are elementary symmetric functions [8]. They equal:

$$S(m_1, m_2, \cdots, m_N)_0 = 1,$$
$$S(m_1, m_2, \cdots, m_N)_1 = m_1 + m_2 + \cdots + m_N,$$
$$S(m_1, m_2, \cdots, m_N)_2 = m_1 m_2 + m_1 m_3 + \cdots + m_{N-1} m_N, \tag{9}$$
$$S(m_1, m_2, \cdots, m_N)_3 = m_1 m_2 m_3 + m_1 m_2 m_4 + \cdots + m_{N-2} m_{N-1} m_N ,$$
$$S(m_1, m_2, \cdots, m_N)_N = m_1 m_2 m_3 \cdots m_{N-1} m_N.$$

For these functions the formula can be written at $k > 1$

$$S(m_1, m_2, \cdots, m_N)_k = \sum_{i_k > i_{k-1} > \cdots > i_2 > i_1 \geq 1} m_{i_1} m_{i_2} m_{i_3} \cdots m_{i_{k-1}} m_{i_k} . \tag{10}$$

The elementary symmetric functions are related to the binomial coefficients C_N^k

$$S(m, m, \cdots, m_N)_k = m^k C_N^k = m^k \frac{N!}{k!(N-k)!} \tag{11}$$

As the operators of generalized Dirac equations (5) include the partial derivatives of the N order and they are polynomials, Lagrangins for these equations must have polynomial structure. Let us denote

$$\Psi(x)_{\mu_1 \mu_2 \cdots \mu_k} = \partial_{\mu_1} \partial_{\mu_2} \cdots \partial_{\mu_k} \Psi(x), \qquad \overline{\Psi}(x)_{\mu_1 \mu_2 \cdots \mu_k} = \partial_{\mu_1} \partial_{\mu_2} \cdots \partial_{\mu_k} \overline{\Psi}(x) \qquad . \tag{12}$$

In the operators of the equations (5) the terms with even and odd degrees of $\hat{\partial}$ must be separated (as $\hat{\partial}^2 = \square$). Therefore, in the Lagrangians the terms including the derivatives of even and odd orders must be separated also. The Lagrangian for arbitrary N may be written as

$$L(x) = L(x)_{free} - \overline{\Psi}(x)\chi(x) - \overline{\chi}(x)\Psi(x), L(x)_{free} = \alpha_0 L_0 + \sum_{n=1}^{N_e} \alpha_{2n} L_{2n} + \sum_{n=0}^{N_{od}} \alpha_{2n+1} L_{2n+1} , \tag{13}$$

where α_k are numbers related to the elementary symmetric functions, $\chi(x)$ is current. The numbers N_e and N_{od} equal $\frac{N}{2}$ and $\frac{N}{2}$ -1 for even N, respectively. Similarly, for odd N $N_e = N_{od} = (N-1)/2$. The terms of Lagrangians including the fields are given by

$$L_0 = \overline{\Psi}(x)\Psi(x), \qquad L_{2n} = \overline{\Psi}(x)_{\mu_1 \mu_2 \cdots \mu_{2n}} \Psi(x)_{\mu_1 \mu_2 \cdots \mu_{2n}} . \tag{14}$$

$$L_{2n+1} = \overline{\Psi}(x)_{\mu_1\mu_2\cdots\mu_{2n+1}} \gamma_{\mu_{2n+1}} \Psi(x)_{\mu_1\mu_2\cdots\mu_{2n}} - \overline{\Psi}(x)_{\mu_1\mu_2\cdots\mu_{2n}} \gamma_{\mu_{2n+1}} \Psi(x)_{\mu_1\mu_2\cdots\mu_{2n+1}} .$$

Using the least action principle (the Ostrogradskij-Hamilton principle) the Ostrogradskij-Euler equations [9, 10], which are generalizations of the Euler-Lagrange equations, can be derived. The equation (5) can be obtained by means of the variation of the Lagrangian *L(x)* with respect to $\overline{\Psi}$. Consider the operators of these equations

$$O_{EL}(\overline{\Psi}) = \frac{\partial}{\partial\overline{\Psi}} + \sum_{n=1}^{N} (-1)^n \partial_{\mu_1}\partial_{\mu_2}\cdots\partial_{\mu_n} \frac{\partial}{\partial\overline{\Psi}_{\mu_1\mu_2\cdots\mu_n}} . \tag{15}$$

Then, the Ostrogradskij-Euler equations, which must coincide with the equations (5), may be written as

$$O_{EL}(\overline{\Psi})L(x) = 0. \tag{16}$$

For the terms in the Lagrangian (13) next expressions may be derived

$$O_{EL}(\overline{\Psi})L_0 = \Psi , \quad O_{EL}(\overline{\Psi})L_{2n} = \Box^n \Psi , \qquad O_{EL}(\overline{\Psi})L_{2n+1} = -2\hat{\partial}\Box^n \Psi . \tag{17}$$

Using last results, by means of a comparison of the equations (8) and (16), relations between the α_k -coefficients in the Lagrangian (13) and the elementary symmetric functions S_k are obtained. It allows one to derive the Lagrangians in terms of the S_k -functions (9) and the L_k -values (14) at arbitrary N :

1. For even *N*

$$L(x) = -\overline{\Psi}(x)\chi(x) - \overline{\chi}(x)\Psi(x) + S_N L_0 + \sum_{n=1}^{\frac{N}{2}} (-1)^n S_{N-2n}L_{2n} + \frac{i}{2}\sum_{n=1}^{\frac{N}{2}} (-1)^{n+1} S_{N-2n+1}L_{2n-1} \tag{18}$$

In particular, at N = 6 the Lagrangian equals:

$$L(x) = -\overline{\Psi}(x)\chi(x) - \overline{\chi}(x)\Psi(x) + S_6 L_0 - S_4 L_2 + S_2 L_4 - S_0 L_6 + \frac{i}{2}(S_5 L_1 - S_3 L_3 + S_1 L_5)$$

2. For odd *N*

$$L(x) = -\overline{\Psi}(x)\chi(x) - \overline{\chi}(x)\Psi(x) + S_N L_0 + \sum_{n=1}^{\frac{N-1}{2}} (-1)^n S_{N-2n}L_{2n} + \frac{i}{2}\sum_{n=0}^{\frac{N-1}{2}} (-1)^n S_{N-2n-1}L_{2n+1} \tag{19}$$

In particular, at N =7 the Lagrangian equals

$$L(x) = -\overline{\Psi}(x)\chi(x) - \overline{\chi}(x)\Psi(x) + S_7 L_0 - S_5 L_2 + S_3 L_4 - S_1 L_6 + \frac{i}{2}(S_6 L_1 - S_4 L_3 + S_2 L_5 - S_0 L_7)$$

NEW CLASSIFICATION OF HADRONS

Different quarks have got the quantum numbers related to a spin (s), a color (c), and flavors (f). For description of hadrons consisting of u -, d -, s -quarks usually the $SU(3,c) \otimes SU(6, fs) \otimes O(3)$ group is exploited [7]. The $O(3)$ -group is used for a description of orbital excitations of the quarks in some hadrons.

Now consider two quark kinds: U -quarks and D -quarks for each color. The members U_k and D_k of the U - quark and the D -quark kinds can be written as: $U_1 = u, U_2 = c, U_3 = t, \quad U_4, \quad U_5, \quad U_6 \cdots$ and $D_1 = d, D_2 = s, D_3 = b, \quad D_4, \quad D_5, \quad D_6, \cdots$, respectively. Such the k number (which is related to generations) can be considered as new quantum number. Therefore, for description of hadrons we propose the $U(N_f, g) \times SU(3,c) \times SU(4, fs) \times O(3)$ -group. In this paper the hadrons consisting of quarks in $1s$ − state are considered. Such hadrons are described by singlets of the $O(3)$ − group. The U_k - and D_k - quarks from one generation belong the $N_f \times 3 \times 4 \times 1$ -representation of the $U(N_f, g) \times SU(3,c) \times SU(4, fs) \times O(3)$ -group.

Usually the symmetry groups such as $SU(3, f), SU(6, fs)$ are considered for particles with equal or near

27

Classification of Particles at Arbitrary Quantity of Generations. I. Hadrons   EEJP Vol.3 No.4 2016

masses, But the differences between the masses for particles of different generations are very large. Indeed, the $U-$ quarks have got masses: $m_u = m(U_1) \approx 0.36$ GeV, (in non-relativistic quark models), $m_c = m(U_2) \approx 1.5$ GeV, $m_t = m(U_3) \approx 177$ GeV. Similarly, the $D-$ quarks have got the masses: $m_d = m(D_1) \approx 0.36$ GeV, $m_s = m(D_2) \approx 0.5$ GeV, $m_b = m(D_3) \approx 4.5$ GeV [11]. Therefore, the use of the $SU(N_f, g)$-group can seem doubtful.

It may be assumed that the laws of a conservation for such quantities as the strangeness , the charm, the beauty, and the truth (by analogy with the law of the conservation of the particle electric charges) do not exist. Indeed, the charm and the truth correspond to the U_k-quarks at $k = 2,3$. Similarly, the strangeness and the beauty correspond to the D_k-quarks for $k = 2,3$. As usual, propose that non-zero anticommutators for creation operators and annihilation operators are given by

$$\{a(\vec{p}_1)_{k_1,\sigma_1}, a(\vec{p}_2)^+_{k_2,\sigma_2}\} = 2 p_{10} \delta_{k_1 k_2} \delta_{\sigma_1 \sigma_2} \delta(\vec{p}_1 - \vec{p}_2),$$

$$\{b(\vec{p}_1)_{k_1,\sigma_1}, b(\vec{p}_2)^+_{k_2,\sigma_2}\} = 2 p_{10} \delta_{k_1 k_2} \delta_{\sigma_1 \sigma_2} \delta(\vec{p}_1 - \vec{p}_2), \qquad (20)$$

where $a(\vec{p})_{k,\sigma}$ ($a(\vec{p})^+_{k,\sigma}$) are the annihilation (creation) operators of the quark for the k-generation with σ quantum numbers (spin projection, flower (U or D), color, and other values), $p = (p_0, \vec{p})$ is the 4-momentum of the quark ($p_{0k} = \sqrt{\vec{p}_k^2 + m_k^2}$). By analogy, $b(\vec{p})_{k,\sigma}$ ($b(\vec{p})^+_{k,\sigma}$) are the annihilation (creation) operators of the antiquark. The anticommutators (20) agree with the orthonormalization condition

$$\langle \vec{p}_1, k_1, \sigma_1 | \vec{p}_2, k_2, \sigma_2 \rangle = 2 p_{10} \delta_{k_1 k_2} \delta_{\sigma_1 \sigma_2} \delta(\vec{p}_1 - \vec{p}_2) \qquad (21)$$

In formulae (20, 21) the conditions $p_{k_1} = p_{k_2}$ are equivalent to $\delta_{k_1 k_2}$. An inclusion of the $\delta_{k_1 k_2}$-factor in the formulae (20, 21) permits to see explicitly the zero results at $k_1 \neq k_2$. Thus, the conservation of such quantities as the strangness , the charm, the beauty, and the truth is the consequence of the anticommutators (20) and the conditions (21).

The classical free field for the quarks is presented in (6). It can be seen that for quantized fields scalar products (where $\overline{\Psi(x)_\alpha} = (\Psi(x)^+ \gamma_0)_\alpha$) are not changed under unitary transformations

$$\Psi(x)^\alpha \to \Psi(x)^{\alpha \prime} = \exp(i\theta_i \Gamma_i) \Psi(x)^\alpha, \qquad (22)$$

$$\overline{\Psi(x)_\alpha} \to \overline{\Psi(x)_\alpha}' = \overline{\Psi(x)_\alpha} \exp(-i\theta_i \Gamma_i),$$

where Γ_i are the generators of the $U(N_f, g)$-group, θ_i are the parameters of the transformation. In particular, the vacuum means of the Lagrangians (18, 19) do not change under transformations (22). Indeed, the S_k-functions (9) are constants and the vacuum means of the L_k-values (14) do not change under the transformations (22). In particular, the transformation (22) leading to permutation of generations in one kind, can be considered. The generation numbers are related to particle masses. The equations (5), the solution (6), and the S_k-functions (9) do not change at the permutations of the masses. Therefore, the scalar products $\overline{\Psi(x)_\alpha} \Psi(x)^\alpha$ are invariant under the generation permutation. Thus the use of the $U(N_f, g)$-group can be valid for a classification of particle generations.

CLASSIFICATION OF MESONS

A representation of the $SU(4, fs)$-group for $q\overline{q} -$ system is reducible: $4 \times 4 = 15 + 1$. A dimension of a representation of the $U(N_f, g)$-group for the $q\overline{q} -$ system is equal to N_f^2. Therefore, the colorless states of the $q\overline{q} -$ system belong to next representations of the $U(N_f, g) \times SU(3,c) \times SU(4, fs) \times O(3)$-group: $N_f^2 \times 1 \times 15 \times 1$ and $N_f^2 \times 1 \times 1 \times 1$. The $SU(4, fs)$-group is a subgroup of the $SU(6, fs)$-group. Therefore, known expansion of the representations $SU(6, fs)$-group with respect to the representations of the

$SU(3, f) \times SU(2, s)$ -group can be used to find similar expansion for the representations $SU(4, fs)$ -group with respect to the representations of the $SU(2, f) \times SU(2, s)$ -group in the case of the U_1 – and D_1 -quarks. For the $15 - plet$ of the $SU(4, fs)$ -group such expansion can be written as $15 = 3 \times 1 + 3 \times 3 + 1 \times 3$. The first term in this expansion corresponds to pseudoscalar mesons (π^+, π^0, π^-), the second - to charged and neutral vector mesons (ρ^+, ρ^0, ρ^-), and third – to neutral vector mesons (ω^0). This expansion can be generalized on the case of different generations.

1. *Pseudoscalar mesons.* At first consider the charged pseudoscalar mesons. The mesons with positive and negative charges will be denoted as

$$P^+{}_{k_1 k_2} = [U_{k_1} \bar{D}_{k_2}], \qquad P^-{}_{k_1 k_2} = [D_{k_1} \bar{U}_{k_2}], \qquad \bar{P}^+{}_{k_1 k_2} = P^-{}_{k_2 k_1}. \tag{23}$$

The spin states of the pseudoscalar mesons are chosen according to Ref [7], for example

$$\left| P^+{}_{k_1 k_2} \right\rangle = \frac{1}{\sqrt{2}} \left| U \uparrow_{k_1} \bar{D} \downarrow_{k_2} - U \downarrow_{k_1} \bar{D} \uparrow_{k_2} \right\rangle = \left| U_{k_1} \bar{D}_{k_2} \uparrow\downarrow \right\rangle_- \tag{24}$$

Consider some well known pseudoscalar mesons: $P^+{}_{11} = \pi^+(140)$, $P^+{}_{22} = D^+_s(1969)$, $P^+{}_{12} = K^+(494)$, $P^+{}_{21} = D^+(1869)$, $P^+{}_{13} = B^+(5278)$.

In the $SU(4, fs)$ -group the neutral mesons can be obtained from the charged mesons by means of the isospin symmetry operators. For $k \geq 2$ a use of the isospin symmetry is not adequate. But the quarks can participate in weak interactions. It is possible to choice the phases for transitions with $W^\pm -$ bosons such as for the isospin operators, i.e., $U \to W^+ D$, $\bar{D} \to -W^+ \bar{U}$. Using these transitions it is possible to obtain the states for the neutral mesons from states for the mesons with the positive charge. Such, although the isotopic invariance is not valid for $k \geq 2$, relations between the matrix elements of transitions at $k = 1$ can be derived the same as in the isotopic symmetry.

For a $U\bar{D} -$ system the relation $\left| U\bar{D} \right\rangle \to W^+ \frac{1}{\sqrt{2}} \left| -U\bar{U} + D\bar{D} \right\rangle$ can be derived. Let us denote

$$P^0{}_{k_1 k_2, U} = [U_{k_1} \bar{U}_{k_2}], \qquad P^0{}_{k_1 k_2, D} = [D_{k_1} \bar{D}_{k_2}], \qquad P^0{}_{k_1 k_2, UD} = \frac{1}{\sqrt{2}} (P^0{}_{k_1 k_2, D} - P^0{}_{k_1 k_2, U}). \tag{25}$$

Then for some neutral pseudoscalar mesons it can be written: $P^0{}_{11,UD} = \pi^0(140)$, $P^0{}_{12,D} = K^0(498)$, $P^0{}_{12,U} = \bar{D}^0(1864)$, $P^0{}_{21,D} = \bar{K}^0(498)$, $P^0{}_{21,U} = D^0(1864)$, $P^0{}_{13,D} = B^0(5279)$, $P^0{}_{31,D} = \bar{B}^0(5279)$. Possibly for neutral mesons, corresponding to different k_1 and k_2 such expressions $(P^0{}_{k_1 k_2} - P^0{}_{k_2 k_1}) / \sqrt{2}$ may be considered. These expressions are similar to the expression for $\pi^0 -$ meson ($d\bar{d} - u\bar{u}) / \sqrt{2}$). For $k_1 = 1, k_2 = 2$ it corresponds to $K^0{}_2 = (K^0(493) - \bar{K}^0(493)) / \sqrt{2}$.

2. *Vector mesons.* In the $SU(4, fs)$ -group the vector mesons correspond two representations of the $SU(2, f)$ -group. One of them includes charged and neutral mesons but second – neutral mesons only. For the representation including charged meson (the 3×3 representations of the $SU(2, f) \times SU(2, s)$ -group) we use the denotations similar to (11) and (12) for charged and neutral mesons, respectively (with substitutions V instead of P). Some charged vector mesons are: $V^+{}_{11} = \rho^+(770)$, $V^+{}_{22} = D_s^{*+}(2112)$, $V^+{}_{12} = K^{*+}(892)$. The neutral vector mesons from the 3×3 representations of the $SU(2, f) \times SU(2, s)$ -group are: $V^0{}_{11} = \frac{1}{\sqrt{2}}(-u\bar{u} + d\bar{d}) = \rho^0(770)$, $V^0{}_{12,D} = K^{*0}(892)$, $V^0{}_{21,D} = \bar{K}^{*0}(892)$, $V^0{}_{12,U} = D^{*0}(2010)$, $V^0{}_{21,U} = \bar{D}^{*0}(2010)$.

States of neutral vector mesons from the 1×3 representations of the $SU(2, f) \times SU(2, s)$ -group denote as

$$\omega_{k_1 k_2, U} = [U_{k_1} \bar{U}_{k_2}] \qquad \omega_{k_1 k_2, D} = [D_{k_1} \bar{D}_{k_2}] \tag{26}$$

The states of some known neutral mesons can be written as: $\frac{1}{\sqrt{2}}\left| \; \omega_{11,U} + \omega_{11,D} \; \right\rangle = \left| \omega^0 (783) \; \right\rangle$,

$\left| \omega_{22,D} \; \right\rangle = \left| \varphi(1020) \; \right\rangle$, $\left| \omega_{22,U} \; \right\rangle = \left| J/\psi(3097) \; \right\rangle$, $\left| \omega_{33,D} \; \right\rangle = \left| \Upsilon(9460) \; \right\rangle$.

3. *Singlet states of the $SU(4, fs)$ -group.* Denote the states corresponding to the $N_f^{\,2} \times 1 \times 1 \times 1$ -representations of the $U(N_f, g) \times SU(3, c) \times SU(4, fs) \times O(3)$ -group as

$$\left| \; \eta_{k_1 k_2} \; \right\rangle = \frac{1}{2} \left| U\uparrow_{k_1} \bar{U}\downarrow_{k_2} + U\downarrow_{k_1} \bar{U}\uparrow_{k_2} + D\uparrow_{k_1} \bar{D}\downarrow_{k_2} + D\downarrow_{k_1} \bar{D}\uparrow_{k_2} \; \right\rangle. \qquad (27)$$

At $k_1 = k_2 = k$ the η_{kk} pseudoscalar mesons are totally neutral. For $k_1 \neq k_2$ the $\eta_{k_1 k_2}$ -mesons have got the zero electric charge, but they are not totally neutral. For example,

$$\left| \; \eta_{12} \; \right\rangle = \frac{1}{2} \left| u\uparrow \bar{c}\downarrow + u\downarrow \bar{c}\uparrow + d\uparrow \bar{s}\downarrow + d\downarrow \bar{s}\uparrow \; \right\rangle \qquad (28)$$

and antiparticle of the η_{12} -meson is the η_{21} -meson.

4. *$U(N_f, g)$ -group or $SU(N_f, g)$ -group?* The $q\bar{q}$ − systems with quarks of N_f generations are described in the $SU(N_f, g)$ -group by means of representations with the ($N_f^{\,2} - 1$) and 1 dimensions. The representation of the 1 dimension corresponds to totally neutral pseudoscalar meson. The representation of the $N_f^{\,2} - 1$ dimension is described by traceless tensor of second rank. Therefore, these traceless tensors give the representations of the $SU(N_f, g) \times SU(3, c) \times SU(4, fs) \times O(3)$ -group which distinguish from the representations of the $U(N_f, g) \times SU(3, c) \times SU(4, fs) \times O(3)$ -group for neutral and vector mesons. In particular, for positively charged pseudoscalar mesons in the $SU(N_f, g) \times SU(3, c) \times SU(4, fs) \times O(3)$ group next states

$$\frac{1}{\sqrt{2}}(P^+_{11} - P^+_{22}), \qquad \frac{1}{\sqrt{6}}(P^+_{11} + P^+_{22} - 2P^+_{33}), \qquad (29)$$

$$\frac{1}{\sqrt{N_f(N_f - 1)}}[P^+_{11} + P^+_{22} + \cdots + P^+_{N_f - 1, N_f - 1} - (N_f - 1)P^+_{N_f N_f}]$$

must exist instead the P^+_{11}, P^+_{22}, $P^+_{33}\cdots$ -states. Probably the states (29) do not exist. Therefore, the $U(N_f, g) \times SU(3, c) \times SU(4, fs) \times O(3)$ -group ought to be used for the classification of the $q\bar{q}$ − mesons. This group can be exploited for the baryons also.

CLASSIFICATION OF BARYONS

Consider q^3 − baryonic systems with quarks in $1s$ − state. It is known (e.g., Refs. [7], [12], [13]) that the representations for q^3 − system in the spaces of flavors and spin are reducible and can be expanded as sums of the symmetric (S), the antisymmetric (A) representations, and two representations of the mixed symmetry (M_S, M_A). Such expansions have to exist in the spaces of the color and the generations also. From the Pauli principle the total antisymmetry of the tensors for q^3 − systems follows. The $U(N_f, g) \times SU(3, c) \times SU(4, fs) \times O(3)$ -group gives representations with determined properties of symmetry (related to the space of generations) in addition to representations of .the $SU(3, c) \times SU(4, fs) \times O(3)$ -group. It allows one to assume an existence of some baryons which are non-antisymmetric representations of the $SU(3, c) \times SU(4, fs) \times O(3)$ -group.

Note that a type of the symmetry for the representation of the q^3 − system in some space can be determined by means of a quantity of equal quantum numbers for the quarks. If in a representation for the q^3 − system the state with three equal numbers of the quark exists, then this representation is symmetric. If maximal number of equal quantum

number of the quarks is equal to two in a representation of a q^3 − system, then this representation has got mixed symmetry. If in a representation for the q^3 − system all the states have got different quantum numbers of the quarks, then this representation is antisymmetric. For quantum numbers of a quark which correspond to variables in a space of the n -dimension, the representations for the q^3 − system of the symmetric, the antisymmetric, and mixed symmetry types have got the dimensions: $N_S(n) = n(n+1)(n+2)/6$, $N_A(n) = n(n-1)(n-2)/6$, and $N_{M_A}(n) = N_{M_S}(n) = n(n^2-1)/3$, respectively.

As Δ^{++}, Δ^-, and Ω^- consist of the same quarks, nucleons and other baryons (which belong to 56-plet of the $SU(6, fs)$ and similar baryons including the quark $U_2 = c$ instead the $D_2 = s$) are described by symmetric 20-plet of the $SU(4, fs)$ and symmetric representation of the $U(N_f, g)$ at k =1 and 2. For k =3 we obtain the *ttt* -baryon (similar to Δ^{++}) and the *bbb* -baryon (similar to Δ^- and Ω^-). Thus, these baryons belong to the $N_S(N_f) \times 1 \times 20 \times 1$ -representation of the $U(N_f, g) \times SU(3, c) \times SU(4, fs) \times O(3)$ -group (for $N_f = 6$ the number $N_S(N_f)$ equals 56). These baryons have got the spin-parity $J^P = \frac{1}{2}^+, \frac{3}{2}^+$. Note that known results derived in the $SU(6, fs)$ -symmetry (such as $\frac{\mu_p}{\mu_n} = -\frac{3}{2}$ and $\mu_z(\gamma p \to \Delta^+) = \frac{2\sqrt{2}}{3} \mu_p$) must remain valid in the $SU(4, fs)$ -symmetry.

The baryon resonances with negative spatial parity corresponding to the quarks with an orbital moment $L = 1$ and mixed symmetry of a q^3 − system (such as $D_{13}(1520), S_{11}(1535)$) belong to the $N_S(N_f) \times 1 \times 20 \times 3$ -representation of the $U(N_f, g) \times SU(3, c) \times SU(4, fs) \times O(3)$ -group. These baryon resonances have got the spin-parity $J^P = \frac{1}{2}^-, \frac{3}{2}^-, \frac{5}{2}^-$.

So we can see that the baryons with low masses belong to the symmetric representation of the $SU(4, fs)$ -group for a q^3 − system (with $J^P = \frac{1}{2}^+, \frac{3}{2}^+$) and the representation of mixed symmetry (with $J^P = \frac{1}{2}^-, \frac{3}{2}^-, \frac{5}{2}^-$). A question arises: what objects correspond to the antisymmetric representation of the $SU(4, fs)$ -group for a q^3 − system. The antisymmetric representation of the $SU(4, fs)$ -group corresponds to the 4-dimension (for two particles of the $\frac{1}{2}$ -spin). The representations of the $SU(4, fs)$ -group can be classified with respect to the representations of the $SU(2, f) \times SU(2, s)$ − group. For the representations of the $SU(2, s)$ − group the designation J^p will be used. In particular, the expansion of the antisymmetric representation of the $SU(4, fs)$ -group with respect to the representations of the $SU(2, f) \times SU(2, s)$ − group for the q^3 − system with quarks in the $1s$ − states may be written as $4 = 2 \times \frac{1}{2}^+$.

ON COLORED HADRON-LIKE SISTEMS

It is well known that hadrons are colorless. But at consideration of any q^3 − system (or $q\bar{q}$ -system) with definite J^p colored states appear together with uncolored states. In a relation with an absence of the color in observed hadrons the questions arises: 1) Why are observed hadrons uncolored? What principles ensure an absence of the color in hadrons? Consider the mass formula corresponding to the approximation of the one-gluon exchange:

$$M = M_0 - \alpha_s \sum_{i>j} \mu_{mag}(m_i, m_j)(\vec{\sigma}_i \lambda_i^a)(\vec{\sigma}_j \lambda_j^a) + \alpha_s \sum_{i>j} \mu_{el}(m_i, m_j)\lambda_i^a \lambda_j^a \qquad (30)$$

The second term corresponds to the color-magnetic interaction and third term- to the color-electric interaction. The

31

Classification of Particles at Arbitrary Quantity of Generations. I. Hadrons   EEJP Vol.3 No.4 2016

M_0 − value includes the sum of quark masses and it can include some additional terms (equal for all baryons of the representation). The $\sum_{i>j} \lambda_i^a \lambda_j^a$ -value can be calculated using the Kasimir operator C_2 for the $SU(3,c)$ -group (e.g., Refs. [7], [14]). In the color space a q^3 -system can be a singlet or an octet or a decuplet. The Kasimir operator for the singlet, the octet, and the decuplet equals 0, 3, and 6, respectively. For q^3 -baryons it can be derived

$$\sum_{i>j} \lambda_i^a \lambda_j^a = 2C_2 - \frac{3}{2}\vec{\lambda}^2 = 2C_2 - 8. \tag{31}$$

From (30) and the values of the Kasimir operator it follows that indeed the colored baryon-like states have bigger masses in a comparison with uncolored baryon. Similar result can be derived for $q\bar{q}$ -mesons. Colored baryon-like states with small masses may belong to the representation of the $SU(N_f,g) \otimes SU(3,c) \otimes SU(4,sf) \otimes O(3)$ -group corresponding to the total symmetric representation of the $SU(N_f,g)$ -group (i.e. they can consist of the quarks for k =1), the octet of the $SU(3,c)$ -group, the mixed representation of the $SU(4,sf)$ -group at L =0. Possibly colored $q^3 -$ baryon-like states are not stable, as the color octets can decay into a gluon and a colorless baryon. Similarly the hadrons of color decuplet can decay into two gluons and colorless hadrons. Thus, observed hadrons have got lower masses than masses of corresponding colored hadron-like states. The color is conserved. A conservation of the color is a consequence of a gauge invariance. In collisions of hadrons colored states and uncolored states are produced. In a final state the color must be absent. Colored states must decay rapidly into uncolored hadrons. Therefore, in reality colored hadron-like states are not observed.

ON MASSIVE PARTNERS OF PHOTONS AND GLUONS

From convergence of integrals for generalized wave equation (which is a partial case of generalized Klein-Gordon equation (1) at $m_1 = 0$) it follows that the photon and the gluons have to be massless members of the photonic and the gluonic kinds, respectively. Other members of these kinds must be massive. It is clear that a convergence of integrals for the Green functions of generalized Klein-Gordon equations do not depends on magnitudes of particle masses in the kinds.

At first consider the photonic kind. Denote the members of the photonic kind as γ_k ($\gamma_1 = \gamma$ is the photon, γ_k for $k > 1$ are massive partners of the photon). As the processes of the photon interactions with charged leptons are described well in frameworks of the quantum electrodynamics, it of interest to investigate the interactions of massive partners of the photon with quarks. The massive partners of the photon have to be coupled with quarks and antiquarks in the state of electrical neutral uncolored vector mesons with negative spatial and charge parities. Now a lot of such mesons are known. Next questions arise in relation with massive partners of the photon: 1) Are the massive partners known or unknown particles? 2) What properties must have the massive partners of the photon, which allow to distinct them from other particles? Consider requirements for the massive partners of the photon.

1. The members of the photonic kind can be emitted and absorbed by charged leptons, similarly to the photon. The amplitudes for interactions of massive partners of photon with quarks and leptons are determined by the electric charge of a quark or a lepton. Therefore, the coupling constants of some γ_k with all the U-quarks are the same, and similarly for D-quarks. The ratio of the coupling constants for the interactions of γ_k with the U-quarks and the D-quarks equals − 2.

2. Some γ_k can have got enough big masses and can decay into mesons. The massive partners of the photon can be produced in the e^+e^- − interaction and can be observed as resonances. Each virtual massive partners of the photon can interact with all the U-quarks and the D-quarks. But the massive partners of the photon decay into such final states that their total energies do not exceed the energies of these γ_k. Therefore, the mesons including heavy quarks cannot be observed in decay products of some γ_k with low masses.

The massive partners of the photon decay into mesons through a production of quark-antiquark pair. As quark have got some color an additional quark-antiquark pair must appear in a final state. These additional quark-antiquark pairs make complicated an analysis of decays of the massive partners of the photon. Therefore, it is of importance the consideration of relations of the massive partners of the photon with leptons.

It is known that the $\rho^0(770)-$, the $\omega^0(783)-$, the $\varphi^0(1020)-$, the $J/\Psi(3097)-$, the $\Upsilon(9460)-$ mesons, and other similar vector mesons consisting of a quark and corresponding antiquark are excited in

the $e^+e^- \to hadrons$ and the $e^+e^- \to e^+e^-$. Therefore it may be assumed that these vector mesons are related to the massive partners of the photon. Then the quantity of the massive partners of the photon equals $2N_f$ (N_f partners related to the uncolored $U_k\bar{U}_k$-pairs and N_f partners -to $D_k\bar{D}_k$-pairs, k=1, 2, ... N_f). This assumption on the massive partners of the photon is related to the model of vector dominance. Indeed it can be shown that some formulae for reaction amplitudes coincide in these two approaches. Therefore, we can hope that this assumption on the massive partners of the photon will not lead to new contradictions with experimental data. Note that at this assumption the masses of the massive partners of the photon can be calculated in quark models for uncolored systems.

Now consider the massive partners of the gluons. Similarly to the massive partners of the photon it can be assumed that the massive partners of the gluons are electrically neutral vector states of $q\bar{q}-$ systems with negative spatial parity, which are the color octet. The masses of the massive partners of the gluons can be calculated in the same quark models similarly to the massive partners of the photon. Indeed, the massive partners of the photon can be presented as uncolored $q\bar{q}-$ systems and the massive partners of the gluons as colored $q\bar{q}-$ systems. Then it can be expected that the masses of the massive partners of the gluons will exceed the masses of the massive partners of the photon for each number of generation. Note that the mass formula (30) must be modified for $q\bar{q}-$ systems. The $\sum_{i.>.j} \vec{\lambda}_i \vec{\lambda}_j$ -value in

(30) must be changed by the $\vec{\lambda}_1 \vec{\lambda}_2$-value, which is equal to *-16/3* for the massive partners of the photon (color singlet) and *2/3* for the massive partners of the gluons (color octet).

CONCLUSION

In present paper it is proposed to classify all the quarks by means two numbers: the electric charge and the generation number. The quarks with the $\frac{2}{3}Q_p$ -charge belong to the $U-$ quarks and the quarks with the $-\frac{1}{3}Q_p$ -charge – to the $D-$ quarks. Thus, it is proposed that the quarks belong to two flavors: *up* and *down*. The flavors of all the quarks are described by the $SU(2,f)$ -group. Then the states of all the quarks in the spin space and in the flavor space are described by the $SU(4, fs)$ -group. The conservations of the strangeness, the charm, the beauty, the truth, and other similar possible numbers in the strong and the electromagnetic interactions are the consequences of conservations of the electric charge and the number of generations.

In Ref. [4] it is shown that minimal quantity of the quark generations equals six (i.e., $N_f \geq 6$). Note that now it is known a half of necessary quantity of quarks. Therefore, it may be proposed that the quarks and hadrons can be classified as representations of the $U(N_f,g) \otimes SU(3,c) \otimes SU(4,sf) \otimes O(3)$-group. The representations of the $U(N_f,g)$ -group for q^3 -systems have got different symmetry properties. According to Pauli principle the representations of the $U(N_f,g) \otimes SU(3,c) \otimes SU(4,sf) \otimes O(3)$ -group for q^3 -systems must be antisymmetric as well as the representations of known $SU(3,c) \otimes SU(6,sf) \otimes O(3)$ -group. Taking into account of the symmetry properties for the representations of the $U(N_f,g)$ -group in the $U(N_f,g) \otimes SU(3,c) \otimes SU(4,sf) \otimes O(3)$- group for q^3 -systems allow derive the states, which are impossible in the $SU(3,c) \otimes SU(6,sf) \otimes O(3)$ -group for u,d,s -quarks (or in the $SU(3,c) \otimes SU(8,sf) \otimes O(3)$ -group for u,d,s,c -quarks).

The Lagrangians (18) give the generalized Dirac equations (5) as consequence of the least action principle. These Lagrangians depend on the particle masses by means of the elementary symmetric functions (9, 10). Therefore, the Lagrangians (18, 19) are invariant under the generation permutations.

REFERENCES
1. Treiman S.B., Jackiw R., Gross D.J. Lectures on current algebra and its applications. - Princeton: Princeton Univ. Pres., 1972; Moscow: Atomizdat, 1977. - P. 93. (in Russion)
2. Kulish Yu., Rybacuk E.V. Necessary generalization of Klein-Gordon and Dirac equations and existence of particle generations // Problems of Atomic Science and Technology. – 2012. – No.1 (77). - P. 16–20.
3. Kulish Yu. V., Rybachuk E.V. Divergences of integrals for Green functions and necessary existence of particle generations // Journal of Kharkiv National Univ. - 2011. – No.955. - Iss.2(50). - P. 4-14.
4. Kulish Yu.V. Elimination of singularities in causal Green functions of generalized Klein-Gordon and Dirac equations on light cone // EEPJ. - 2016. - Vol. 3. – No.3. – P. 73-83.

33

Classification of Particles at Arbitrary Quantity of Generations. I. Hadrons   **EEJP Vol.3 No.4 2016**

5. Nguen Van Xieu. Lectures on theory of unitary symmetry for elementary particles. – Moscow: Atomizdat, 1967. – 344p. (in Russion)
6. Bogolubov N.N. Theory of symmetry of elementary particles. High-energy physics and theory of elementary particles. - Kiev: Naukova dumka, 1967. - P. 5-112. (in Russion)
7. Close F.E. An introduction to quarks and partons. - London, New York, San Francisco: Academic Press, 1979; Moscow: Mir, 1982. – P. 150. (in Russion)
8. Korn G.A., Korn T.M. Mathematical handbook for scientists and engineers. Definitions, theorems and formulas for reference and review. – New York, San Francisco, Toronto, Ljndon, Sydney: Mc Graw Book Company, 1968; Moscow: Nauka, 1978. - P.34. (in Russion)
9. Esl'sgol'ts L.E. Variational calculus. – Moscow: Gostechizdat, 1952. (in Russion)
10. Myshkis A.D. Mathematics. Special curses for higher technical schools. – Moscow: Nauka, 1971. - 632p. (in Russion)
11. Zima V.G., Nurmagambetov A.Yu. Particle physics from atoms to quarks. – Kharkov: Karazin N.V. Kharkov National University, 2014. – 266p. (in Russion)
12. Feynman R.P., Kislinger M., Ravndal F. Current matrix elements from a relativistic quark model // Phys. Rev. D. - 1971.-Vol.3. – No.11. - P. 2706 – 2732.
13. Feynman R.P. Photon-hadron interactions. – Massachusetts: W.A. Benjamin, Inc. Reading, 1972; Moscow: Mir, 1975. - 390 p. (in Russion)
14. Gasiorowicz S. Elementary particle physics. - New York-London-Sydney: John Wiley&Sons, Inc; Moscow: Nauka, 1969. – 744p. (in Russion)

CLASSIFICATION OF PARTICLES AT ARBITRARY QUANTITY OF GENERATIONS. II. LEPTONS

Yu.V. Kulish

Ukrainian State University of Railway Transport
Sq. Feuerbach 7, Kharkiv region, 61050, Ukraine
E-mail: Yu.V.Kulish@gmail.com
Received November 22, 2016

The hypothesis on quark nature of the leptons is proposed. Leptons are compacted $\overline{q}^3$-systems. It ensures the equality of modules for the electric charges of the proton and the electron. The classification of particles based on the $U(N_f, g) \times SU(3,c) \times SU(4, fs) \times O(3)$-group is proposed at arbitrary quantity N_f of the quark generations. The $U(N_f, g)$-group corresponds to the quark generations, the $SU(3,c)$-group describes the color variables, the $SU(4, fs)$-group corresponds to the variables in the spin (*s*) and flavor (*f*) spaces, and the $O(3)$-group describes the orbital excitations of quarks. In consequence of the Pauli principle leptons consist of antiquarks from 3 different generations. Minimal quantity of leptons with definite electric charge equal 20. Excited double charged l^{--}-leptons and $\overline{l}^{++}$-antileptons with the $J^p = \frac{1}{2}^+$ and $J^p = \frac{1}{2}^-$ are predicted, respectively. They can be resonances in $e^-\pi^-, e^-K^-, e^+\pi^+, e^+K^+,\ \mu^-\pi^-, \mu^-K^-, \mu^+\pi^+, \mu^+K^+$-systems.
KEY WORDS: leptons, quarks, excited leptons, lepton-meson resonances

КЛАСИФІКАЦІЯ ЧАСТИНОК ПРИ ДОВІЛЬНІЙ КІЛЬКОСТІ ПОКОЛІНЬ. ІІ. ЛЕПТОНИ
Ю.В Куліш
Український державний університет залізничного транспорту
м. Фейєрбаха 7, Харків, 61050, Україна

Запропоновано гіпотезу про кваркову природу лептонів. Лептони являють собою щільно запаковані $\overline{q}^3$-системи. Це забезпечує рівність модулів електричних зарядів протона та електрона. Запропоновано класифікацію частинок на основі $U(N_f, g) \times SU(3,c) \times SU(4, fs) \times O(3)$ групи при довільній кількості поколінь кварків N_f Група $U(N_f, g)$ відповідає поколінням кварків, група $SU(3,c)$ описує кольорові змінні, група $SU(4, fs)$ - відповідає змінним в просторах спіну (*s*) та ароматів (*f*), і група $O(3)$ описує орбітальні збудження кварків. Внаслідок принципа Паулі, лептони складаються з антикварків 3 різних поколінь. Мінімальна кількість лептонів з певним електричним зарядом дорівнює 20. Передбачено існування збуджених двічі заряджених l^{--}-лептонів та $\overline{l}^{++}$-антилептонів з $J^p = \frac{1}{2}^+$ та $J^p = \frac{1}{2}^-$,відповідно. Вони можуть бути резонансами в $e^-\pi^-, e^-K^-, e^+\pi^+, e^+K^+,\ \mu^-\pi^-, \mu^-K^-, \mu^+\pi^+, \mu^+K^+$-системах.
КЛЮЧОВІ СЛОВА: лептони, кварки, збуджені лептони, лептон-мезонні резонанси

КЛАССИФИКАЦИЯ ЧАСТИЦ ПРИ ПРОИЗВОЛЬНОМ КОЛИЧЕСТВЕ ПОКОЛЕНИЙ. ІІ. ЛЕПТОНЫ
Ю.В. Кулиш
Украинский государственный университет железнодорожного транспорта
пл. Фейербаха 7, Харьков, 61050, Украина

Предложена гипотеза о кварковой природе лептонов. Лептоны являются плотно упакованными $\overline{q}^3$- системами. Это обеспечивает равенство модулей электрических зарядов протона и электрона. Предложена классификация частиц на основе группы $U(N_f, g) \times SU(3,c) \times SU(4, fs) \times O(3)$ – при произвольном количестве поколений кварков N_f. Группа $U(N_f, g)$ соответствует поколениям кварков, группа $SU(3,c)$ описывает цветовые переменные, группа $SU(4, fs)$ - соответствует переменным в пространствах спина (*s*) и ароматов (*f*), и группа $O(3)$ описывает орбитальные возбуждения кварков. Вследствие принципа Паули лептоны состоят из антикварков 3 разных поколений. Минимальное количество лептонов с определенным электрическим зарядом равно 20. Предсказано существование возбужденных дважды заряженных l^{--}-лептонов и $\overline{l}^{++}$-антилептонов с $J^p = \frac{1}{2}^+$ и $J^p = \frac{1}{2}^-$, соответственно. Они могут быть резонансами в $e^-\pi^-, e^-K^-, e^+\pi^+, e^+K^+,\ \mu^-\pi^-, \mu^-K^-, \mu^+\pi^+, \mu^+K^+$-системах.
КЛЮЧЕВЫЕ СЛОВА: лептоны, кварки, возбужденные лептоны, лептон-мезонные резонансы

35

Classification of Particles at Arbitrary Quantity of Generations. II. Leptons   EEJP Vol.3 No.4 2016

As it is known the atoms consist of electrons, protons, and neutrons. A spin of all these particles equals ½. The electron belongs to leptons. The proton and the neutron belong to baryons (hadrons with the ½-spin). The leptons and the hadrons have got distinguish properties:

1. The quantity of the known leptons equals 12 ($e^-, \mu^-, \tau^-, \nu_e, \nu_\mu, \nu_\tau$ and their antiparticles) distributed in three generations. The quantity of hadrons (in particular, baryons) is very big.

2. The leptons participate in electroweak and gravitation interactions, whereas the hadrons participate in strong, electroweak, and gravitation interactions.

3. The leptons have not got excited states, whereas each hadron has a lot of excited states.

4. At perturbation (e.g., at the capture of a photon) leptons emit the photon and transit to initial state. At perturbation hadrons can transit in excited states, which can decay in other hadrons.

5. The leptons are point-like particles, i.e., their form factors are constants in the measured region of a momentum transfer. Form factors of hadrons have got essential dependences on momentum transfer. An existence of hadron form factors is related to a decrease of a probability of a transition of this hadron in initial state at a capture of a virtual photon

6. All the leptons are fermions and they have got the $\frac{1}{2}$ spin. Hadrons have got integer spin (mesons) and half-integer spin (baryons).

In spite of these distinctions of the leptons and the hadrons, the electric charge for any hadrons equals the product of the electron charge and the integer number with big accuracy of measurements. Therefore, it is of interest to study a problem of proportionality for the electric charges of leptons and hadrons [1].

The present paper is devoted to investigations of leptons in framework of the approach, which ensures in general case the proportionality of the electrical charges of hadrons and leptons. In particular case this approach must ensure the equality of the electrical charges for the proton and the positron.

ON ELECTRIC CHARGES OF PROTON AND ELECTRON

Let us consider a problem of the equality for the absolute values of the Q_e-electron charge and the Q_p-proton charge. It means that a value

$$Q_e + Q_p = \varepsilon_{ep} \tag{1}$$

must equal zero with any accuracy. It is known that in quantum theory of fields the interactions can change electric charges of particles and their masses (it is related to the renormalizations). Therefore, the bare charges and the masses (without interactions) distinguish from these physical values (with an inclusion of interactions).

In Ref. [2], using the gauge invariance, it is shown that a change of the electric charge is determined by interactions of the massless particles. The change of lepton charges can be determined by interactions of the leptons with the photons and possibly gravitons. But the change of hadron charges can be determined by interactions of the hadrons with the photons, the gluons, and possibly gravitons. Therefore, it may be assumed that at equal modules of bare charges the physical value ε_{ep} in (1) has got a non-zero quantity. For example, it may be assumed that the physical value ε_{ep} has got small magnitude related to gravitation interactions, which is essentially less than up-to-date accuracy of measurements. A non-zero value of ε_{ep} can be important in the astrophysics.

The elimination of divergences in the axial Adler-Bell-Jackiw anomaly [3] is important for a proof of a renormalization in the electroweak theory. This anomaly is determined by Feynman diagram corresponding to the loop with the fermion of the $\frac{1}{2}$ – spin and with two photons as well as an axial neutral current for the I_3-third isospin component.

The contribution of a fermion to the ABJ-anomaly equals the product the $Q^2 I_3$-coefficient and the linearly divergent integral, where Q is the electric charge of the fermion. The I_3-value equal $-\frac{1}{2}, \frac{1}{2}, -\frac{1}{2}, \frac{1}{2}$ for the charged leptons $l^-(e^-, \mu^-, \tau^-)$, neutrinos, the *down*-quarks D_k, the *up*-quarks U_k, respectively. The contribution of a charged fermiom to the ABJ-anomaly gives the linear divergence, but a sum of contributions for the charged lepton, the neutrino, D_k-quark, and U_k-quark is proportional to $[0 - Q_e^2 + 3Q_p^2(\frac{4}{9} - \frac{1}{9})]/2 = (Q_p^2 - Q_e^2)/2$ for each generation. Thus, if $\varepsilon_{ep} \neq 0$ (even if ε_{ep} has got small magnitude, which is essentially less than up-to-date accuracy of measurements), then the ABJ-anomaly diverges linearly and the electroweak theory is non-renormalized. In

consequence of good agreement of the electroweak theory with experimental data we must conclude that Q_p equals $-Q_e$ identically. In relation with this the question arises: what essence leads to the equality of the absolute values of the proton and the electron charges.

HYPOTHESIS ON QUARK NATURE OF LEPTONS

To explain the equality of the absolute values of the proton and the electron charges propose that these particles consist of similar particles. We shall consider the positron, as it has got positive electrical charge and the charges of the proton and the positron must equal identically. Then each particle in the positron must correspond to the particle in the proton with the same electrical charge. As the proton consists of three quarks the positron must consist of three quarks also. It may be proposed that other antileptons (leptons with positive electric charge) and antineutrinos consist of quarks. Then the electron and other leptons with negative electric charge as well as neutrinos consist of antiquarks.

In each generation a charged antilepton and an antineutrino exist. These particles have got the $\frac{1}{2}$-spin and they correspond to a representation of the 4-dimension of the $SU(4, sf)$-group. This representation may be identified with the antisymmetric representation for a q^3−system. Note that baryons, which belong to antisymmetric representation of the $SU(6, sf)$- (and $SU(4, sf)$-) group, are unknown [4]. Therefore, it may be assumed that the q^3−systems classified by the symmetric representation and mixed symmetry representation of the $SU(6, sf)$- (and $SU(4, sf)$-) group are baryons, whereas the q^3−systems classified by the antisymmetric representation of the $SU(6, sf)$- (and $SU(4, sf)$-) group are antileptons.

In Ref. [5] it is shown that the fourfold integrals corresponding to the Green functions of the Klein-Gordon and the Dirac equations diverge. For the $\frac{1}{2}$-spin particles the next generalization of the non-homogeneous Dirac equation is proposed in Refs. [5, 6]

$$\left(-i\hat{\partial} + m_1\right)\left(-i\hat{\partial} + m_2\right).....\left(-i\hat{\partial} + m_{N_f}\right)\Psi(x) = \chi(x). \tag{2}$$

The classical solution of the homogeneous equation (2) is given by

$$\Psi^\alpha(x)_{free} = \sum_s \sum_{k=1}^{N_f} \int d^4 p\, \delta\left(q^2 - m_k^2\right)\left[C_k u^\alpha{}_{k,s}(q) e^{-iqx} + \tilde{C}_k v^\alpha{}_{k,s}(q) e^{iqx}\right], \tag{3}$$

where α is the bispinor index, s corresponds to spin projection, $u^\alpha{}_{k,s}(q)$ and $v^\alpha{}_{k,s}(q)$ are the bispinors, C_k and $\tilde{C}_k$ are arbitrary constants. The Green functions (which are 4×4-matrixes) for this equation may be written as

$$\overline{S}(x) = \frac{1}{(2\pi)^4} \int \frac{(\hat{q} + m_1)(\hat{q} + m_2)....\left((\hat{q} + m_{N_f})\right)}{\left(-q^2 + m_1^2\right)\left(-q^2 + m_2^2\right)...\left(-q^2 + m_{N_f}^2\right)} d^4 q. \tag{4}$$

The N_f-number equals to the quantity of generations for the $\frac{1}{2}$-spin fermions and order of the equation (2). The integrals in (4) can converge at $N_f \geq 5$. The study of a continuity of the causal Green functions (4) in all the space-time (and on the light cone too) has been shown that the quantity of fermion generations $N_f \geq 6$ [7]. In Ref. [8] the classification of hadrons with respect to the $U(N_f, g) \times SU(3, c) \times SU(4, fs) \times O(3)$-group is proposed at arbitrary quantity N_f of fermion generations. The $U(N_f, g)$-group corresponds to the quark generations, the $SU(3, c)$-group describes the color variables, the $SU(4, fs)$-group corresponds to the variables in the spin (*s*) and flavor (*f*) spaces (which is subgroup of the known $SU(6, fs)$-group), and the $O(3)$-group describes the orbital excitations of quarks [4].

Propose that leptons (antileptons) are colorless, i.e., they are described by singlets of the $SU(3, c)$−group, which correspond to antisymmetric representations for $q^3 - (\overline{q}^3 -)$ systems. Because a quantity of the leptons and the

37

Classification of Particles at Arbitrary Quantity of Generations. II. Leptons   EEJP Vol.3 No.4 2016

antileptons is small in a comparison with a quantity of baryons, it may be proposed that quarks and anriquarks in antileptons and in leptons, respectively, are in the $1s-$ state with the $L=0$ orbital moment. It means that leptons (antileptons) are singlets of the $O(3)-$ group, which correspond to symmetric representations for q^3- $(\overline{q}^3-)$ systems. Then from the Pauli principle follows that the antileptons (leptons) belong to the antisymmetric representations of the $U(N_f,g)-$ group for q^3- $(\overline{q}^3-)$ systems. The dimension of these representations equals $N_A(N_f)=N_f(N_f-1)(N_f-2)/1\bullet2\bullet3$. Therefore, the minimal quantity of the generations for the antileptons (the leptons) equals 20 (for $N_f=6$ [8]). These leptons have got the $\dfrac{1}{2}$-spin.

The antileptons (e.g., the positron) and the proton have got the same spatial parity, as all the quarks are in the $1s-$ state. Therefore the spatial parities of the leptons (e.g., the electron) and the proton must be opposite.

Denote the charged antileptons and the antineutrinos, which consist of the quarks from the number k_1,k_2,k_3 generations as $\overline{l}^+_{k_1k_2k_3}$ and $\overline{\nu}_{k_1k_2k_3}$, respectively, with the k_1,k_2,k_3 numbers disposed in increasing order. Denote corresponding the charged leptons and the neutrinos as $l^-{}_{k_1k_2k_3}$ and $\nu_{k_1k_2k_3}$, respectively. The antileptons consisting of the quarks from first, second, and third generations must exist among $N_A(N_f)$ antileptons. For such antileptons the M_0- value, which for baryons give the sum of quark masses (for example, in the mass formula (30) of Ref. [8]) is minimal among all the generations. Possibly these antileptons are the positron and the electron antineutrino.

The wave function of the charged antilepton (including the positron) may be written as:

$$\left|\overline{l}^+_{k_1k_2k_3},S_z=\frac{1}{2}\ \right\rangle=\frac{1}{6\sqrt{6}}\varepsilon_{c_1c_2c_3}\varepsilon^{N_f}{}_{g_1g_2g_3}(k_1,k_2,k_3)\Big|U\uparrow_{c_1g_1}U\downarrow_{c_2g_2}D\uparrow_{c_3g_3}-U\downarrow_{c_1g_1}U\uparrow_{c_2g_2}D\uparrow_{c_3g_3}+$$
$$+U\downarrow_{c_1g_1}D\uparrow_{c_2g_2}U\uparrow_{c_3g_3}-U\uparrow_{c_1g_1}D\uparrow_{c_2g_2}U\downarrow_{c_3g_3}+ \qquad (5)$$
$$+D\uparrow_{c_1g_1}U\uparrow_{c_2g_2}U\downarrow_{c_3g_3}-D\uparrow_{c_1g_1}U\downarrow_{c_2g_2}U\uparrow_{c_3g_3}\ \Big\rangle,$$

where c_1,c_2,c_3 are the indices of the $SU(3,c)$-group, the $\varepsilon_{c_1c_2c_3}$ - tensor is the antisymmetric tensor of third rank. The g_1,g_2,g_3 indices are the numbers of the generations. The $\varepsilon^{N_f}{}_{g_1g_2g_3}(k_1,k_2,k_3)$- tensor is the antisymmetric tensor of the N_f-rank with six non-zero components, which correspond to the permutatons of the g_1,g_2,g_3-indices from $\varepsilon_{123\cdots N_f}=1$. For example, at $N_f=6$ and $k_1=2,k_2=4,k_3=5$ this tensor is given by $\varepsilon^6{}_{g_1g_2g_3}(2,4,5)=\varepsilon_{1g_13g_2g_36}$ and $\varepsilon^6{}_{245}(2,4,5)=\varepsilon^6{}_{524}(2,4,5)=\varepsilon^6{}_{452}(2,4,5)=-\varepsilon^6{}_{425}(2,4,5)=$ $-\varepsilon^6{}_{254}(2,4,5)=-\varepsilon^6{}_{542}(2,4,5)=1$. The wave function of the positively charged antilepton is determined by 216 terms.

The wave function of the antineutrino is given by:

$$\left|\overline{\nu}_{k_1k_2k_3},S_z=\frac{1}{2}\ \right\rangle=\frac{1}{6\sqrt{6}}\varepsilon_{c_1c_2c_3}\varepsilon^{N_f}{}_{g_1g_2g_3}(k_1,k_2,k_3)\Big|-D\uparrow_{c_1g_1}D\downarrow_{c_2g_2}U\uparrow_{c_3g_3}+D\downarrow_{c_1g_1}D\uparrow_{c_2g_2}U\uparrow_{c_3g_3}-$$
$$-D\downarrow_{c_1g_1}U\uparrow_{c_2g_2}D\uparrow_{c_3g_3}+D\uparrow_{c_1g_1}U\uparrow_{c_2g_2}D\downarrow_{c_3g_3}- \qquad (6)$$
$$-U\uparrow_{c_1g_1}D\uparrow_{c_2g_2}D\downarrow_{c_3g_3}+U\uparrow_{c_1g_1}D\downarrow_{c_2g_2}D\uparrow_{c_3g_3}\ \Big\rangle.$$

The wave function (6) is derived from (5) by means of the changes $U\leftrightarrow D$ and by general sign similarly to the derivation of the wave function of the neutron from the wave function of the proton in the quark model of baryons [9,10].

The wave function of the neutrinos we derive from (6) by means of the substitutions $U\rightarrow\overline{U},D\rightarrow\overline{D}$:

$$\left|\nu_{k_1k_2k_3},S_z=\frac{1}{2}\ \right\rangle=\frac{1}{6\sqrt{6}}\varepsilon_{c_1c_2c_3}\varepsilon^{N_f}{}_{g_1g_2g_3}(k_1,k_2,k_3)\Big|-\overline{D}\uparrow_{c_1g_1}\overline{D}\downarrow_{c_2g_2}\overline{U}\uparrow_{c_3g_3}+\overline{D}\downarrow_{c_1g_1}\overline{D}\uparrow_{c_2g_2}\overline{U}\uparrow_{c_3g_3}-$$
$$-\overline{D}\downarrow_{c_1g_1}\overline{U}\uparrow_{c_2g_2}\overline{D}\uparrow_{c_3g_3}+\overline{D}\uparrow_{c_1g_1}\overline{U}\uparrow_{c_2g_2}\overline{D}\downarrow_{c_3g_3}- \qquad (7)$$
$$-\overline{U}\uparrow_{c_1g_1}\overline{D}\uparrow_{c_2g_2}\overline{D}\downarrow_{c_3g_3}+\overline{U}\uparrow_{c_1g_1}\overline{D}\downarrow_{c_2g_2}\overline{D}\uparrow_{c_3g_3}\ \Big\rangle.$$

The wave function of the charged lepton (including the electron) may be presented as

$$\left| l^-{}_{k_1 k_2 k_3}, S_z = \frac{1}{2} \right\rangle = \frac{1}{6\sqrt{6}} \varepsilon_{c_1 c_2 c_3} \varepsilon^{N_f}{}_{g_1 g_2 g_3}(k_1, k_2, k_3) \left| \bar{U}\uparrow_{c_1 g_1} \bar{U}\downarrow_{c_2 g_2} \bar{D}\uparrow_{c_3 g_3} - \bar{U}\downarrow_{c_1 g_1} \bar{U}\uparrow_{c_2 g_2} \bar{D}\uparrow_{c_3 g_3} + \right.$$

$$+ \bar{U}\downarrow_{c_1 g_1} \bar{D}\uparrow_{c_2 g_2} \bar{U}\uparrow_{c_3 g_3} - \bar{U}\uparrow_{c_1 g_1} \bar{D}\uparrow_{c_2 g_2} \bar{U}\downarrow_{c_3 g_3} + \qquad (8)$$

$$\left. + \bar{D}\uparrow_{c_1 g_1} \bar{U}\uparrow_{c_2 g_2} \bar{U}\downarrow_{c_3 g_3} - \bar{D}\uparrow_{c_1 g_1} \bar{U}\downarrow_{c_2 g_2} \bar{U}\uparrow_{c_3 g_3} \right\rangle .$$

Now we consider the consequences of the antisymmetry of the representation of the $U(N_f, g)$− group for the set of quarks from the 1, 2, 3- numbers of the generations in antileptons:

$$\bar{l}^+_{123} = [ucb, ctd, tus], \bar{v}_{123} = [dst, bdc, sbu] . \qquad (9)$$

From (9) it is seen that leptons and antileptons include antiquarks and quarks with big masses. Even the antileptons consisting of the quark from the 1, 2, 3- numbers of the generations (possibly the positron and the electron antineutrino) include the t-quark, which has got the $m(t) \approx 177 GeV$ mass [11]. Note that masses of U_k − quarks with $k \geq 3$ must be greater than $m(t)$. From (9) it can be seen that each antilepton include three U_k-quark and three D_k-quarks. Therefore it is of interest to derive the M_0-term, which for baryons give the sum of quark masses (for example, in the mass formula (30) of Ref. [8]). Using (5), the mass of the $l^+{}_{k_1 k_2 k_3}$ -antilepton may be written as

$$M_0(\bar{l}^+_{k_1 k_2 k_3}) = \left\langle \bar{l}^+_{k_1 k_2 k_3} \left| \sum_i m_i \right| \bar{l}^+{}_{k_1 k_2 k_3} \right\rangle = \frac{6 \times 6}{216} \varepsilon^{N_f}{}_{g_1 g_2 g_3}(k_1, k_2, k_3) \varepsilon^{N_f}{}_{g_4 g_5 g_6}(k_1, k_2, k_3)$$

$$\left\langle U\uparrow_{g_4} U\downarrow_{g_5} D\uparrow_{g_6} \left| m(U_{g_1}) + m(U_{g_2}) + m(U_{g_3}) + m(D_{g_1}) + m(D_{g_2}) + m(D_{g_3}) \right| U\uparrow_{g_1} U\downarrow_{g_2} D\uparrow_{g_3} \right\rangle =$$

$$= \frac{1}{3}\left[\sum_g m(U_{g_1}) + \sum_{g_2} m(U_{g_2}) + \sum_{g_3} m(D_{g_3}) \right] = \qquad (10)$$

$$= \frac{1}{3}\left[2m(U_{k_1}) + 2m(U_{k_2}) + 2m(U_{k_3}) + m(D_{k_1}) + m(D_{k_2}) + m(D_{k_3}) \right] .$$

In this formula are not written the color indices. The summation with respect of these indices gives the 6 factor. The m_i mass operators in the $\sum_i m_i$ -operator are proportional to unique operator in the color and the spin spaces and they are diagonal operators in the space of generations. Therefore, such structure of the mass operators permits one to take the same results for six terms in (5). As analogy, the antineutrino masses are given by

$$M_0(\bar{v}_{k_1 k_2 k_3}) = \frac{1}{3}\left[2m(D_{k_1}) + 2m(D_{k_2}) + 2m(D_{k_3}) + m(U_{k_1}) + m(U_{k_2}) + m(U_{k_3}) \right] . \qquad (11)$$

In particular, for the antileptons which consist of the quarks from the number 1, 2, 3 generations the M_0 -values are

$$M_0(\bar{l}^+_{123}) = \frac{1}{3}\left[2m(u) + 2m(c) + 2m(t) + m(d) + m(s) + m(b) \right] \qquad (12)$$

$$M_0(\bar{v}_{123}) = \frac{1}{3}\left[2m(d) + 2m(s) + 2m(b) + m(u) + m(c) + m(t) \right] .$$

DIAMOND-GRAPHITE ANALOGY OF LEPTONS AND BARYONS

It is known that the diamond and the graphite consist of the carbon atoms. In spite of properties of them are different. The graphite is fairly soft material, but the diamond is the hardest material.

Pencils with graphite cores are used to write. It means that at small perturbation the graphite transits to other states. Indeed, in initial state we have got the pencil and the clean paper, but in a final state we have got the pencil and this paper with drawn line. The mass of the graphite core can change. It corresponds to a transition of the pencil graphite to other states. Therefore, the graphite is similar to hadrons, in particular – to baryons. The analogy of the graphite and the baryons (nucleons) can be continued. The carbon atoms in the graphite are located on the planes. The nucleons consist of the quarks from the same generation.

As the diamond is the hardest solid, the state of the diamond does not change at an interaction with other solids. Thus, the diamond is similar to the leptons (antileptons). In addition note that the carbon atoms in the diamond are located in the space and they yield the space lattice. It is the analogy of a proposition that the leptons (antileptons) consist of the quarks (antiquarks) from different generations.

39

Classification of Particles at Arbitrary Quantity of Generations. II. Leptons   EEJP Vol.3 No.4 2016

EXCITED LEPTONS AND POSSIBLE EXPERIMENTAL TESTS

A consideration of the q^3 – systems with the quarks in the $(1s)^2 1p$ – states allows one to study the baryons with the negative parity [4]. In such systems the quark orbital moment equals one. The physical states belong to the representations with mixed symmetry of the $O(3)$ – group. Then the uncolored baryons are described by the representations with mixed symmetry of the $SU(6, fs)$ – group and the $SU(4, fs)$ – group of the dimensions 70 and 20, respectively.

Let us study the leptons (antileptons) as the $\bar{q}^3 - (q^3)$ – systems with the quarks in the $(1s)^2 1p$ – states. The expansion of the representations of the $SU(4, fs)$ – groups for the mixed symmetry with a respect of the $SU(2, f) \times SU(2, s)$ – group for the q^3 – system is given by:

$$20 = 4 \times \frac{1}{2}^- + 2 \times \frac{3}{2}^- + 2 \times \frac{1}{2}^- . \tag{13}$$

In the expansion (13) the representations of the $SU(2, s)$ -group are presented by J^p -values. The product of the representations with mixed symmetry for the $SU(2, s)$ – and the $O(3)$ – groups can be expanded as the sum of the symmetric, mixed symmetric, and antisymmetric representations. Consider the antisymmetric representation of the $SU(4, fs) \times O(3)$ – group. This representation can be obtained as the product of the mixed symmetric representations of the $SU(4, fs)$ – group and the $O(3)$ – group. The product of the antisimmetric representations of the $U(N_f, g)$ –, the $SU(3, c)$ –, and the $SU(4, fs) \times O(3)$ – groups agrees with the Pauli principle. The expansion (13) is valid for the q^3 – systems (i.e., for the antileptons). Similar expansion can be written for the $\bar{q}^3$ – system (i.e., for the leptons), but in this case the parity must be positive.

The representation of the $SU(2, f)$ – group of the dimension 4 corresponds to excited leptons (antileptons). Denote these excited antileptons (which consist of the quarks) and leptons as

$$\bar{l}^*(4) = \{\bar{l}^{*-}, \bar{l}^{*o}, \bar{l}^{*+}, \bar{l}^{*++}\}, \qquad l(4) = \{l^{*--}, l^{*-}, l^{*0}, l^{*+}\}. \tag{14}$$

The representation of the $SU(2, f)$ – group of the dimension 4 is symmetric. So to obtain the antisymmetric representation of the $SU(4, fs) \times O(3)$ – group we have to consider the antisymmetric representation of the $SU(2, s) \times O(3)$ – group. This representation corresponds to $J = \frac{1}{2}$. Such, we predict that excited l^{*--} - leptons and l^{*++} - antileptons with the $\frac{1}{2}$ -spin can exist. Note that the representation of the $SU(2, f)$ – group of the dimension 4 can occur at other modes for products of the representations of the $U(N_f, g) \times SU(3, c) \times SU(2, s) \times O(3)$ -group. As the representation of the $O(3)$ – group corresponding to the quarks in the $(1s)^2 1p$ – states has got mixed symmetry, the representations $U(N_f, g) \times SU(3, c) \times SU(2, s)$ must have got mixed symmetry too. In particular, for the symmetric representation of the $SU(2, s)$ -group the $\bar{l}^*(4)$ -antileptons and the $l^*(4)$ -leptons can exist in two cases: the antisymmetric representation of the $U(N_f, g)$ -group in the state of the color octet and the mixed symmetric representation of the $U(N_f, g)$ -group in the state of the color singlet. In these cases the $\bar{l}^*(4)$ -antileptons with $J^p = \frac{1}{2}^-$ and the $l^*(4)$ -leptons with $J^p = \frac{1}{2}^+$ can exist. For the quarks from the first, the second, and the third generations the $\bar{l}^{*++}$ - and the $\bar{l}^{*-}$ -antileptons consist of the $u, c, t-$ and the $d, s.b-$ quarks, respectively. Therefore, we may assume that for the masses of the $\bar{l}^*(4)$ -antileptons the inequalities $m(\bar{l}^{*-}) < m(\bar{l}^{*o}) < m(\bar{l}^{*+}) < m(\bar{l}^{*++})$ are valid. If the contributions of the color-magnetic and the color-electric interactions in the mass formula (30) of Ref. [8] are additional, then the relations

$$m(\bar{l}^{*+}) - m(\bar{l}^{*0}) = m(\bar{l}^{*0}) - m(\bar{l}^{*-}) = \tag{15}$$

$$= \frac{1}{3}[m(U_{k_1}) + m(U_{k_2}) + m(U_{k_3}) - m(D_{k_1}) - m(D_{k_2}) - m(D_{k_3})]$$

may be valid for the antileptons consisting of the quarks from the k_1, k_2, k_3 -numbers of the generations.

The analogy between the $\bar{l}^{*-}$-antileptons and the $\Delta -$ baryons, which consist of the quarks in the $(1s)^2 1p -$ states, may be proposed. Among the $\Delta -$ baryons with negative parity the $\Delta(1620)$ -resonance ($S_{31}(1620)$ -resonance in the $\pi N -$ system) with $J^p = \frac{1}{2}^-$ has got the minimal mass [12]. In quark models the mass difference between the $\Delta(1620)$ -resonance and the nucleon mainly determined by the $\vec{L}\vec{S} -$ interactions [4]. If we assume that the $\vec{L}\vec{S} -$ interactions give additional contributions to the masses of excited baryons and antileptons, then we may expect that the masses of the $\bar{l}^{*o} -$ antileptons and the $\bar{l}^{*+} -$ antileptons equal approximately 700 MeV. Such transitions between quarks as $u \to d\pi^+, d \to u\pi^-, u \to sK^+, s \to uK^-, \quad u \to sK^{*+}, s \to uK^{*-}$ $u \to d\rho^+, d \to u\rho^-, u \to sK^{*+}, s \to uK^{*-}$ can occur in hadrons and in leptons. These transitions induce the $P_{33}(1232) \to N\pi, D_{13}(1520) \to N\pi, S_{11}(1535) \to N\pi, S_{31}(1620) \to N\pi$ decays. Similarly these transitions can induce the $l^*(4) \to l\pi$, $l^*(4) \to l\rho$, $\bar{l}^*(4) \to \bar{l}\pi$, $\bar{l}^*(4) \to \bar{l}\rho$ decays. One can expect that these decays must be induced by strong interactions. It is of interest to study the decays of the $\bar{l}^{*++}$ -antilepton and the l^{*--} -leptons. As these excited antilepton and lepton ought to have got fairly large masses, they must be resonances. It can be used for the test of the hypothesis on quark nature of leptons.

For the tests of proposed hypothesis it is of interest to investigate the resonances in the $e^-\pi^-, e^-\rho^-, e^-K^-, e^-K^{*-}$, $\mu^-\pi^-, \mu^-\rho^-, \mu^-K^-, \mu^-K^{*-}$, $e^+\pi^+, e^+\rho^+, e^+K^+, \mu^+\pi^+, \mu^+\rho^+, \mu^+K^+, \mu^+K^{*+}$, $e^+K^{*+}, \mu^+\pi^+, \mu^+\rho^+, \mu^+K^+, \mu^+K^{*+}$ -systems. The resonances in these systems can be investigated in hadron reactions. However, it can be more convenient to investigate these resonances in the reactions of the lepton-antilepton interactions:

$$e^+e^- \to \bar{l}^{*++}l^{*--}, \qquad \mu^+\mu^- \to \bar{l}^{*++}l^{*--}. \tag{16}$$

ON STRONG INTERACTIONS OF LEPTONS

According to the quark nature of leptons it may be assumed that some strong transitions between quark systems, which usually considered as leptons or antileptons can become possible. Such strong transitions can lead to decays of $\pi^\pm -, K^\pm -$ mesons into charged lepton (antilepton) and neutrino (antineutrino). These decays are well known. But they are weak. Therefore, non-zero amplitudes of such strong transitions will contradict to experimental data. Compare similar strong $e^+ \to \pi^+ \bar{V}_e$ - and $p \to \pi^+ n$ - transitions. The spin structure of the amplitudes for these transitions is the same: $\bar{u}(p_2)\gamma_5 u(p_1)\varphi_\pi$. As usual assume that the π^+ -meson is the $u\bar{d}$ -pair and the proton and the neutron are the *uud*-system and the *ddu*-system, respectively. Then the $e^+ \to \pi^+ \bar{V}_e$ - and the $p \to \pi^+ n$ - transitions are determined by a $u \to \pi^+ d$ -transition between the quarks. In the $p \to \pi^+ n$ - transition the proton becomes the neutron directly after an emission of the π^+ -meson by the *u*-quark.

Assume that e^+ - and $\bar{V}_e$ - consist of the quarks from the first, the second, and the third generations. Then these antileptons are the antisymmetric combinations of different quarks (9). The *ucb*- and the *uts*- systems from the positron transit to the *cdb*- and the *tds*- systems from the antineutrino after the emission of the pion, respectively. But the the *ctd*-system from the positron cannot transits to the *usb*-system from the antineutrino at the emission of the pion. Thus, the positron does not transit immediately to the antineutrino after the emission of the pion. Therefore, it may be concluded that strong $e^+ \to \pi^+ \bar{V}_e$ -transition (with the $\bar{u}(p_2)\gamma_5 u(p_1)\varphi_\pi$ -amplitude) is forbidden. Similarly, strong $\mu^+ \to \pi^+ \bar{V}_\mu$ -, $e^+ \to K^+ \bar{V}_e$ -, $\mu^+ \to K^+ \bar{V}_\mu$ - , $e^+ \to \rho^+ \bar{V}_e$ -, $\mu^+ \to \rho^+ \bar{V}_\mu$ -, $e^+ \to K^{*+} \bar{V}_e$ -, $\mu^+ \to K^{*+} \bar{V}_\mu$ -transitions must be forbidden. As result, these transitions are induced by the weak interactions.

It is of interest to consider the transitions between a baryon and a antilepton, such as $p \to e^+\gamma$, $p \to \mu^+\gamma$, $p \to e^+\pi^0$, $p \to \mu^+\pi^0$. These transitions have not been observed yet. Usually it is explained by a violation of the conservation laws for the baryonic and the leptonic numbers. The proton belongs to symmetric representation of the

41

Classification of Particles at Arbitrary Quantity of Generations. II. Leptons   EEJP Vol.3 No.4 2016

$U(N_f, g)$-group $B^{\{g_1, g_2, g_3\}}$ and according to the hypotheses on quark nature of leptons the antileptons belong to the antisymmetric representation $\overline{L}^{[g_1, g_2, g_3]}$ of this group. Denote the representation of the $U(N_f, g)$-group for $q\overline{q}$ − mesons as $M^{g_1}{}_{g_2}$. Then the amplitudes of the transitions of the B-baryons to the $\overline{L}$ − antileptons and the M-mesons may be written as

$$T(B \rightarrow \overline{L}M) = B^{\{g_1 g_2 g_3\}} \overline{L}_{[g_4 g_2 g_3]} M^{g_4}{}_{g_1} A(B \rightarrow \overline{L}M) = 0, \qquad (17)$$

where $A(B \rightarrow \overline{L}M)$ is a part of the amplitude corresponding to particle momenta, the color, the spin, and the flavor variables. The amplitudes of strong transitions (17) vanish as they express through the products of the symmetric and antisymmetric tensors in the space of generations. In particular, from (17) it follows that the $p \rightarrow e^+ \gamma$ -, $p \rightarrow \mu^+ \gamma$ -, $p \rightarrow e^+ \pi^0$ -, $p \rightarrow \mu^+ \pi^0$ -transitions are forbidden. Note that the amplitudes of radiative decays of the pronon can be derived from (17) by means of the model of vector dominance.

CONCLUSION

The proposed hypothesis on quark nature of leptons ensures the equality of the modules of the electron and the proton electric charges. The antisymmetry of the representations of the $U(N_f, g)$-group and the $SU(4, fs)$-group of q^3-systems for antileptons allows one to explain distinctions of the properties for leptons (antileptons) and hadrons. Indeed, the antisymmetric representation of the $SU(4, fs)$-group corresponds to two particles of the $\frac{1}{2}$-spin in the ground state (the $(1s)^3$-state), e.g., positron and antineutrino for q^3-systems. Next excited states occur for q^3-systems in $(1s)^2 1p$-state. Among excited states the leptons (antileptons) with double electric charge must exist. In consequence of big mass values for the quarks from the third generation and the antisymmetry of the representation of the $U(N_f, g)$-group the mass difference between the excited and the ground states have to be rather large.

Therefore, the leptons (antileptons) ought to behave at relatively small momentum transfer as point-like particles.

It may be assumed that the leptons (antileptons) can participate in strong interactions at high energies. It means that the strong interactions of the leptons (antileptons) are biased to the high-energy region. The leptons (antileptons) can be interpreted as strongly packed antibaryons (baryons).

It is of important to explain the mass spectrum of the baryons and the antileptons for the consistence of proposed classification of particles and the hypothesis on quark nature of leptons. There can be doubts in possibility to do this by means of the mass formula. It can be seen from the M_0-value for the nucleons and the leptons (antileptons). The M_0-value for the nucleons and $\Delta(1232)$ approximately equal $1.02 GeV$ whereas according to (12) the minimal values of M_0 for the electron (positron) and electron neutrino (antineutrino) equal $M_0(e^-) \approx 2m(t)/3 = 118 GeV$ and $M_0(\nu_e) \approx m(t)/3 = 59 GeV$. Last values exceed essentially the experimental ones ($m(e) = 0.51 MeV, m(\nu_e) < 5eV$). As it is known the color-magnetic interactions reduce the nucleon masses and enlarge the $\Delta(1232)$ masses. This allows obtain the values of the nucleon and the $\Delta(1232)$-isobar masses near to experimental ones. But it cannot be expected that taking into account of the color-magnetic interaction allows one to derive the values of the electron and the electron neutrino masses near to experimental values.

Assume that quarks interact by means of tensor mesons in an addition to the gluon exchange. Amplitudes of the quark interactions by means of the $J^p = 2^+$-meson exchange are proportional to the quark 4-momenta [13]. In the rest frame these amplitudes are proportional to the quark masses. Therefore, the $J^p = 2^+$-meson exchange may be just essential for heavy quarks (i.e. for leptons (antileptons)) and it can be invisible for hadrons consisting of light quarks (e.g., for the nucleons and the $\Delta(1232)$-isobars). In Refs. [14, 15] it is shown that interaction currents for higher spin particles (i.e. particles with the 2-spin) must obey the theorem on currents and fields as well as the theorem on continuity of current derivatives. In Ref. [13] the currents of the interactions of the $J^p = 2^+$-boson with the $\frac{1}{2}$-spin fermions obey the theorem on currents and fields.

In proposed hypothesis on quark nature of leptons the excited leptons (antileptons) with double electric charge are predicted. These excited leptons (antileptons) ought to be the meson-lepton (meson-antileptons) resonances. These

mesons can be pseudoscalar or vector. The investigations such resonances may be very important for the test of proposed hypothesis.

Weak interactions of the quarks in higher orders can lead to such decays, as $\mu \to e\gamma, \mu \to e\gamma\gamma$. They can be investigated in the $\mu e \to \gamma\gamma -, \gamma e \to \gamma\mu -$ processes [16].

A situation with calculations of amplitudes for interactions of leptons and antileptons, represented as antiquark and quark systems, is similar to a situation with calculations of amplitudes of soft hadron processes in the quantum chromodynamics. As it is known, the QCD is the theory of strong interactions. But in the QCD the amplitudes of soft hadron reactions cannot be calculated. In particular, the coupling constants of the $\pi NN-, \pi N\Delta -$ interactions cannot be calculated by means of the QCD Lagrangian with known the constant of the quark-gluon interaction and the quark masses. On the other hand, amplitudes of some hadron reactions can be calculated with reasonable accuracy in models with hadrons represented as elementary particles. In such calculations the values of interaction constants and particle masses known from experimental data are used. Therefore, it is naturally that leptonic processes are described well in the framework of the electroweak theory with leptons and antileptons considered as elementary particles.

REFERENCES
1. Akhiezer A.I., Rekalo M.P. Electrical charge of elementary particles // Uspekhi fizicheskikh nauk. – 1974. - Vol. 114. - P.478-508. (in Russion)
2. De Alfaro V., Fubini S., Furlan G., Rosseti C. Currents in hadron physics. – North-holland Publ. Comp. Amsterdam; American Elseviev Publ. Comp. Inc. – London, New York 1973; Moscow: Nauka, 1976. - P. 602. (in Russion)
3. Treiman S.B., Jackiw R., Gross D.J. Lectures on current algebra and its applications.-Princeton Univ. Pres.-Princeton. – 1972; Moscow: Atomizdat, 1977. – P. 93. (in Russion)
4. Close F.E. An introduction to quarks and partons. - Academic Press. - London, New York, San Francisco. - 1979; Moscow: Mir, 1982. - P.150 (in Russion)
5. Kulish Yu. V., Rybachuk E.V. Divergences of integrals for Green functions and necessary existence of particle generations // Journal of Kharkiv National University. - 2011. – No.955. - Is.2/50/. - P. 4-14.
6. Kulish Yu., Rybacuk E.V. Necessary generalization of Klein-Gordon and Dirac equations and existence of particle generations // Problems of Atomic Science and Technology. - 2012. – No. (77). - P. 16–20.
7. Kulish Yu.V. Elimination of singularities in causal Green functions of generalized Klein-Gordon and Dirac equations on light cone // East Europ. J. Phys. – 2016. – Vol. 3. – No. 3. – P. 73-83.
8. Kulish Yu.V. Classification of particles at arbitrary quantity of generations. I. Hadrons // East Europ. J. Phys. – 2016. – Vol. 3. – No. 4. – P. 22-33.
9. Kokkedee J.J.J. The quark model. - W.A. Benjamin, Inc. - New York, Amsterdam, 1969; Moscow: Mir, 1971. - 244 p. (in Russion)
10. Shelest V.P., Zinoviev G.M., Miranskij V.A. Models of strong-interacting elementary particles. Vol. 1. – Moscow: Atomizdat, 1975. – 232p. (in Russion)
11. Zima V.G., Nurmagambetov A.Yu. Particle physics from atoms to quarks. – Kharkov: V.N. Karazin Kharkov National University, 2014. – 266p. (in Russion)
12. Particle data group. Review of particle properties // Phys. Lett. – 1988. – Vol. 204. – No. 1. – P.1-486.
13. Kulish Yu.V. Interactions of elementary particles similar to gravitational ones // Problems of atomic science and technology. - 2001. – No. 6(1). – P.80-83.
14. Kulish Yu.V., Rybachuk E.V. Properties of high-spin boson interaction currents and elimination of power divergences // Problems of atomic science and technology. -2001. – No. 6(1). –P.84-87.
15. Kulish Yu.V., Rybachuk E.V. Properties of interaction currents for massive higher spin bosons // The Journal of Kharkiv National University, physical series "Nuclei, Particles, Fields". – 2003. – No.585. – Iss.1(21). – P.49-55.
16. Gakh G.I. Non-conservation of muonic number and $\mu \to e\gamma\gamma -$, $\mu e \to \gamma\gamma -, \gamma e \to \gamma\mu -$ processes // Yad. Fiz. – 1979. – Vol. 30. – Iss. 1(7). – P. 198. (in Russion)

PLASMA WALL TRANSITION AND EFFECTS OF GEOMETRY IN PRESHEATH

S. Ahmad[1], K. Chaudhary[2]

[1]Department of Physics, Government Postgraduate College Mansehra, Pakistan
[2]Department of Physics, Government College University Lahore, Pakistan
E-mail: saeedgcuahmad87@gmail.com
Received December 01, 2016

When plasma interacts with the wall of a conductor, electrons due to high mobility reach the wall first and develop negative potential on the wall and very near to the wall plasma is divided into sheath and presheath regions. The quasi-neutral plasma is shielded from the wall by a space charge sheath of the positive ions of the order of few electrons Debye's lengths (λ_D). At the sheath edge quasi neutrality breaks down from presheath side. In asymptotic limit $\varepsilon = \lambda_D/L \to 0$ varying area of geometry affects the structure of the presheath scale. In addition to geometry, collisions and ionization also affects the presheath structure. But the sheath region is universal and is independent of either of geometry, ionization rate and collision frequency. The region which play the role of a link between these two regions has characteristics of both regions and is known as intermediate region. Even in the absence of ionization source and collision expanding area of geometry can accelerates the ions towards the wall. The characteristic length of the geometric presheath depends on radius of curvature $R_c = A/A'$, where "A" is the area of geometry and "$A' = dA/dz$". If either of ionization or collisions is present along with the expanding area of geometry then dominant factor for the acceleration of ions in the presheath region is not the expanding area of geometry.
KEYWORDS: Debye's length, sheath, presheath, Bohm's criterion, ion acoustic speed, Boltzman's relation, Tonks Langmiur problem

When plasma interacts with the wall of a conductor, the electrons due to high mobility reach the wall first and develop negative potential on the wall and very near to the wall plasma is divided into two regions. The quasi-neutral plasma is shielded from the wall by a space charge sheath of the positive ions of the order of few electrons Debye's lengths (λ_D) [1]. Langmuir in history for the first time in 1929 used the terms plasma and sheath for a gas discharge [2]. Up to 1951 all the work on plasma wall transition was done assuming collisionsless plasma. Boyd in 1951 for the first time using diffusion controlled theory for collision dominated plasma, introduced Bohm's criterion [3]. Allen and Thonemann in 1954 confirmed Bohm's criterion in equality form and stated boundary conditions for sheath and the presheath region for the case of marginal form of Bohm's criterion. Harrison and Thompson in 1959 analytically solved Tonks Langmiur problem and find kinetic Bohm criterion [4]. According to this criteria for planar geometry at the sheath edge ions must have speed equal to ion acoustic speed $(v_i = c_S)$ in order to enter in the sheath region. This condition is known as Bohm's criteria in marginal form [1]. It was investigated by Riemann as well as by Sternberg that when the area expands or contracts then the standard Bohm's criterion must be changed and non-marginal form of Bohm's criteria is used [5]. The reason of the non-marginal Bohm's criterion is that as geometry contracts pressure increases, so density increases and velocity must be less than ion sound velocity at the sheath edge, in order to conserve steady state current density following towards the wall [4,6]. The region in which ions are accelerated to ion acoustic speed (c_S) is called the presheath region. In the presheath region number density of electrons and ions is equal, i.e, $(n_i = n_e)$. The presheath is dominated by either of the four basic mechanism which are collision of neutrals with ions, geometric current concentration, applied magnetic field, and ionization rate [7]. This paper clarifies the effects of collisions, ionization and especially of geometry on presheath. As the characteristic length of the geometric presheath depends on radius of curvature $R_c = A/A'$, where "A" is the area of geometry and $A' = dA/dz$ [8]. So, we can define three types of geometries depending on change in area of the geometry. If $A' = 0$ we have planar geometry, for $A' > 0$ we have widening geometry and for $A' < 0$ we have contracting geometry [1]. In this paper only widening geometry of spherical and cylindrical shape will be discussed. We have proved mathematically and graphically that the expanding area of geometry can accelerate charged particles. There are many practical applications in which effects of widening geometry are important. Some of these applications are plasma nozzle, plasma probe, limiters and diverters of tokamak, magnetoplasmadynamic thruster, Hall thruster, and the variable specific impulse magnetoplasma rocket (VASIMR) [9,10,11].

BASIC MODEL AND EQUATIONS

In this paper the effects of expanding area of geometry on one dimensional plasma (along z-axis) in front of a wall is discussed. Assuming the wall at $z = z_w$ and sheath edge at $z = x = 0$. As $z \to -\infty$ we have quasi neutral plasma [5]. On the left side of the sheath edge is the presheath and on right side is sheath. The ionization rate in the plasma depends

on the source of ionization. There are collisions in the plasma of mean free path λ. Our case is time independent. We are assuming hot ions $(T_i \neq 0)$ in the absence of applied magnetic field. The electric field **E** is in z direction only. As shown in the Fig. 1 below.
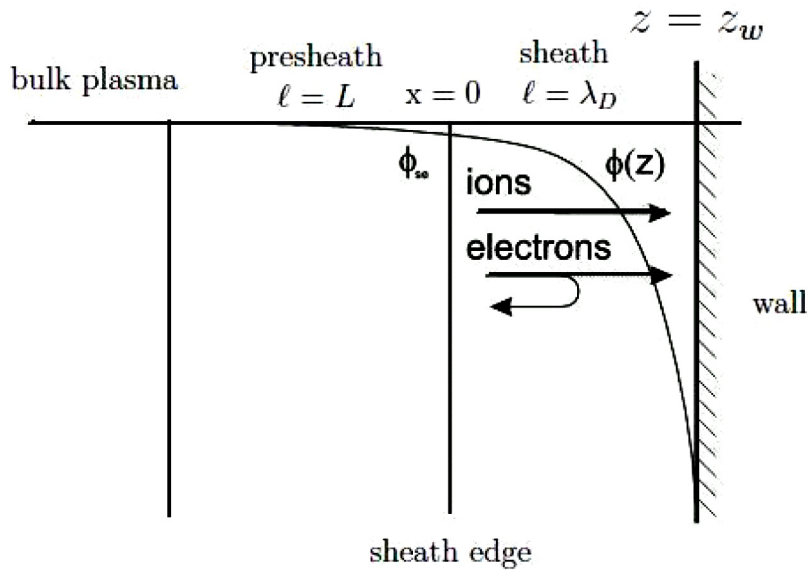
Fig. 1. Plasma wall interaction

For one dimensional case

$$\mathbf{v_i} = v_i \mathbf{e_z}, \qquad \nabla = \mathbf{e_z} \frac{d}{dz}, \qquad div = \frac{1}{A}\frac{dA}{dz} = \frac{A'}{A}. \tag{1}$$

Where A is the area, which specify the geometry of the plasma. For spherical shape we have $A = 4\pi(R \pm z)^2$ [12]. Here the plasma region is described by $z < 0$ and sheath edge is at $z = 0$. Momentum balance equation for such a system is of the form,

$$m_i v_i \frac{dv_i}{dz} + e\frac{d\phi}{dz} + \frac{\gamma_i kT_i}{n_i}\frac{dn_i}{dz} = -\left(v_{ci} + \frac{S_i}{n_i}\right)m_i v_i. \tag{2}$$

Equation of continuity, in one dimension along z axis is,

$$\frac{d}{dz}(n_i v_i) = S_i - \frac{A'}{A}n_i v_i. \tag{3}$$

Poisson's equation is,

$$\frac{d^2\phi}{dz^2} + \frac{A'}{A}\frac{d\phi}{dz} = -\frac{e}{\varepsilon_0}(n_i - n_e) \tag{4}$$

and Boltzman's relation for electrons is,

$$n_e = n_0 e^{(e\phi/kT_e)}. \tag{5}$$

Normalization

The normalization variables are,

$$s = \frac{z}{\ell}, \quad \varphi = -\frac{e\phi}{kT_e}, \quad \hat{n}_{i,e} = \frac{n_{i,e}}{n_0}, \quad u = \frac{v_i}{c_s}, \quad v(u) = \frac{L}{c_s}v_{ci},$$

$$\sigma = -\frac{L}{c_s}\frac{S_i}{n_s}, \quad a = \frac{L}{A}\frac{dA}{dz}, \quad \tau = \frac{\gamma T_i}{T_e + T_i}, \tag{6}$$

where

$$c_s = \sqrt{\frac{kT_e + \gamma kT_i}{m_i}}, \qquad \lambda_D = \sqrt{\frac{\varepsilon_0 kT_e}{n_0 e^2}}. \tag{7}$$

Using eqn. (6) and eqn. (7) our normalized set of equations is,
Boltzman's relation

$$\hat{n}_e = e^{-\varphi}. \tag{8}$$

Poission's equation.

$$\hat{n}_i - \hat{n}_e = \frac{\lambda_D^2}{\ell^2}\left(\frac{d^2\varphi}{ds^2} + a\frac{\ell}{L}\frac{d\varphi}{ds}\right). \tag{9}$$

Continuity equation.

$$\frac{d}{ds}\left(\hat{n}_i u\right) = \frac{\ell}{L}\left(\sigma - a\hat{n}_i u\right). \tag{10}$$

Momentum balance equation.

$$u\frac{du}{ds} - \frac{d\varphi}{ds} = -\frac{\ell}{L}\left(v + \frac{\sigma}{\hat{n}_i}\right)u - \tau\left(\frac{1}{\hat{n}_i}\frac{d\hat{n}_i}{ds} - \frac{1}{\hat{n}_e}\frac{d\hat{n}_e}{ds}\right). \tag{11}$$

Eqn. (8), eqn. (9), eqn. (10), and eqn. (11), i.e, Boltzman's relation, Poission's equation, continuity equation, and momentum balance equation respectively are basic equation of our model in normalized form. It is important for practical applications to study the transition from the presheath to sheath region for $\varepsilon = \lambda_D/L \to 0$ [1].

Asymptotic sheath theory

In inner region or sheath region scale length is Debye length $\ell_i = \lambda_D$. In this region the space coordinate changes to $\xi = s_i = z/\lambda_D$. So, Poisson's eqn. (9) for sheath region in limiting case $\varepsilon = \lambda_D/L \to 0$, is

$$\hat{n}_i - \hat{n}_e = \frac{d^2\varphi}{d\xi^2}. \tag{12}$$

Continuity eqn. (10) for sheath region in limiting case $\varepsilon = \lambda_D/L \to 0$, becomes,

$$\frac{d}{d\xi}\left(\hat{n}_i u\right) = o\left(\varepsilon\right) \tag{13}$$

and momentum eqn. (11) for sheath region in limiting case $\varepsilon = \lambda_D/L \to 0$, becomes,

$$u\frac{du}{d\xi} - \frac{d\varphi}{d\xi} + \tau\left(\frac{1}{\hat{n}_i}\frac{d\hat{n}_i}{d\xi} - \frac{1}{\hat{n}_e}\frac{d\hat{n}_e}{d\xi}\right) = o\left(\varepsilon\right). \tag{14}$$

If we plot φ verses ξ, at the sheath edge $\varphi \to 0$ [12].

Asymptotic presheath theory

In outer region or presheath region we have scale length $\ell_0 = L$. In this region the space coordinate is $x = s_0 = z/L$. Poission's eqn. (9) for the presheath region in limiting case $\varepsilon = \lambda_D/L \to 0$, is

$$\hat{n}_i - \hat{n}_e = o\left(\varepsilon^2 \frac{d^2\varphi}{dx^2}\right). \tag{15}$$

Continuity eqn. (10) for the presheath region becomes

$$\frac{d}{dx}\left(\hat{n}_i u\right) = \sigma - a\hat{n}_i u, \tag{16}$$

and momentum eqn. (11) for the presheath region in limiting case $\varepsilon = \lambda_D/L \to 0$, using eqn. (16) after simplification becomes,

$$\left(u - \frac{1}{u}\right)\frac{du}{dx} = a - \frac{\sigma}{\hat{n}_i}\left(u + \frac{1}{u}\right) - vu. \tag{17}$$

Eqn. (17) shows when $u = 1$, we have a singular point and this point is known as sheath edge. It is the point at which quasi neutrality breaks down from the presheath side. If we plot φ verses x, at the sheath edge $\varphi \to \infty$ [13]. It has been observed that the asymptotic solutions of the potential profiles for plasma presheath and sheath for very small but finite value of λ_D/L do not match smoothly. The asymptotic presheath solution at the sheath edge turns into a singularity $d\phi/dz \to -\infty$ and on the other hand on sheath scale (z/λ_D) the sheath edge is characterized by $(d\phi/dz \to 0)$ [14]. In order to have smooth transition intermediate scale had been used in literature.

Intermediate scale

For intermediate scale, space coordinate is ζ and is defined as $\zeta = z/\ell_m$. Using $\varphi = 0$, $u = 1$, $\hat{n}_i = \hat{n}_e = 1$, and $\frac{d\hat{n}_e}{d\varphi} = \frac{d\hat{n}_i}{d\varphi} = -1$ which are values of different variables at the sheath edge [8]. Hence at the sheath edge eqn. (17) can be written as,

$$\left(u - \frac{1}{u}\right)\frac{du}{dx} = a_s - 2\sigma_s - v_s. \tag{18}$$

Where "s" denotes the value of different variables at the sheath edge. Using Boltzman's relation for electrons, "u" can be written as $u = 1 + \varphi$. At $u = 1$ eqn. (18) shows a singularity. For singular transition right hand side of eqn. (18) can be taken equal to -1. Substituting the value of $u = 1 + \varphi$ and after simplification eqn. (18) becomes

$$\varphi^2 + x = o\left(\varepsilon^2 \frac{d^2\varphi}{dx^2}\right). \tag{19}$$

Using Boltzman's relation, eqn. (14) which is the momentum equation for sheath region and Poission's equation, i.e, eqn. (12) we get

$$\frac{d^2\varphi}{d\xi^2} = \frac{\varphi^2}{1-\tau} + o(\varepsilon\xi). \tag{20}$$

The relation between space coordinates of sheath, presheath and intermediate scale is $\left(\zeta = \frac{z}{\ell_m} = \frac{L}{\ell_m}x = \frac{\lambda_D}{\ell_m}\xi\right)$. Using this relation eqn. (19) for intermediate scale is

$$\varphi^2 + \frac{\ell_m}{L}\zeta = o\left(\frac{\lambda_D^2}{\ell_m^2}\frac{d^2\varphi}{d\zeta^2}\right), \tag{21}$$

and eqn. (20) is,

$$\frac{\lambda_D^2}{\ell_m^2}\frac{d^2\varphi}{d\zeta^2} = \frac{\varphi^2}{1-\tau} + o\left(\frac{\ell_m}{L}\zeta\right), \tag{22}$$

Eqn. (20) and eqn. (22) have uniform representation so, using this property and $w = \left(\frac{L}{\ell_m}\right)^{\frac{1}{2}}\varphi = -\left(\frac{L}{\ell_m}\right)^{\frac{1}{2}}\frac{e\phi}{kT_e}$, $\ell_m = (1 - \tau_s)^{2/5}\lambda_D^{4/5}L^{1/5}$ we get [9],

$$\frac{d^2w}{d\zeta^2} = w^2 + \zeta. \tag{23}$$

Equation (23) is universal differential equation for intermediate scale which had been widely used in literature to explain the variation of potential and electric field in intermediate scale. Eqn. (23) for inner expansion of outer solution gives presheath solution and for outer expansion of inner solution gives sheath solution [5,13,14]. So, far we have discussed some of the basic equations in plasma-wall transition which have already been developed to explain the mechanism of plasma wall transition. In the following section a new equation will be developed using equations of

presheath and intermediate scale which will explain effect of geometry in presheath.

Generalized equation for Presheath

The generalized equation for presheath scale having the effect of geometry, ionization and collision can be developed using momentum balance equation for presheath. The reduced form of eqn. (17), using equation of continuity for the presheath region and eqn. (19) is

$$2\varphi\frac{d\varphi}{dx} = -2\sigma - v\left(1+\sqrt{-x}\right) + a. \tag{24}$$

On R.H.S of this equation first term is for ionizational effect, 2nd for collisional effect and third for geometrical effects in the presheath region.

RESULTS AND DISCUSSION

We can deduce some of the important results from equation (24). We are mainly focusing on geometrical effects with and without ionization and collision. These effects are discussed one by one with graphical presentation in the following sections.

Geometrical effects $\left(\sigma = 0,\ v = 0,\ a \neq 0\right)$

In the absence of ionization $\left(\sigma = 0\right)$, and collisions $\left(v = 0\right)$, the important factor is A'/A [10]. Change in area of geometry will affect only presheath region. Assuming cylindrical and spherical geometries the effect of change in area of geometry will be discussed in this section.

Spherical geometry

For spherical geometry of area " A " the presheath region in front of a spherical geometry have $a = -2\left/\left(\frac{r}{L}-x\right)\right.$.

In this case eqn. (24) can be written as

$$\varphi = -\sqrt{2\ln\left(\frac{r}{L}-x\right)+c}. \tag{25}$$

The dependence of potential behavior on radius of spherical probes can be seen from the following plot (Fig. 2). We are using $r_1 = 0.8$ mm, $r_2 = 0.4$ mm, $r_3 = 0.1$ mm, $r_4 = 0.04$ mm, and $L = 4.5$ mm [15]. From the Fig. 2 it is obvious that at the sheath edge there is an electric field even in the absence of ionization and collision in plasma for spherical geometry. The value of potential at sheath edge decreases with the increase in radius of the sphere.
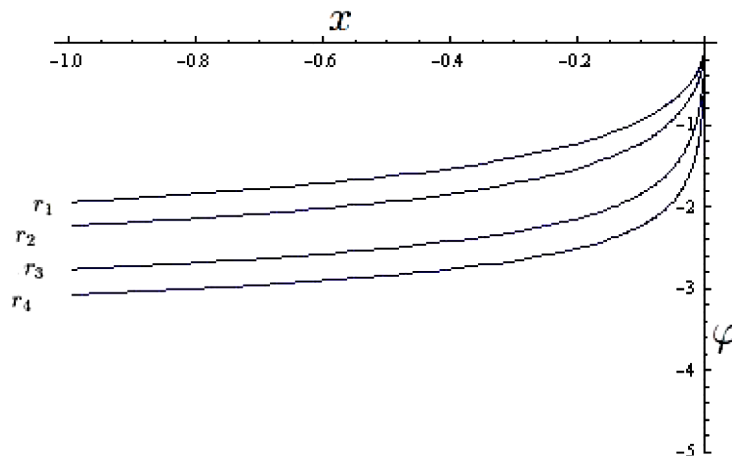
Fig. 2: Variation of φ with x for different values of radius of spherical probe

Cylindrical geometry

The presheath region in front of a cylinder of radius "r" and height "h" is described by, $A = 2\pi\left(r - z\right)h$.

Considering geometrical effects and substituting $a = -1\left/\left(\frac{r}{L}-x\right)\right.$ for cylindrical geometry, eqn.(24) can be written as

$$\varphi = -\sqrt{\ln\left(\frac{r}{L} - x\right) + c}.$$ (26)

Using sheath edge conditions and for cylindrical probe of different values of radius and height (r_1, h_1)=(95 μm, 60 mm), (r_2, h_2)=(47.5 μm, 30 mm), (r_3, h_3)=(25 μm, 15 mm), and (r_4, h_4)=(8 μm, 7 mm) and L = 130 mm we get φ verses x as shown in Fig. 3 [16,17]. Again it is clear from the plot that at the sheath edge there is an electric field even in the absence of ionization and collision in plasma for cylindrical geometry. The value of potential at sheath edge decreases with the increase in radial size of the cylinder.
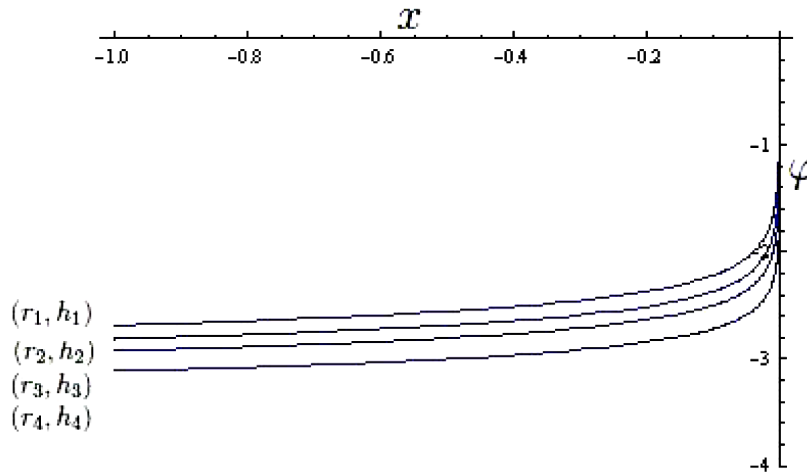
Fig. 3. Variation of φ with x for different values of radius and length of cylindrical probe

Collisionless case $\left(v = 0, \ \sigma = constant, \ a \neq 0\right)$

If we add effect of ionization in the presence of varying area of geometry then there will be no change in sheath region. Considering constant ionization rate $\left(\sigma = 1\right)$ and taking $v = 0$, eqn. (24) after integration for spherical geometry can be written as

$$\varphi = -\sqrt{-2x + 2\ln\left(\frac{r}{L} - x\right) + c}.$$ (27)

Where "c" is the constant of integration which can be calculated using boundary conditions and using characteristic of geometry. Whereas for cylindrical geometry eqn. (27) is

$$\varphi = -\sqrt{-2x + \ln\left(\frac{r}{L} - x\right) + c}.$$ (28)

In this case we can see from curves (b) in Fig. 4 and Fig. 5 that more potential penetrates into the presheath region from the wall. The main reason is that in this case more number of electrons gain energy from ionization source and reach the wall and develop more negative potential on the wall as compared to geometrical effects only.

No ionization case $\left(\sigma = 0, \ v = constant, \ a \neq 0\right)$

Now we are considering combined effect of geometry and colllisions on the structure of plasma presheath without any ionization source just like collision dominated plasma in fusion devices. Considering constant collisions frequency and taking $\sigma = 0$, eqn. (24) after integration using boundaries conditions for spherical geometry becomes

$$\varphi = -\sqrt{-x\left(1 + \frac{2}{3}\sqrt{-x}\right) + 2\ln\left(\frac{r}{L} - x\right) + c}.$$ (29)

For cylindrical geometry eqn. (29) becomes

$$\varphi = -\sqrt{-x\left(1 + \frac{2}{3}\sqrt{-x}\right) + \ln\left(\frac{r}{L} - x\right) + c}.$$ (30)

Again in this case we can see from the from curves (c) in Fig. 4 and Fig. 5 that more potential penetrates from wall into the presheath region due to small collisional cross section of electrons neutral collisions as compared to ions neutral collisional cross section. Hence electrons reach the wall in very short duration of time and develop more negative potential on the wall.

Combined effect of constant ionization rate, constant collision frequency and geometry
$$\left(\sigma = constant, \ \ v = constant, \ \textbf{and} \ \ a \neq 0\right)$$

If we consider constant collision frequency, constant ionization rate and take geometrical effects then after integration eqn. (24), using boundaries conditions for spherical geometry becomes

$$\varphi = -\sqrt{-x\left(3 + \frac{2}{3}\sqrt{-x}\right) + 2\ln\left(\frac{r}{L} - x\right) + c}. \tag{31}$$

Whereas for cylindrical geometry eqn. (31) becomes

$$\varphi = -\sqrt{-x\left(3 + \frac{2}{3}\sqrt{-x}\right) + \ln\left(\frac{r}{L} - x\right) + c}. \tag{32}$$

From curves (d) in Fig. 4 and Fig. 5, we can see that the penetration of the potential of the wall in the case of combined effect of ionization, collision and geometry is more than as that of only geometrical effects, combined effect of geometry and either of the ionization and collision. This is due to the reason that electrons which are more mobile as compared to ions, in the presence of ionization source and collisions in plasma quickly reach the wall due to high energy as compared to without ionization source and collisions in plasma. Hence electrons develop more negative potential on the wall as compared to in the presence of geometrical effects only.
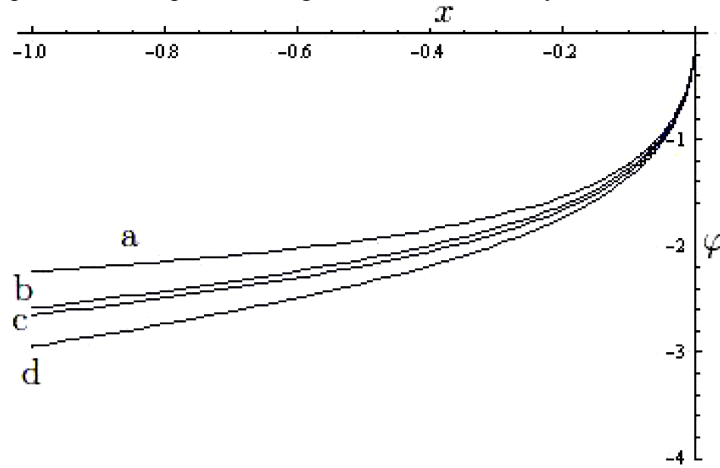
Fig. 4. Variation of φ with x for spherical geometry considering (a) Only geometry (b) Geometry and constant ionization rate (c) Geometry and constant collision frequency (d) Geometry, constant ionization rate and constant collision frequency
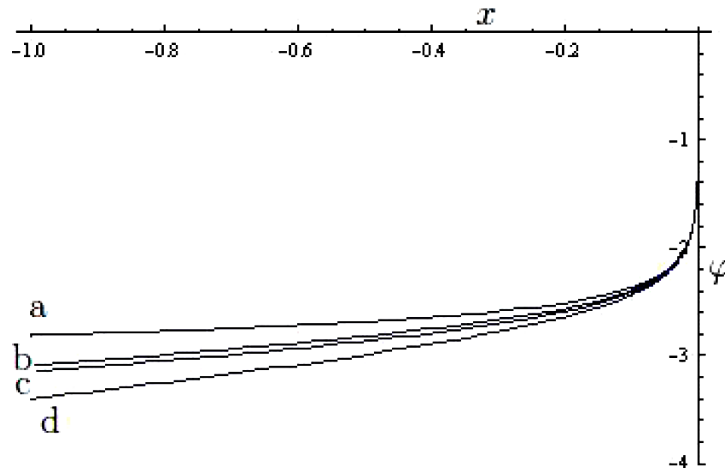
Fig. 5. Variation of φ with x for cylindrical geometry considering (a) Only geometry (b) Geometry and constant ionization rate (c) Geometry and constant collision frequency (d) Geometry, constant ionization rate and constant collision frequency

CONCLUSION

The presheath structure depends on ionization, collisions, and geometry in the absence of applied magnetic field. The geometrical effects play important role in ion dynamics in the presheath region and the expanding area of cylindrical or spherical geometry can accelerate ions even in the absence of ionizations and collisions in plasma. If we assume only geometrical effects, just like plasma in expanding area of loval nozzle, in the absence of collisions and ionization source, then there will be no effect on the sheath region. If we increase the area of spherical or cylindrical geometry then for a geometry of larger area at the sheath edge less amount of negative potential penetrates into plasma. If we assume collisionless plasma, in the presence of geometrical effects and ionization source just like in Tonks Langmuir problem, then sheath region remains same as without effects of ionization. Whereas more potential of the wall penetrates into the presheath region as compared to without effect of ionization. If we assume collisions dominated plasma in the presence of geometrical effects without any ionization source then, again there will be no effect on sheath region. On the otherhand both collisional effects and geometrical effects accelerate ions in the presheath region and more potential of the wall penetrates into the presheath region as compared to without effects of collisions. If we summarize above discussion we can say that in the presence of effects of ionization or collision in addition to geometrical effects for cylindrical and spherical geometries more negative potential of the wall penetrates into the presheath region. However sheath region is universal and does not depend on either of ionization, collisions or geometry.

REFERENCES

1. Riemann K.U. The Bohm criterion and sheath formation // J. Phys. D: Appl. Phys. – 1991. – Vol. 24. – P.493.
2. Langmuir I. Oscillation in ionized gases // Proc. Natl. Acad. Sci. – 1928. – Vol.14. – P.626-627.
3. Riemann K.U. Consistent analysis of a weakly ionized plasma and its boundary layer // phys. Fluids B. – 1993. – Vol.3. – P.456.
4. Caruso A., Cavaliere A. The structure of the collisionless plasma-sheath transition // Nuovo Cimento. – 1962. – Vol.26. – P.1389.
5. Riemann K.U. The plasma sheath matching problem // J. Tech. Phys. – 2005. – Vol. 41. – No.1- P.89-90.
6. Lieberman M A and Lichtenberg A J. Principles of Plasma Discharges and Materials Processing. Ch.5.-New York: Wiley, 1994. – P.123-125.
7. Riemann K.U. Tsendin L. Unipolar ion sheath // J. Appl. Phys. – 2001. – Vol.90. – No.11. – P.5487-5490.
8. Valentini H.B. Two-Fluid Theory of Presheath and Space Charge Sheath in Low Pressure Plasmas // Contributions to Plasma Physics. – 1991. – Vol. 31. – P.221-229.
9. Tonks L. and Langmiur I. A General Theory of the Plasma of an Arc // Phys. Review Letters. – 1929. – Vol. 34. – P.876.
10. Riemann K.U., Meyer P. Bohm criterion for the collisional sheath - comment // Physics of plasmas. – 1996. – Vol. 3. – No.12. – P.4751-4753.
11. Escobar D., Ahedo E. Low frequency azimuthal stability of the ionization region of the hall thruster discharge // Physics of Plasmas. – 2014. – Vol. 21. – No.4. – P.043505.
12. Riemann K.U. Theory of plasma sheath transition // J. Tech. Phys. – 2000. – Vol. 41. – No.1- P.89-121.
13. Riemann K.U. The influence of collisions on the plasma sheath transition // Physics of plasmas. – 1997. – Vol.4. – No.11. – P.4158-4166.
14. Riemann K.U. Theory of the plasma-sheath transition in an oblique magnetic-field // Contributions to Plasma Physics. – 1994. – Vol. 34. – No.2. – P.127-132.
15. Martinez M., Ahedo E. Magnetic mirror effects on a collisionless plasma in a convergent geometry // Physics of Plasmas. – 2011. – Vol.18. – P.033509.
16. Lieberman M.A., Lichtenberg A.J. Principles of Plasma Discharges and Materials Processing. Ch.3. – New York: Wiley, 1994. – 180 p.
17. Ahedo E., Escobar D. Two-region model for positive and negative plasma sheaths and its application to Hall thruster metallic anodes // Physics of Plasmas. – 2008. – Vol. 15. – P.23-28.

CABLE FREE TRANSMISSION OF ELECTRICITY: FROM NIKOLA TESLA TO OUR TIME

B.V. Borts[1], I.V. Tkachenko[1], V.I. Tkachenko[1,2]

[1] *National Science Center "Kharkov Institute of Physics and Technology"*
The National Academy of Sciences of Ukraine
61108, Kharkov,1, Akademicheskaya str., tel./fax 8-057-349-10-78
[2] *V.N. Karazin Kharkiv National University*
61022, Kharkov,4, Svobody sq., tel./fax 8-057-705-14-05
E-mail: tkachenko@kipt.kharkov.ua

Model of Earth charge resonant oscillations excitations based on Tesla experiment, was offered. Solutions of d'Alembert wave equations for electric and magnetic potentials of the charged perfectly conductive sphere were found. Graphic analyses of perturbed potential distribution on the Earth surface was provided. It was shown that obtained solution provides adequate description of Tesla experiment on wireless transfer of electricity conducted in Colorado Springs in 1899 – 1900. In the very low-frequency area of the electro-magnetic oscillations spectrum it was offered to consider the Earth as capacitors battery, consisting of two put one into another perfectly conductive spheres, between which thin dielectric layers is placed. Own oscillation frequencies of the Earth charge were determined in this area. It was shown that these frequencies most precisely correspond to experimentally measured Schumann resonances.

KEYWORDS: Tesla's experiment, electricity on the Earth, cable free transmission, potential distribution, very low-frequency of the electro-magnetic oscillations, Schumann resonance frequency

БЕСПРОВІДНА ПЕРЕДАЧА ЕЛЕКТРИКИ: ВІД МИКОЛИ ТЕСЛА ПО ТЕПЕРІШНІЙ ЧАС
Б.В. Борц[1], І.В. Ткаченко[1], В.І. Ткаченко[1,2]
[1] *Національний науковий центр "Харківський фізико-технічний інститут"*
Національної академії наук України,
61108, г. Харків, вул. Академічна 1, tel./fax 8-057-349-10-78
[2] *Харківський національний університет імені В.Н. Каразіна,*
61022, г. Харків, пл. Свободи 4, tel./fax 8-057-705-14-05

Запропоновано модель збудження резонансних коливань заряду Землі, заснована на експериментах Тесли. Знайдено рішення хвильових рівнянь Даламбера для електричного і магнітного потенціалу зарядженої, ідеально провідної сфери. Надано графічний аналіз розподілу збуреного потенціалу на поверхні Землі. Показано, що отримане рішення адекватно описує експерименти Тесли по бездротовій передачі електрики, що проведені в Колорадо-Спрінгс в 1899 - 1900 р.р.
У наднизькочастотній області спектра електромагнітних коливань запропоновано розглядати Землю як конденсаторну батарею, що складається з двох вкладених одна в іншу ідеально проводять сфер, між якими знаходиться тонкий діелектричний прошарок. У цій області частот визначені власні частоти коливань заряду Землі. Показано, що ці частоти найбільш точно відповідають експериментально виміряним першим резонансам Шумана.

КЛЮЧОВІ СЛОВА: експеримент Тесли, електрика Землі, бездротова передача, розподіл потенціалу, наднизькочастотні електромагнітні коливання, резонанси Шумана

БЕСПРОВОДНАЯ ПЕРЕДАЧА ЭЛЕКТРИЧЕСТВА: ОТ НИКОЛЫ ТЕСЛА ДО НАШЕГО ВРЕМЕНИ
Б.В. Борц[1], И.В. Ткаченко[1], В.И. Ткаченко[1,2]
[1] *Национальный научный центр "Харьковский физико-технический институт"*
Национальной академии наук Украины,
61108, г. Харьков, ул. Академическая 1, tel./fax 8-057-349-10-78
[2] *Харьковский национальный университет имени В.Н. Каразина,*
61022, г. Харьков, пл. Свободы 4, tel./fax 8-057-705-14-05

Предложена модель возбуждения резонансных колебаний заряда Земли, основанная на экспериментах Теслы. Найдены решения волновых уравнений Даламбера для электрического и магнитного потенциала заряженной, идеально проводящей сферы. Дан графический анализ распределения возмущенного потенциала на поверхности Земли. Показано, что полученное решение адекватно описывает эксперименты Тесла по беспроводной передаче электричества, проведенные в Колорадо-Спрингс в 1899 - 1900 г.г. В сверхнизкочастотной области спектра электромагнитных колебаний предложено рассматривать Землю как конденсаторную батарею, состоящую из двух вложенных одна в другую идеально проводящих сфер, между которыми находится тонкая диэлектрическая прослойка. В этой области частот определены собственные частоты колебаний заряда Земли. Показано, что эти частоты наиболее точно соответствует экспериментально измеренным первым резонансам Шумана.

КЛЮЧЕВЫЕ СЛОВА: эксперимент Теслы, электричество Земли, беспроводная передача, распределение потенциала, сверхнизкочастотные электромагнитные колебания, резонансы Шумана

Idea of wireless transfer of electric energy appeared with physicists and engineers almost simultaneously with formation of electrical engineering science as and independent area of techniques (1870-1890). During this and further

periods of formation and development, the electrical devices are based on wire electric energy transfer. It is obvious that transfer of a large quantity of energy through wires constitutes a complicated task.

In case of wireless transfer of electric energy the task becomes much more complicated. However some economic advantages of this method (economy of conducting metal, construction materials, simplification of circuits architecture) give a basis for research of such method of electric energy transfer.

Nikola Tesla is considered to be the pioneer in the field of wireless transfer of electric energy [1].

In Colorado-Springs laboratory (1899-1900) Tesla conducted test of wireless energy transfer system, using the giant high-frequency transformer with frequency $\omega_0 = 1.5 \cdot 10^5$ Hz and wave length $\lambda_0 = 2 \cdot 10^3$ m for the first time [2].

In his experiments he switched on 200 electric bulbs placed 26 miles ($\approx$ 42 km) away from his laboratory. Power of each bulb constituted 50W, and the total energy consumption constituted 10 kW or 13,6 h.p. According to Tesla calculations coefficient of efficiency of energy transfer constituted 95%. He asserted that by means of 300-power vibrator he could switch-on dozen of electric garlands each consisting of 200 bulbs placed in different parts of the earth.

Very soon after this experiments Tesla moved to New York, on Long Island and further did not work on the wireless electricity transfer topic.

German electrical engineer Winfried Otto Schumann studied the transfer of electric signals in the very-low frequency area of frequency spectrum. In 1952 he used the model of resonator of the Earth-ionosphere cavity for description of such wave processes [3]. Schumann discovered the resonance frequency of electric signals, which were later called "Schumann resonances". These resonances constitute set of picks in the frequency spectrum which are created by standing electromagnetic waves between the Earth conducting surface and external conducting border of the ionosphere. Dimensional analyses using the light speed c and length of earth circle $2\pi R_E$ allowed him to determine the frequency order for minimally possible resonance $\omega_E = c/2\pi R_E = 7.5$ Hz.

It is interesting to note that long before this in Colorado-Springs, Tesla, while studying the thunderstorm activity of the local area, also discovered the resonance fluctuations of the Earth electric field in this frequency range. But there were continuation of the experiments as he started the experiments on the wireless electricity transfer.

Thus the described above experiments demonstrate the possibility of wireless transfer of electricity and electrical signals either in high-frequency or in very low-frequency range of frequencies.

At present time the topic of Schumann resonances attracts the interest of researches not only from the point of their theoretical description but also due to the possibility of their practical implementation. Schumann resonances theory is presented in monograph [4]. Numerical methods of such resonances description based on their presentation in the form of standing waves in the Earth ionosphere provide the results comparable with real data [5].

From the practical point of view, Schumann resonances can be used for transfer of electrical signals on the long distances. They are closely connected with global thunderstorm activity of the Earth and correspondingly can become an instrument for climate research. Schumann resonances can also be involved for the research of changes in the lower ionosphere of the Earth, earthquake forecasts, and research of other celestial bodies' properties.

At present time another type of wire transfer of electric energy becomes relevant – wireless charging and power supply units.

Phenomenon of electromagnetic induction is used in such systems for energy transfer from the source (transmitter) to the receiver, which is explained by appearance of the electric current in the closed circle under change of magnetic flux running through this circle. However the distance of electric energy transfer is small under this method and cannot be compatible with methods presented above.

Summarizing the mentioned above it can be stated that practical solution of the problem of wireless transfer of electricity on the long distances, despite rather well-grounded theoretical study of this issue, remains in the condition close to initial stage.

Aim of paper. The present paper offers physical maximally approached to Tesla experiment condition, model of resonance oscillations of the Earth charge. Estimation of resonance frequencies in the high-frequency and very-low frequency area of wave spectrum were conducted using the proposed model.

THEORETICAL MODEL

Let's consider the model for conducting the wireless transfer of electricity. In this model, in the equilibrium state the Earth constitutes the rigid ideally conductive sphere on which the negative charge is evenly distributed. The equilibrium state means absence of charges motion in the sphere. Assumption on the ideal conductivity of the sphere is based on a rather high level of ground conductivity. High conductivity of the ground was demonstrated in Tesla experiments for many times and also is confirmed with its use for ground connection of different electrical devices

Estimations of the Earth charge from different sources provide the following value, for example, $q_E = -5.7 \cdot 10^5$ κ[6], or $q_E = -6.0 \cdot 10^5$ κ[7,8].

When calculating in equilibrium state, we will model the Earth as ideally conducting rigid sphere with surface

charge $\sigma_E = Q_E / 4\pi R_E^2$ taking as a basis the Earth charge $Q_E = -6.0 \cdot 10^5$ C. Here $R_E = 6.3710 \cdot 10^6$ m – is an average radius of the Earth [6].

As it follows from Gauss theorem in the equilibrium state, intensity of electric field is equal to $\vec{E}_E(r) = \dfrac{Q_E}{r^2}\dfrac{\vec{r}}{r}$

for radiuses $r > R_E$. Potential corresponding to this field is specified with the expression $\varphi_E(r) = Q_E / r$.

Charge oscillations on the sphere e $\tilde{q}(\vec{r},t) = q(\vec{r},t) - Q_E$ caused from outside, result in formation of perturbed scalar potential $\tilde{\varphi}(\vec{r},t) = \varphi(\vec{r},t) - \varphi_E(r)$ and corresponding disturbed current density $\tilde{\vec{j}}(\vec{r},t)$.

Let's determine the relation of the perturbed charge with the perturbed potential which was realized in Tesla experiments.

In this experiments the perturbed charges were created by transfer of part of the Earth charge which, in the simplified form, can be presented as spherical capacitor with capacity C_E and full charge Q_E on the attached to it spherical capacitor with significantly lower capacity C_{Sp} $\left(C_{Sp} << C_E \right)$ and charge Q_{Sp} . Spherical capacitors with capacity C_E and C_{Sp} are connected to the battery in-parallel as the negative plates of the capacitors are connected to the same contact. When the capacitors are connected in-parallel the total charge is constant and is equal Q_E and the potential difference on the capacitors is the same, so the expressions are true:

$$\frac{\tilde{q}(\vec{r},t)}{C_{Sp}} = \varphi_E(R_E) + \tilde{\varphi}(\vec{r},t),$$

$$\frac{Q_E - \tilde{q}(\vec{r},t)}{C_E} = \varphi_E(R_E) + \tilde{\varphi}(\vec{r},t) \qquad (1)$$

Connection of perturbed charge with perturbed potential $\tilde{q}(\vec{r},t) = -C_E \tilde{\varphi}(\vec{r},t)$ follows from the second equality (1).

Dependence of oscillations of scalar $\tilde{\varphi}(\vec{r},t)$ and vector $\tilde{\vec{A}}(\vec{r},t)$ potentials on perturbed charge density and current density on the sphere with capacity C_E is described with D'Alembert equations [9]:

$$\Delta\tilde{\varphi}(\vec{r},t) - \frac{1}{c^2}\frac{\partial^2}{\partial t^2}\tilde{\varphi}(\vec{r},t) = -4\pi\tilde{\rho}(\vec{r},t),$$

$$\Delta\tilde{\vec{A}}(\vec{r},t) - \frac{1}{c^2}\frac{\partial^2}{\partial t^2}\tilde{\vec{A}}(\vec{r},t) = -\frac{4\pi}{c}\tilde{\vec{j}}(\vec{r},t), \qquad (2)$$

on condition of gauge invariance

$$\text{div}\tilde{\vec{A}}(\vec{r},t) = -\frac{1}{c}\frac{\partial}{\partial t}\tilde{\varphi}(\vec{r},t),$$

where $\tilde{\rho}(\vec{r},t) = \rho(\vec{r},t) - \rho_E$, $\tilde{\rho}(\vec{r},t) = \tilde{q}(\vec{r},t)/V_E$, $\rho(\vec{r},t) = q(\vec{r},t)/V_E$, $\rho_E = Q_E/V_E, V_E$ - the Earth volume, c - light speed, Δ - Laplace operator, t - time, $\vec{r}$ - spatial value.

Solution of equations (2) should correspond to the condition of potentials limitation on the infinity: $\left| \tilde{\varphi}(\vec{r},t), \tilde{\vec{A}}(\vec{r},t) \right| = O(1/r)$ under $r \to \infty$, and also their limitation on the sphere surface: $\left| \tilde{\varphi}(\vec{r},t), \tilde{\vec{A}}(\vec{r},t) \right| < \infty$ under $r = R_E$.

It follows from the gauge invariance that in conditions of Tesla experiments, the oscillated vector potential $\tilde{\vec{A}}(\vec{r},t)$ is of the same order with the oscillated scalar potential as $\left| \tilde{\vec{A}}(\vec{r},t) \right| \Big/ \left| \tilde{\varphi}(\vec{r},t) \right| \approx \lambda_0\omega_0/c = 1$.

Thus while studying the task of wireless transfer of electricity, space time change of vector potential $\tilde{\vec{A}}(\vec{r},t)$ should be described together with the change in space of the time of scalar potential $\tilde{\varphi}(\vec{r},t)$.

It can be shown from the continuity equation and condition of gauge invariance taking into account $\tilde{\rho}(\vec{r},t) = -C_E \tilde{\varphi}(\vec{r},t)/V_E$, that $\tilde{\vec{j}}(\vec{r},t) = -c \cdot C_E \cdot \tilde{\vec{A}}(\vec{r},t)/V_E$.

Based on the task symmetry, the vector potential has only the radial component i.e. $\tilde{\vec{A}}(\vec{r},t) = (\tilde{A}_r(\vec{r},t),0,0)$.

Thus the equation of radial projection of the vector potential is transferred in the following way:

$$\Delta \tilde{A}_r(\vec{r},t) - \frac{1}{c^2}\frac{\partial^2}{\partial t^2}\tilde{A}_r(\vec{r},t) = 4\pi \frac{C_E}{V_E}\tilde{A}_r(\vec{r},t).$$

Thus in the result of usage of the connections between the oscillated potentials and charges oscillation found above, the equations (2) can be presented in the following way:

$$\Delta \Psi(\vec{r},t) - \frac{1}{c^2}\frac{\partial^2}{\partial t^2}\Psi(\vec{r},t) = 4\pi \frac{C_E}{V_E}\Psi(\vec{r},t) \qquad (3)$$

where $\Psi(\vec{r},t) = \{\tilde{\varphi}(\vec{r},t), \tilde{A}_r(\vec{r},t)\}$ - function, which possesses the value either of the first or of the second expression in braces, $|\Psi(\vec{r},t)| = O(1/r)$ under $r \to \infty$, $|\Psi(\vec{r},t)| < \infty$ under $r = R_E$.

Distorted electric and magnetic field strengths are determined with simple differentiation of scalar and vector potentials: $\tilde{\vec{H}}(\vec{r},t) = \mathrm{rot}\,\tilde{\vec{A}}(\vec{r},t)$, $\tilde{\vec{E}}(\vec{r},t) = -\mathrm{grad}\,\tilde{\varphi}(\vec{r},t) - c^{-1}\partial \tilde{\vec{A}}/\partial t$.

SOLUTION FOR THE DISTORTED ELECTRIC POTENTIAL

Let us consider the equation (3) for the distorted electrical potential of the charged rigid sphere $\tilde{\varphi}(\vec{r},t)$ on condition $|\tilde{\varphi}(\vec{r},t)| < \infty$.

We suppose that its dependence on time in the form $\tilde{\varphi}(\vec{r},t) = \tilde{\varphi}'(\vec{r}) \cdot \exp(-i\omega_0 t)$.

Then the equation (3) for electric potential is transformed into Helmholtz equation [10] for the the perturbed potential:

$$\Delta \tilde{\varphi}'(\vec{r}) + k^2 \tilde{\varphi}'(\vec{r}) = 0 \qquad (4)$$

where $k^2 = \frac{\omega_0^2}{c^2} - 4\pi \frac{C_E}{V_E} = \frac{\omega_0^2}{c^2}\varepsilon(\omega_0)$, $\varepsilon(\omega_0) = \left(1 - \frac{\Omega_e^2}{\omega_0^2}\right)$, $\Omega_e = \sqrt{4\pi c^2 C_E/V_E} \approx 81.189$ Hz – analogue of

Langmuir frequency of sphere electron oscillation, the prime sign is further omitted in notation of distorted potential.

It should be noted that Ω_e frequency is calculated for ideally conducting sphere placed in vacuum when $C_E = R_E$.

In the real situation, the Earth can be presented as capacitors battery consisting of two put one into another spheres with a layer with dielectric capacity $\varepsilon(\omega_0)$ and thickness $d << R_E$ placed between them. Capacity of such capacitors battery will be equal to $C_{EB} = \varepsilon(\omega_0)S_E/4\pi d$, where $S_E = 4\pi R_E^2$ - square of the Earth surface.

This precise definition as to the capacity of the Earth charge does not influence further discussions, but will be used below in order to match the obtained theoretical visions with experimental data.

Lets find the solution of equation (4) for the perturbed scalar potential $\tilde{\varphi}(\vec{r})$.

For this we will pass to spherical coordinates:

$$\frac{1}{r^2}\frac{\partial}{\partial r}\left(r^2\frac{\partial \tilde{\varphi}}{\partial r}\right) + \frac{1}{r^2 \sin\theta}\frac{\partial}{\partial \theta}\left(\sin\theta\frac{\partial \tilde{\varphi}}{\partial \theta}\right) + \frac{1}{r^2 \sin^2\theta}\frac{\partial^2 \tilde{\varphi}}{\partial \varphi^2} + k^2\tilde{\varphi} = 0 \qquad (5)$$

where $r \geq R_E$, $0 \leq \theta \leq \pi$ - polar angle, $0 \leq \varphi \leq 2\pi$ - azimuth angle.

Expression for the perturbed potential we will present in the form of product of two functions depending on radial and angle variables (variable separation method):

$$\tilde{\varphi}(r,\theta,\varphi) = R(r)Y(\theta,\varphi) \qquad (6)$$

After insertion of this expression into equation (6) we receive:

$$\frac{1}{R(r)}\frac{\partial}{\partial r}\left(r^2\frac{\partial R(r)}{\partial r}\right)+k^2r^2 = -\frac{1}{Y(\theta,\varphi)\sin\theta}\frac{\partial}{\partial\theta}\left(\sin\theta\frac{\partial Y(\theta,\varphi)}{\partial\theta}\right)-$$
$$-\frac{1}{Y(\theta,\varphi)\sin^2\theta}\frac{\partial^2 Y(\theta,\varphi)}{\partial\varphi^2}=\nu(\nu+1)$$

(7)

where $\nu(\nu+1)$ – is a constant.

Equations for functions, depending on angles follow from (7):

$$\frac{1}{\sin\theta}\frac{\partial}{\partial\theta}\left(\sin\theta\frac{\partial Y(\theta,\varphi)}{\partial\theta}\right)+\frac{1}{\sin^2\theta}\frac{\partial^2 Y(\theta,\varphi)}{\partial\varphi^2}+\nu(\nu+1)Y(\theta,\varphi)=0$$

(8)

Function depending on radius:

$$\frac{d}{dr}\left(r^2\frac{dR(r)}{dr}\right)+\left(k^2r^2-\nu(\nu+1)\right)R(r)=0$$

(9)

First we will find the solutions of equation (8) for the angles.
In order to divide the variable we assume

$$Y(\theta,\varphi)=\Theta(\theta)\Phi(\varphi).$$

(10)

Then from (9) we receive:

$$\sin^2\theta\left[\frac{1}{\Theta(\theta)\sin\theta}\frac{\partial}{\partial\theta}\left(\sin\theta\frac{\partial\Theta(\theta)}{\partial\theta}\right)+\nu(\nu+1)\right]=-\frac{1}{\Phi(\varphi)}\frac{\partial^2\Phi(\varphi)}{\partial\varphi^2}=\mu^2$$

(11)

where μ - real constant.

Thus from (11) we have two equations for determination of dependence of perturbed potential on angles θ and φ :

$$\sin^2\theta\left[\frac{1}{\Theta(\theta)\sin\theta}\frac{\partial}{\partial\theta}\left(\sin\theta\frac{\partial\Theta(\theta)}{\partial\theta}\right)+\nu(\nu+1)\right]=\mu^2$$

(12)

$$\frac{\partial^2\Phi(\varphi)}{\partial\varphi^2}=-\mu^2\Phi(\varphi).$$

(13)

After insertion of $\cos\theta=x$, the equation (12) is transferred to the following form:

$$(1-x^2)\frac{d^2\Theta(x)}{dx^2}-2x\frac{d\Theta(x)}{dx}+\left[\nu(\nu+1)-\frac{\mu^2}{1-x^2}\right]\Theta(x)=0.$$

(14)

For real $\Theta(x)$, x under integral $\mu=m=0,1,2,3....$ and $\nu=n=0,1,2,3....$ the equation (14) has the solution in the form of attached Legendre polynomials of the n order, rank m :

$$P_{n,m}(x)=(1-x^2)^{\frac{m}{2}}\frac{d^m P_n(x)}{dx^m}=(1-x^2)^{\frac{m}{2}}\frac{1}{2^n n!}\frac{d^{n+m}}{dx^{n+m}}\left[(x^2-1)^n\right],$$

(15)

or in the integral form:

$$P_{n,m}(x)=\frac{(n+1)...(n+m)}{\pi i^m}\int_0^\pi\left(x+\sqrt{x^2-1}\cos\psi\right)^n\cos m\psi\, d\psi\,.$$

(16)

The attached Legendre polynomials are characterized with the following properties:

$$P_{n,0}(x)=P_n(x),\quad m=0;$$
$$P_{n,m}(x)=0,\qquad m>n,$$

(17)

where $P_n(x)$ - Legendre polynomial of the n order.

As it follows from (17) for the attached Legendre polynomials $m=0,1,2,3....,n$ on condition $m\le n$.
Equation (13) for integral value $\mu=m$ is integrated in elementary functions:

$$\Phi(\varphi) = C_1 \cos m\varphi + C_2 \sin m\varphi. \tag{18}$$

Further we calculate that $C_2 = 0$.

Let us find the solution of equation (9) for radial dependence of perturbed potential.

Substitution of a new variable $R(r) = r^{-\frac{1}{2}} U(r)$ into equation (9) makes it the following:

$$\frac{d^2 U(r)}{dr^2} + \frac{1}{r}\frac{dU(r)}{dr} + \left(k^2 - \frac{(n+1/2)^2}{r^2}\right) U(r) = 0. \tag{19}$$

Bessel and Neumann functions of the half-integer order [10, 11] constitute the solution of equation (18). Common solution of the original equation (8) has the following view:

$$R(r) = \left[A_1 J_{n+1/2}(kr) + A_2 N_{n+1/2}(kr) \right] \Big/ \sqrt{kr} \tag{20}$$

where A_1 and A_2 - are the constants.

We consider that A_2 is equal to zero, as when argument kr tends to zero (on the sphere surface under $r = R_E$ it is possible when $k \to 0$) the solution should be limited.

Thus we will write the expression for the perturbed electric potential of the charged sphere:

$$\tilde{\varphi}(r,\theta,\varphi) = B_1 (kr)^{-\frac{1}{2}} J_{n+1/2}(kr) P_{n,m}(x) \cos m\varphi \tag{21}$$

where: $B_1 = A_1 C_1$ - constant determined from border conditions for the solution dependence on radius ; $x = \cos\theta$.

SOLUTION FOR SCALAR AND VECTOR POTENTIALS. CONNECTION TO THE CONDITIONS OF TESLA EXPERIMENT
Scalar potential

Solution (20) should correspond to the border conditions on the sphere surface. As it follows from the experiments conducted by Tesla in Colorado-Springs, perturbations of the Earth charge can be schematically described in the following way: conductor was connected with one end to the specific point of the conductive sphere (the Earth) with capacitance C_E. Capacitor with capacity C_{Sp} was connected to the second part of this conductor with length $l << R_E$. By means of a transformer of his own construction Tesla transferred a specific part of the charge on the capacitor C_{Sp} and then again injected it on the capacitor C_E. Thus at the specific moments of transformer operation, potential was imposed in the specified point on the sphere surface C_E :

$$\tilde{\varphi}(R_E, \theta_0, \varphi_0) = \Phi_0, \tag{22}$$

where Φ_0 - amplitude of the imposed in Tesla experiment potential ($|\Phi_0| << |Q_E/R_E| \approx 10^9$ V).

Based on the border condition (22) the constant in the expression for the perturbed potential on the Earth surface (21) in the point with angle coordinates, for example, $\theta_0 = 0, \varphi_0 = 0$ is determined with the expression:

$$B_1 = \frac{\sqrt{kR_E}}{J_{1/2}(kR_E)} \Phi_0 \tag{23}$$

Thus the solution (21) with a constant (23) describes distribution of the perturbed potential on the Earth surface.

It should be noted that setting of the coordinate of the point of application of the perturbed potential on the Earth surface is automatically determined the position of the pole of the spherical system of coordinates: $r = R_E, \theta_0 = 0, \varphi_0 = 0$.

It goes from the view of the border condition (22), in solution (21) it should supposed that $m = 0$. In this case the perturbed potential is described with Legendre polynomial and does not depend on azimuth angle φ.

Vector potential

We will consider the border conditions for vector potential have the view (22) where it is necessary to replace $\tilde{\varphi}(R_E, \theta_0, \varphi_0) \to \tilde{A}_r(R_E, \theta_0, \varphi_0)$ and $\Phi_0 \to J_0$ where J_0 - amplitude of the currency density in Tesla experiments in the point on pole with coordinates: $r = R_E, \theta_0 = 0, \varphi_0 = 0$.

Then we will write the solution for radial projection of the vector potential:

$$\tilde{A}_r\left(r,\theta,\varphi\right) = D_1\left(kr\right)^{-\frac{1}{2}} J_{n+1/2}\left(kr\right) P_{n,m}\left(x\right)\cos m\varphi, \tag{24}$$

where $D_1 = \dfrac{\sqrt{kR_E}}{J_{1/2}\left(kR_E\right)} J_0$.

Based on the experimental data, taken from [12], meanings of perturbed potential amplitudes and currency density can be estimated: $\Phi_0 \approx \left(3.5....4.0\right)\cdot 10^6$ V, $J_0 \approx 300/S_0$ A/mm^2 where S_0 current-carrying square in the cross-section of the conductor of the secondary coil of Tesla transformer (in mm^2)

Graphic analyses of distribution of the perturbed electric potential on the Earth surface

Let us build the diagram of potential distribution on the Earth surface in the spherical coordinates system Potential on the Earth surface will be presented in the form of sum of the Earth electrostatic potential and its perturbation:

$$\varphi\left(R_E,\theta,\varphi\right) = \varphi_E\left(R_E\right) + \tilde{\varphi}\left(R_E,\theta,\varphi\right). \tag{25}$$

In the process of graphic analyses, we will impose the electrostatic potential of the Earth $\varphi_E\left(R_E\right)$ with the unit radius sphere. We will consider that $\left|\tilde{\varphi}\left(R_E,\theta,\varphi\right)\right|/\left|\varphi_E\left(R_E\right)\right| << 1$.

In the numerical calculations, the potential in dimensionless units $\hat{\varphi}\left(R_E,\theta,\varphi\right)$ was imposed with the expression:

$$\hat{\varphi}\left(R_E,\theta,\varphi\right) = 1 + \tilde{\varphi}\left(R_E,\theta,\varphi\right)/\varphi_E\left(R_E\right) = 1 + Amp\cdot\tilde{\varphi}\left(R_E,\theta,\varphi\right). \tag{26}$$

The Figure presents the results of the Earth potential from different meanings n for the amplitude of perturbed potential $Amp = 0.1$.

Under $n = 0$ the perturbed potential does not depend on angles θ and φ and one sign relatively to the Earth equilibrium potential.

Dependence of the sign of the perturbed potential on the number $n \geq 1$ is presented on Fig.1 below.

It follows from Fig.1 that perturbed potential of the Earth on the upper pole of the sphere ($\theta_0 = 0, \varphi_0 = 0$) is determined with condition (22) i.e. is equal to Φ_0.

It goes from the figures that number of zones N of one sign on the sphere width is equal $N = n+1$, where n is a number of zeros of Legendre polynomials $P_n\left(x\right)$ in the interval $-1 \leq x \leq +1$ [10, 11].

n				
1	2	3	4	5
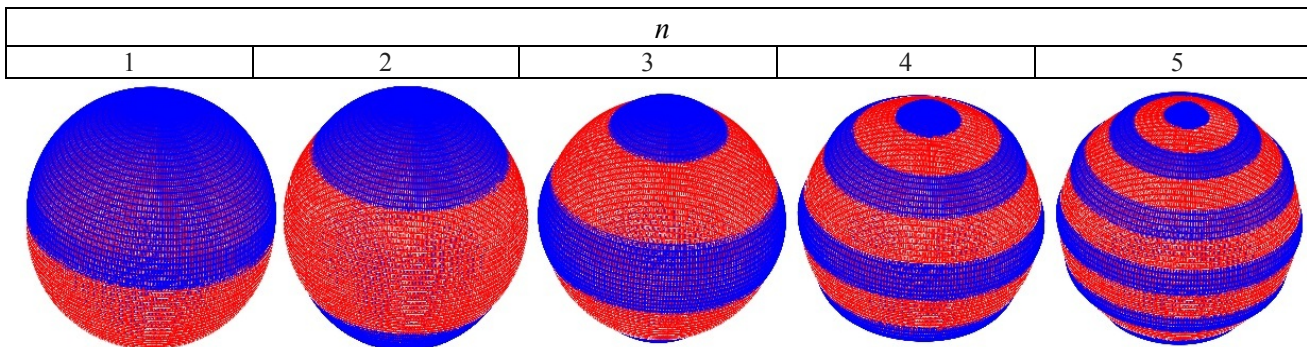
Figure. Dependence of sign of potential distribution on the Earth surface on the n number for $Amp = 0.1$.

In Tesla experiments the meaning of n number should be rather big: $n = n_0 >> 1$ as the Tesla generator wave length on the sphere width constitutes $\lambda_0 = 2$ km [2]. This wave length can be determined for relation $\lambda_0 = \lambda_{n_0} = 2\pi R_E/\left(n_0 + 1\right)$. It goes from this that n_0 is rather big : $n_0 \approx 2\pi R_E/\lambda_0 \approx 20015 >> 1$.

Thus in case of ideally conductive sphere the Tesla generator imposes the own charge oscillations placed on the conductive rigid sphere. Due to the task symmetry, the azimuth oscillations mode is equal to zero $m = 0$. Tesla

generator frequency ω_0 is connected with wave length of the perturbed potential on the width λ_0 with relation:

$$\omega_0 = \omega_{n_0} = \frac{c}{\lambda_0} = \frac{c(n_0 + 1)}{2\pi R_E}. \tag{27}$$

In common case the frequencies and wave lengths of the own high-frequency oscillations of the ideally conductive charge sphere are determined from the equalities:

$$\omega_n = \frac{c}{\lambda_n} = \frac{c(n+1)}{2\pi R_E}. \tag{28}$$

Schumann resonances and Tesla experiments in wireless transfer of electricity

In capacitors battery the oscillation frequencies or Schumann resonances [3], $\tilde{\omega}_n$ slightly differ in relative numbers from the frequencies of the own oscillations of the conductive sphere, i.e. $\tilde{\omega}_n = \omega_n + \Delta_n$ where $|\Delta_n| \ll \omega_n$. The mentioned above divergence between the frequencies is presented in Table [13].

Table.

Comparison of Schumann resonances with the own frequencies of the ideally conductive sphere

Frequency (Hz)	Number of mode n				
	0	1	2	3	4
Schumann resonances[13], $\tilde{\omega}_n$	7.8	14.3	20.8	27.3	33.8
Sphere resonances, ω_n	7.5	15	22.5	30	37.5
Divergence, $\Delta_n = \tilde{\omega}_n - \omega_n$	0.3	-0.7	-1.7	-2.7	-3.7

Let us consider the reasons of divergences of resonance Schumann frequencies from the own frequencies of the conductive sphere.

For this the dielectric permittivity of the layer in spherical capacitor can be conditionally presented in the form:

$$\varepsilon(\tilde{\omega}_n) = \left(1 - \frac{\Omega_n^2}{\tilde{\omega}_n^2}\right) \tag{29}$$

where Ω_n - own oscillations frequencies of the capacitors battery, $\Omega_n^2 = (1 + \alpha_n)\tilde{\omega}_n^2, \alpha_n \ll 1$.

Expression (29) describes the input of dielectric layer into the own frequencies of the ideally conductive sphere.

For the capacitors spherical battery on resonance frequencies we have:

$$\left(k_n^2\right)_B = \frac{\tilde{\omega}_n^2}{c^2} - \frac{4\pi C_{EB}}{V_E} = \frac{\tilde{\omega}_n^2}{c^2} - \frac{3\varepsilon(\tilde{\omega}_n)}{R_E d}. \tag{30}$$

For the ideally conductive sphere:

$$\left(k_n^2\right)_S = \frac{\omega_n^2}{c^2}. \tag{31}$$

Second summand in the right part (31) $4\pi C_E / V_E$ is not taken into consideration due to its smallness in relation to $4\pi C_{EB} / V_E$.

The wavelength of the ideally conductive sphere and capacitors battery is determined with a number of zeros of Legendre function. Equality $\left(k_n^2\right)_B = \left(k_n^2\right)_S = (n+1)^2 / (2\pi R_E)^2$ follows from this.

From the expressions (30) and (31), assuming that $\tilde{\omega}_n = \omega_n + \Delta_n$, where $|\Delta_n| \ll \omega_n$ we will determine the conditions under which the displaced, due to the presence of dielectric layer resonance frequencies of the ideally conductive ionosphere, correspond to Schumann resonances:

$$\Delta_n = -\frac{6\pi^2}{(n+1)^2} \frac{R_E}{d} \alpha_n \omega_n. \tag{32}$$

Assuming, for example, that the thickness of dielectric layer is small ($d \ll R_E$), from Table 1 and equality (32)

we will determine the meaning of parameter α_n:

$$\alpha_n = \frac{1}{6\pi^2}\frac{d}{7.5 R_E}(n-0.3)(n+1). \tag{33}$$

Expression for lowest Schumann resonances $\tilde{\omega}_n$ follows from (32) and (33):

$$\tilde{\omega}_n = \omega_n\left(1+\frac{(0.3-n)}{7.5(n+1)}\right), \tag{34}$$

where $n = 0,1,2,3,\ldots$.

Expression (34), unlike presented in [3] expression $\tilde{\omega}_n = 6.0\sqrt{n(n+1)}$, determines Schumann resonances, presented in Table 1, with a high level of accuracy.

Taking into account the daily frequency changes of the first harmonic of Schumann resonance, the figure 7,5 in the expression (34) can obtain the meanings in the ranges from 7 to 11 [14].

Thus, the present section provides determination of resonance of very low-frequency oscillations of the charged spherical capacitor with dielectric layer, which correspond to Schumann resonances.

CONCLUSIONS

Model of the Earth charge resonance oscillations excitation based on Tesla experiment was offered.

The task is directed on the research of D'Alembert equations for electric and magnetic potentials of the charged ideally conductive sphere. Based on the offered model connection of the perturbed charge and currency density with perturbed potentials was determined. It was shown that for high-frequency, harmonically changing in time disturbances of potentials the D'Alembert equations are transferred in Helmholtz equations, solutions of which in axial-symmetric case are expressed through Legendre polynomials. Substitution of border conditions into obtained solutions allow to describe the dependence of the Earth perturbed charged on the polar angle. Based on the found solution, graphic analyses of perturbed potential distribution on the ideally conductive Earth surface was provided. Obtained solution describes adequately Tesla experiments on the wireless electricity transfer, conducted in Colorado-Springs in 1899-1900.

In the very low-frequency spectrum area the Earth constitutes capacitors battery consisting of two placed one in another spheres, with a thin layer with dielectric permittivity $\varepsilon(\omega_0)$ and thickness $d \ll R_E$ placed between them.

The own oscillations frequencies of the Earth charge were determined in this frequencies range. It was shown that value of these frequencies most precisely corresponds to experimentally measured Schumann resonances.

REFERENCES

1. Nikola Tesla "Tesla. Colorado-Springs. Dnevniki [Diaries]. 1899-1900": Samara: Izdatelskiy dom "Agni", 2008. – 460p. (in Russian)
2. John O'Neil. Elektricheskiy Prometey [Electric Prometheus] // Izobretatel i racionalizator [Inventor and Innovator]. – 1979. – No. 4–11. (in Russian)
3. Schumann W.O. On the free oscillations of a conducting sphere which is surrounded by an air layer and an ionosphere shell // Z. Naturforsch. – 1952. - Vol.7A. – P.149–154. (in German)
4. Nickolaenko A, Hayakawa M. Schumann Resonance for Tyros. - Springer Geophysics, Japan, 2014. - 348 p.
5. Toledo-Redondo S., Salinas A., Morente-Molinera J.A., Méndez, Fornieles J., Portí J., Morente J.A. Parallel 3D-TLM algortithm for simulation of the Earth- A. ionosphere cavity // J. Comp. Phys. – 2013. – Vol.236. – P.367–379.
6. Tablicy fizigheskih velichin [Tables of physical quantities.]. Ed. Akad. I.K. Kikoin. - M.: Atomizdat, 1976. – 1008p. (in Russian)
7. Vernadskiy V.I. Himicheskoe stroenie biocferi Zemli i ee okruzhenie [The chemical structure of the Earth's biosphere and its environment.]. - M.: Nauka, 2001. – 376p. (in Russian)
8. Sivuhin D. V. Obshchiy kurs fiziki. Ucheb. posobie: Dlya vuzov [The general course of physics. Handbook for University]. Vol. 5. – T.III. Elektrichestvo [Electricity]. — 4-e isd., stereot. — M.: Fizmatlit; Izd-vo MFTI, 2004. – 656p.
9. Тамм I.E. Osnovy teorii electrichestva: Ucheb. posobie dlya vuzov [Fundamentals of the theory of electricity. Handbook for University].— 10-e izd., ispr.—M.: Nauka. Gl. red. fiz.-mat. lit., 1969. - 504p. (in Russian)
10. Kuznecov D.S. Specialnie funkcii [Special functions.]. - M.: Visshaya shkola, 1965 – 424p. (in Russian)
11. Tihonov A.N., Samarskiy A.A. Uravneniya matematicheskoy fiziki [The equations of mathematical physics]. - M.: Nauka, 1977. – 735p. (in Russian)
12. Tesla, Nikola, 1856-1943. Nikola Tesla on his work with alternating currents and their application to wireless telegraphy, telephony, and transmission of power: an extended interview / Leland Anderson, editor. Originally published: Denver, Colo: Sun Pub., 1992, 242p.
13. Simões F., Pfaff R., Freudenreich H. Observation of Schumann Resonances in the Earth's Ionosphere // Geophysical Research Letters. – 2011. – Vol. 38. – P.L22101, doi:10.1029/2011GL049668.
14. https://ru.wikipedia.org/wiki/Rezonans_Shumana

60

East European Journal of Physics

East Eur. J. Phys. Vol.3 No.4 (2016) 60-65

REFINING ANCIENT LEAD BY VACUUM DISTILLATION

V.D. Virich[1], Yu.V. Gorbenko[1], G.P. Kovtun[1], S.S. Nagorny[2], T.S. Potina[1], D.A. Solopikhin[1], A.P. Shcherban[1]

[1]National Science Center "Kharkov Institute of Physics and Technology"
Kharkiv, Ukraine
[2]INFN – Gran Sasso Scientific Institute, I-67100 L'Aquila, Italy
E-mail: shcherban@kipt.kharkov.ua
Received November 3, 2016

A complex method for refining lead by distillation in vacuum has been described. A brief comparative description of different methods of lead refining was submitted. Analysis of different methods showed that to increase the efficiency of lead deep cleaning the development of complex refining processes is required. The computational studies of the behavior of impurity elements in the ancient lead are performed. The ideal coefficients of impurities separation α_i are calculated at lead distillation temperatures. The range of volatile and nonvolatile impurities was detected by magnitude α_i in lead. Performed computational studies of the impurity elements behavior in lead formed the basis for developing an integrated method of deep refining of ancient lead. To implement this approach the special distillation device was developed, and the procedure of deep purification of lead was described.The results of the study of the deep refining ancient lead have been demonstrated. The cleaning high efficiency of the proposed approach, combined with high performance and yield of the suitable product, was shown. A pilot batch of ancient lead containing base metal > 99.998 wt. % suitable for growing high quality scintillation crystals $PbWO_4$ and $PbMoO_4$ has been produced.
KEYWORDS: ancient lead, deep refining, separation coefficients, vacuum distillation, low-background scintillation crystals

РАФІНУВАННЯ АНТИЧНОГО СВИНЦЮ ДИСТИЛЯЦІЄЮ У ВАКУУМІ
В.Д. Віріч[1], Ю.В. Горбенко[1], Г.П. Ковтун[1], С. С. Нагорний[2], Т.С. Потіна[1], Д.О. Солопіхін[1], О.П. Щербань[1]
[1]Національний Науковий Центр "Харківський фізико-технічний інститут", м. Харків, Україна
[2]INFN - Gran Sasso Scientific Institute, I-67100 L'Aquila, Italy

Описано комплексний метод рафінування свинцю дистиляцією у вакуумі. Дана коротка порівняльна характеристика різних методів рафінування свинцю. Аналіз різних методів показав, що для підвищення ефективності глибокого очищення свинцю необхідне відпрацювання комплексних процесів рафінування. Виконано розрахункові дослідження закономірності поведінки домішкових елементів в античному свинці. Розраховані ідеальні коефіцієнти поділу домішок α_i при температурах дистиляції свинцю. За величиною α_i в свинці виявлено спектр легколетких і труднолетких домішок. Виконані розрахункові дослідження поведінки домішкових елементів в свинці лягли в основу розробки комплексного методу глибокого рафінування античного свинцю. Для реалізації такого підходу розроблено спеціальний дистиляційний пристрій і описана процедура глибокого рафінування свинцю. Наведено результати дослідження глибокого рафінування античного свинцю. Показано високу ефективність очищення запропонованого підходу в поєднанні з високою продуктивністю і виходом придатного продукту. Отримано дослідну партію античного свинцю з вмістом основного металу > 99,998 мас. %, придатного для вирощування якісних сцинтиляційних кристалів $PbWO_4$ і $PbMoO_4$.
КЛЮЧОВІ СЛОВА: античний свинець, глибоке очищення, коефіцієнти розподілу, вакуумна дистиляція, низько-фонові сцинтиляційні кристали

РАФИНИРОВАНИЕ АНТИЧНОГО СВИНЦА ДИСТИЛЛЯЦИЕЙ В ВАКУУМЕ
В.Д. Вирич[1], Ю.В. Горбенко[1], Г.П. Ковтун[1], С. С. Нагорный[2], Т.С. Потина[1], Д.А. Солопихин[1], А.П. Щербань[1]
[1]Национальный Научный Центр "Харьковский физико-технический институт", г. Харьков, Украина;
[2]INFN – Gran Sasso Scientific Institute, I-67100 L'Aquila, Italy

Описан комплексный метод рафинирования свинца дистилляцией в вакууме. Дана краткая сравнительная характеристика различных методов рафинирования свинца. Анализ различных методов показал, что для повышения эффективности глубокой очистки свинца необходима разработка комплексных процессов рафинирования. Выполнены расчетные исследования закономерности поведения примесных элементов в античном свинце. Рассчитаны идеальные коэффиценты разделения примесей α_i при температурах дистилляции свинца. По величине α_i в свинце выявлен спектр легколетучих и труднолетучих примесей. Выполненные расчетные исследования поведения примесных элементов в свинце легли в основу разработки комплексного метода глубокого рафинирования античного свинца. Для реализации такого подхода разработано специальное дистилляционное устройство и описана процедура глубокого рафинирования свинца. Приведены результаты исследования глубокого рафинирования античного свинца. Показана высокая эффективность очистки предложенного подхода в сочетании с высокой производительностью и выходом годного продукта. Получена опытная партия античного свинца с содержанием основного металла > 99,998 мас. %, пригодного для выращивания качественных сцинтилляционных кристаллов $PbWO_4$ и $PbMoO_4$.
КЛЮЧЕВЫЕ СЛОВА: античный свинец, глубокая очистка, коэффиценты разделения, вакуумная дистилляция, низкофоновые сцинтилляционные кристаллы

Lead is an excellent material for passive protection in low-background experiments as well as for the production of lead tungstate and molybdate crystals for use as optical waveguides in low-background experiments for registration of rare nuclear decays [1]. Molybdates and tungstates of lead are also the promising scintillators for use at cryogenic temperatures [2]. However, the conventional lead containing a radioactive isotope ^{210}Pb the activity of which can be tens or even thousands of Bq/kg, which is unacceptable to create the low-background scintillation devices. Период полураспада [210]Pb составляет 22,3 года. Therefore, a radioactivity of lead, smelted hundreds and thousands of years ago, can be very low [3-5].

Besides a purity of the radioactive scintillation detectors the strict requirements are imposed to content of stable of chemical elements, in particular, to the content of transition metals (Fe V, Cr, Mn, Ni, Co, etc.) leading to a reduction of optical and scintillation properties of crystals. Their content should not exceed $\sim (0.1...1)$ ppm [6].

The developed methods of refining must have high performance, high cleaning efficiency (> 100 fold), high yield of suitable product ($> 95\%$) and minimal ($< 1\%$) unrecoverable losses of the refined metal.

One method for deep refining of metal is a distillation in vacuum [7, 8]. An interest in the distillation is due to the fact that this method allows to achieve a high degree of purification of metals with a high yield of good product, and it is environmentally friendly. However, a simple distillation does not provide the required degree of deep cleaning of lead with removal of certain impurities. A comprehensive approach to distillation purification of lead is more effective one.

The aim of this work was to study the regularities of behavior of impurity elements in lead during distillation purification, as well as the study of the complex process of deep refining ancient lead in combination with vacuum distillation.

EXPERIMENTAL METHODS FOR REFINING LEAD

Producing high purity lead requires multi-step processes that combine different methods of deep cleaning.

Electrolytic methods [9] allow to get a lead with total content of metal impurities of 1...100 ppm, however, to produce a metal with impurities concentration which meets to modern demands, it is subjected to further purification. In addition, when electrochemical methods of cleaning lead are used, the emission of harmful gases and vapors inevitably occurred, so careful precautions are needed.

The heating under vacuum at the temperatures of 750…1250 K is an effective method to remove the separate impurities (As, Te, Zn) from lead. However, the weak removal of contaminants such as Bi, Mg and Sb is observed at vacuum heating [10].

The zone re-crystallization can also be used for deep cleaning of lead. Refinement of lead by zone melting has been widely discussed, wherein the behavior of Sn, Cu, Ag, Au, Mg, Na, Bi, Sb was studied quantitatively and that of Co, Ni, Fe, Ge, Cd, As – qualitatively. Sn, Sb, Bi, Mg as well as Na with distribution coefficient close to one ($K \sim 1$) [11] are the impurities which difficult to remove at zone recrystallization of lead. The disadvantage of this method is the low yield (60...70%) of suitable product.

An effective way of lead refining is the method of distillation under a vacuum. The method involves manufacturing to produce a high-purity grades of lead [12].

Computational analysis of impurities behavior in lead

Theoretical basis of the distillation method of refining metals are presented in [13-15]. The distillation method for refining is based on the difference in the compositions of shared liquid mixture and steam formed therefrom. This difference is estimated by the value of relative volatility α of separable component (as applied to the refining process by distillation this value is called the separation coefficient).

In the case of ideal dilute solution, where the activity coefficients of main and impurity elements $\gamma_A = \gamma_B = 1$, the ideal separation coefficient α_i for the molecular evaporation is defined as

$$\alpha_i = \frac{p_A^0 \sqrt{M_B}}{p_B^0 \sqrt{M_A}},$$ (1)

where p_A^0, p_B^0 are the vapor pressure of pure main and impurity components A and B; M_A and M_B – the molecular weight of A and B, respectively.

Using expression (1), the ideal separation coefficients of impurities α_i, the values of which are given in Table 1 below, were calculated at temperatures of lead distillation.

By a magnitude α_i the impurities in lead can be separated into volatile (Zn, Te, Mg, Sr, Tl, Bi, Ca, Li at al.) with $\alpha_i \sim 10^{-2}…10^{-5}$, and nonvolatile (Mn, Ag, Al, Ni, Co, Cu, Sn, Si, Cr, Fe, U at al) with $\alpha_i \sim 10^2…10^9$. For most of impurity elements the values of α_i are significantly different from 1, which suggests an efficient cleaning of lead. Vapor pressure values of the elements at given temperatures were taken from paper [16].

Listed in Table 1 the values of α_i are used to calculate the efficiency of purification of the melt (x_p/x_0) vs the mass change (G_p/G_0) at 1100 K and dependence of the degree of purification of condensate (x_κ/x_0) vs fraction of distillation (G_κ/G_0) at 1200 K. The parameters are as follows: x_0, x_P and x_K - initial and final content of impurities in the melt and in

the condensate of component A, weight %; G_0, G_P and G_K - the initial and final mass of melt and condensate. Such calculations for separate impurities are given in [17]. Calculations indicate that for impurities with $\alpha_i < 10^{-2}$ the removal of volatile impurities from lead by distillation them from the melt will be effective procedure which accompanied by a loss of base metal < 5%. Removal of low-volatile impurities by distillation of lead into condensate will be effective one with the yield of suitable condensate of more than 95% already at $\alpha_i > 5 \cdot 10^1$. These data were taken into account when creating the distillation device and for the choice of mode of lead distillation process.

Table 1

Calculated values of the ideal coefficients of impurities separation α_i at molecular distillation of lead under vacuum

	T=1100 K	T=1200 K	T=1300 K
Na	$7.2 \cdot 10^{-5}$	-	-
Mg	$6.4 \cdot 10^{-4}$	$1.0 \cdot 10^{-3}$	$1.6 \cdot 10^{-3}$
Zn	$1.5 \cdot 10^{-4}$	-	-
Li	$4 \cdot 10^{-3}$	$5.3 \cdot 10^{-3}$	$6.7 \cdot 10^{-3}$
Tl	$8.5 \cdot 10^{-2}$	$9.8 \cdot 10^{-2}$	$1.1 \cdot 10^{-1}$
Te	$8.2 \cdot 10^{-2}$	$3.5 \cdot 10^{-1}$	-
Bi	$6.3 \cdot 10^{-2}$	$7,4 \cdot 10^{-2}$	$8.8 \cdot 10^{-2}$
Ca	$4.4 \cdot 10^{-2}$	$3.4 \cdot 10^{-2}$	$4.3 \cdot 10^{-2}$
Sr	$1.2 \cdot 10^{-2}$	$1.4 \cdot 10^{-2}$	$2.4 \cdot 10^{-2}$
Ba	$1.2 \cdot 10^{-1}$	$1.5 \cdot 10^{-1}$	$1,8 \cdot 10^{-1}$
Pb	**1**	**1**	**1**
In	$3.8 \cdot 10^1$	$2.5 \cdot 10^1$	$1.8 \cdot 10^1$
Sb	$5.9 \cdot 10^1$	$3.6 \cdot 10^1$	$2.5 \cdot 10^1$
Mn	$1.4 \cdot 10^2$	$6.3 \cdot 10^1$	$3.3 \cdot 10^2$
Ga	$5.3 \cdot 10^2$	$2.6 \cdot 10^2$	$1.4 \cdot 10^2$
Ag	$6.3 \cdot 10^2$	$2.6 \cdot 10^2$	$1.4 \cdot 10^2$
Al	$4.4 \cdot 10^3$	$1.6 \cdot 10^3$	$6.7 \cdot 10^2$
Ni	$1.2 \cdot 10^4$	$3.1 \cdot 10^3$	$6.1 \cdot 10^2$
Be	$1.6 \cdot 10^4$	$4.4 \cdot 10^3$	$1.6 \cdot 10^3$
Co	$3.8 \cdot 10^4$	$9 \cdot 10^3$	$2.7 \cdot 10^3$
Sn	$4.9 \cdot 10^4$	$1.7 \cdot 10^4$	$7.4 \cdot 10^3$
Sc	$5.6 \cdot 10^4$	$1.4 \cdot 10^4$	$4.6 \cdot 10^3$
Cu	$1.2 \cdot 10^5$	$3 \cdot 10^4$	$9.8 \cdot 10^3$
Nd	$2.7 \cdot 10^5$	$7,8 \cdot 10^4$	$3.4 \cdot 10^4$
U, V, TI, La, Fe, Si, Au, Ge, Cr	$> 10^5$	$> 10^5$	$> 10^5$

Initial lead

The subject of study was the ancient lead. The sunken 36-meter ship, which went from Spain to Italy, was discovered by archaeologists at the bottom of the Mediterranean Sea near the island of Sardinia in 1988. The more than 1,500 ingots of lead with weight of about ~ 33 kg each (Fig. 1) were on board among the transported cargo. The ship with the lead located on it, which spent about two thousand years on the seabed at a depth of 30 m, was perfectly shielded from exposure of cosmic rays.

Fig. 1. The ingots of archaeological lead with stamps (photo INFN / Cagliari Archeological Superintendence).

Distillation device and a procedure of deep refining of lead

The main stages of the complex process of lead refining were as follows. The first stage – filtration of lead combined with heating to remove surface contaminants and various impurities as well as gas-forming impurities. The second stage – re-condensation of metal into superheated liquid phase to remove the low-volatile and volatile impurity elements.

The special distillation device was developed for the implementation of complex method of deep refining [18, 19]. The apparatus for the distillation was produced of high-pure dense graphite of MPG-7 grade with a minimum content of impurities, having a chemical inertness with respect to lead. Fig. 2 shows a scheme of a distillation device for refining lead.

A feature of lead is that it belongs to a low-melting metals (T_{melt} = 600.5 K) and has a low vapor pressure at the melting temperature (4.3×10^{-7} Pa) [16]. Earlier studies on vacuum distillation of other fusible metals (Cd, Zn, Te, etc.) show that acceptable rates of evaporation in the processes of distillation correspond to pressures of the vapor at a level (27...80) Pa, that for lead corresponds to the melt temperature 1200...1250 K [16]. These features were taken into account when developing the new approach to the process of lead refining.
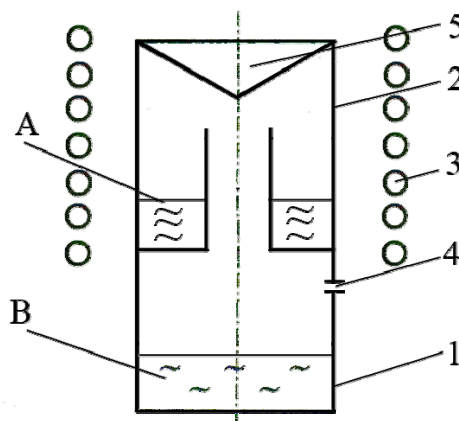
Fig. 2. Scheme of the distillation device for refining lead: A - initial lead; B - refined metal; 1 - condenser 2 - crucible 3 - heater, 4 – hole (aperture) 5 - steam deflector.

The operation of the device for lead refining by vacuum distillation consists as follows. The initial lead was pre-warmed and subjected filtration under vacuum. Then, the filtered lead weighing about 1.5 kg was placed in the crucible 2, the device chamber was evacuated and supported under a pressures of not more than 10^{-1} Pa during refining. Lead melt was heated up to 1220 K, then it was evaporated and collected in the condenser 1 at a temperature about 1120 K in the form of refined metal B. The removal of low-volatile impurities (Cu, Fe, Si, Ni, Co , V, Cr, Au, Ag, Al, Tl, Sb, Sn, Mn, etc.), remaining in a lead residue in the crucible 2, was occurring during evaporation of lead to 95% of the initial charge. Volatile impurities, that partly transferred into the condenser together with lead during its condensation, were removed through a hole 4 in the condenser due to the exposure of purified condensate during the refining process (~ 5 hours) at a temperature ($T_{cond.} \approx 0.8T_{evapor}$). Te lead was subjected to a double distillation according to the described procedure. After each distillation process, the residue in the crucible was about 30...50 g. The Fig. 3 shows a photo of refined lead after distillation.

Fig. 3. The distillates of the refined ancient lead by the weight of ~ 1 kg each.

RESULTS AND DISCUSSION

Content of impurities in lead samples was determined by laser mass spectrometry of high resolution with double focusing according to Mattauhu Duke MS-3101 with registration on the film, to measure optical density of which the microphotometer registering IFO-451 was used.

The main advantages of mass spectrometers having ion source and laser dual focus are on the one hand, the high absolute and relative sensitivity, and on the other hand, the possibility of simultaneous registration with subsequent quantitative determination of almost all elements (from lithium to uranium). Random error of the analysis results is characterized by the value of relative standard deviation 0.15…0.30.

Analysis of impurity elements in the initial ancient and refined lead was performed for 72 elements. The content of the main impurity elements in the initial and refined lead is shown in Table. 2. Moreover, the table indicates only the impurity elements, the content of which in the initial lead was at a level exceeding the limit of sensitivity of the laser mass spectrometer. The concentration of other impurities in the refined lead was below the detection limit of the method of laser mass spectrometry: for Rb, Y, Zr, Nb, Ru, Pt, Au $< 1 \cdot 10^{-2}$ ppm; for Sc, In, Te $< 1 \cdot 10^{-1}$ ppm; for Se, Pd < 1 ppm.

The purity of the initial lead on the sum of impurities is about ~ 99.7 wt. %. It should be noted that the main impurity elements in the initial lead are Cu, Ag, Sn, Sb, and their multiplicity of distillation removal is the value from ~ 100 to 600. The purity of lead after refining with taking into account these and the other impurities is > 99.998 wt. %.

A number of impurities (Na, K, Ca, S, As) there are also in the initial lead, and the removal efficiency of this elements is low - 1.5...2.5. Such situation for sodium can be explained by the fact that its content is at the sensitivity limit of the method definition, and calcium, sulfur and arsenic is apparently transferred to the refined metal in the form of stable compounds. Nevertheless, the proposed lead refining procedure (heating, filtration and a double distillation) provide a high (more than 100 fold) the efficiency of metal purification.

Table 2

The content of the main impurity elements in ancient lead before and after refining by distillation under vacuum

Element	before refining	after refining
	content, ppm	
Na	0.05	0.05
Mg	0.08	< 0.03
Al	0.12	0.009
Si	0.044	< 0.04
S	0.76	0.4
K	0.1	0.045
Ca	0.2	0.16
Mn	0.12	< 0.07
Fe	0.1	< 0.08
Ni	0.37	< 0.1
Zn	< 0.2	< 0.2
Cu	23	< 0.05
As	1.6	0.8
Ag	300	< 0.5
Cd	< 0.8	< 0.8
Sn	1800	7.7
Sb	560	6.3

The authors of this work have produced earlier a pilot batch of the Greek archaeological lead with an upper limit for a wide range of elements at the level 0.1...0.6 ppm [17, 18]. On the basis of obtained high purity Greek lead the high-quality scintillation single crystal of tungstate lead $PbWO_4$ was grown. The crystal was successfully used as an optical fiber in a low-background experiment to search for double beta decay [106]Cd with the help of scintillator [106]CdWO_4 in an underground laboratory in Gran Sasso, Italy [20].

Thus, proposed in this paper the complex method of lead refining allow to produce a final product of more than 2 orders of magnitude purer compared with the initial metal. The obtained so ancient lead is supposed to use for the growth of scintillation crystal of tungstate and molybdate of lead.

CONCLUSIONS

The computational studies of the behavior of impurity elements in the ancient lead were carried out. Ideal coefficients of impurities separation (α_i) were determined at the temperatures of distillation and condensation of lead, on the basis of these coefficients the range of low-volatile and volatile impurities was identified during refining of lead by distillation under a vacuum.

A complex method of refining in combination with vacuum distillation was proposed and investigated in the work for the deep cleaning of ancient lead. To implement such method, the special distillation device has been developed and tested. The purification efficiency of the proposed method is better by more than two orders of magnitude relative to the initial purity.

The pilot batch (~ 2.5 kg) of ancient lead of a purity > 99.998 wt % suitable for the growing scintillation crystals $PbWO_4$ and $PbMoO_4$ was fabricated.

REFERENCES

1. Danevich F.A. et al. Application of PbWO$_4$ crystal scintillators in experiment to search for 2β decay of ^{116}Cd // Nuclear Instruments and Methods in Physics Research. A. – 2006. – Vol. 556. – P. 259 – 265.
2. Danevich F.A. et al. Feasibility study of PbWO$_4$ and PbMoO$_4$ crystal scintillators for cryogenic rare events experiments // Nuclear Instruments and Methods in Physics Research A. – 1991. – Vol. 622. – P. 608 – 613.
3. Alessandrello A., Cattadori C., Fiorentini G. et al. Measurements on Radioactivity of Ancient roman Lead to be Used as Shield in Searches for Rare Events // Nucl. Instrum. Methods. – 1991. – Sect. B. – Vol. 61. – No. 1. – P. 106 – 117.
4. Alessandrello A., Allegretti F., Brofferio C. et al. Measurements of Low Radioactive Contaminations in Lead Using Bolometric Detectors // Nucl. Instrum. Methods. – 1993. – Sect. B. – Vol. 83. – No. 4. – P. 539 – 544.
5. Danevich F.A., Kim S.K., Kim H.J. et al. Ancient Greek lead findings in Ukraine // Nucl. Instrum. Methods. – 2009. – Sect. A. – Vol. 603. – No. 3. – P. 328 – 332.
6. Kovtun G.P., Boiko R.S., Danevich F.A. at al. Proizvodstvo i svojstva nizkofonovyh scintillyatorov vol'framatov kadmiya i svinca dlya poiska dvojnogo beta-raspada [Development and properties of cadmium and lead tungstate low-background scintillators for double beta decay experiments] // Yaderna fizyka ta energetyka [Nuclear physics and atomic energy]. – 2014. – Vol. 15. – No. 1. – P. 92 – 100. (In Russian)
7. Ivanov V.E., Papirov I.I., Tihinskij G.F, Amonenko V.M.. Chistye i sverhchistye metally [Pure and very pure metals] // M.: Metallurgiya, 1965. – 170 p. (In Russian)
8. Pazuhin V.A., Fisher A.Ya. Razdelenie i rafinirovanie metallov v vakuume [Separation and refining of metals in vacuum]. – M.: Metallurgiya, 1969. – 204 p. (In Russian)
9. Kozin L.F., Morachevskij A.G. Fiziko-himiya i metallurgiya vysokochistogo svinca [Physical chemistry and metallurgy of high purity lead]. – M.: Metallurgiya, 1991. – 223 p. (In Russian)
10. Aleksandrov B.N., Udovikov V.I. Povedenie primesej v svince pri vakuumnom progreve, distillyacii i zonnoj plavke [Behavior of impurities in lead at warming, distillation and zone melting up the vacuum]. Fizika kondensirovannogo sostoyaniya [Condensed matter physics] // Har'kov: FTINT AN USSR, 1973. – No. 25. (In Russian)
11. Aleksandrov B.N., D'yakov I.G. Zonnaya ochistka alyuminiya i svinca [Zone-refining of aluminum and lead] // Fizika metallov i metallovedenie [The Physics of Metals and Metallography], 1962. – Vol. 14. – No. 2. – 267 p. (In Russian)
12. Esyutin V.S., Nurgaliev D.N. Vakuum-distillyacionnaya ochistka svinca ot primesej v apparate nepreryvnogo dejstviya [Vacuum-distillation lead purification from impurities in the unit of continuous action] // Cvetnye metally. – 1975. – No. 12. – P. 28-30. (In Russian)
13. Devyatyh G.G., Elliev YU.E. Vvedenie v teoriyu glubokoj ochistki veshchestv [Introduction to the theory of deep cleaning substances]. – Metallurgiya, 1973. – 320 p. (In Russian)
14. Belyaev A.I. Fiziko-himicheskie osnovy ochistki metallov i poluprovodnikovyh materialov. – M.: Metallurgiya, 1973. – 320 p. (In Russian)
15. Devyatyh G.G., Elliev YU.E. Glubokaya ochistka veshchestv [Deep cleaning substances]. – M.: Vysshaya shkola, 1974. – 180 p. (In Russian)
16. Nesmeyanov A.N. Davlenie para himicheskih ehlementov [The vapor pressure of the chemical elements]. – M.: Izd–vo AN SSSR [Publisher of the USSR Academy of Sciences], 1961. – 396 p. (In Russian)
17. Boiko R.S., Virich V.D., Danevich F.A. et al. Ultrapurification of Archaeological Lead // Inorganic Materials. - 2011. - Vol. 47. – No. 6. – P. 645 – 648.
18. Kovtun G.P., Shcherban' A.P., Solopikhin D.A. et al. Purification of Cadmium and Lead for Low Background Scintillators. Proc. 1st Int. Workshop Radiopure Scintillators for EURECA (RPScint'2008). – Kyiv, 2009. – P. 59 – 63.
19. Patent № 94547, C2. Ukraine. Ustrojstvo dlya rafinirovaniya metallov distillyaciej v vakuume [An apparatus for refining metals by distillation in vacuum]. Shcherban' A.P., Kovtun G.P., Solopihin D.O. Byul. – No. 9. – 2011. (In Russian)
20. Tretyak V.I. et al. First results of the experiment to search for 2β decay of ^{106}Cd with ^{106}CdWO$_4$ crystal scintillator in coincidence with four crystals HPGe detector // EPJ Web of Conference 65 (2014) 01004.

SPECTRAL CHARACTERISTICS OF ULTRAFINE PARTICLES Zn_2SiO_4-Mn, PRECIPITATED FROM AN AQUEOUS SOLUTION ON THE SUBSTRATE IN ELECTRIC OR MAGNETIC FIELDS

V.I. Tyutyunnikov

Pryazovskyi State Technical University
Mariupol, St. Universitetskaya, 7, 87500, Ukraine
e-mail: vladimir-tjutjunnikov@rambler.ru
Received December 2, 2016

The spectral parameters ultrafine particles Zn_2SiO_4-Mn, precipitated on the substrate in a magnetic or electric field have been investigated. For getting fine particles industrial phosphor K-60 (Zn_2SiO_4-Mn) was used. Luminescence spectra were obtained on a sample when exposed to ultraviolet light or a beam of charged oxygen ions. When excited by ultraviolet spectral characteristics have difference for samples with different dimensions of the crystals. As for the industrial design luminescence spectrum had a band with λ_{max} = 521 nm, and for the ultrafine crystals willemite spectral band had λ_{max} = 550 nm. Analysis ionoluminescence spectra showed that the reduction of crystal size Zn_2SiO_4-Mn not affect the spectral characteristics of the excitation beam with low energy oxygen ions. The luminescence spectrum when exposed to low-energy ions (1-3 KeV) has a band with λ_{max} = 521 nm and a half-width $\Delta\lambda$ = 41 nm. When measuring the width of the forbidden zone has been established bandgap dependence on the size of the phosphor crystals. The width of the band gap increases with decreasing crystal size to nanoscale sizes. A significant effect was obtained when deposited on a substrate in the nanoscale crystal magnetic or electric field. As for the industrial design the bandgap was 4.16 eV, and for the besieged in the magnetic and electric field of 4.27, 4.29 eV, respectively.
KEY WORDS: the spectrum, ultra-fine crystals, photoluminescence, ionoluminescence, magnetic field, electric field

СПЕКТРАЛЬНІ ПОКАЗНИКИ ДРІБНОДИСПЕРСНИХ ЧАСТИНОК Zn_2SiO_4-Mn, ОСАДЖЕНИХ З ВОДНОГО РОЗЧИНУ НА ПІДЛОЖКУ У ЕЛЕКТРИЧНОМУ ТА МАГНІТНОМУ ПОЛІ
В.І. Тютюнников

Приазовський Державний Технічний Університет
м. Маріуполь, вул. Університетська, 7, 87500, Україна

Досліджувалися спектральні параметри ультрадисперсних частинок Zn_2SiO_4-Mn , осаджених на основу в магнітному або в електричному полі. Для отримання дрібнодисперсних частинок використовували промисловий люмінофор К-60 (Zn_2SiO_4-Mn). Спектри люмінесценції отримували за впливом на зразок ультрафіолетом або пучком заряджених іонів кисню. При збудженні ультрафіолетом спектральні характеристики мали відмінність для зразків з різною розмірністю кристалів. Отже для промислового зразка спектр люмінесценції мав смугу з λ_{max} = 521нм, а для ультрадисперсних кристалів віллеміта спектральна смуга була λ_{max} = 550нм. Аналіз спектрів іонолюмінесценції показав, що зміншення розмірів кристалів Zn_2SiO_4-Mn не впливає на спектральні показники при збудженні пучком іонів кисню низьких енергій. Спектр люмінесценції під час дії іонами низьких енергій (1-3 KeV) має смугу з λ_{max} = 521нм і напівшириною $\Delta\lambda$ = 41нм. Під час вимірювання ширини забороненої зони була встановлена залежність ширини забороненої зони від розмірів кристалів люмінофора. Ширина забороненої зони збільшується під час зменшення розмірів кристалів до нанорозмірних величин. Значний ефект був отриманий під час осадження на підложку нанорозмірних кристалів в магнітному або електричному полі. Отже для промислового зразка ширина забороненої зони склала 4,16 еВ, а для осаджених у магнітному та електричному полі 4,27; 4,29 еВ відповідно.
КЛЮЧОВІ СЛОВА: спектр, ультрадисперсні кристали, фотолюмінісценція, іонолюмінесценція, магнітне поле, електричне поле

СПЕКТРАЛЬНЫЕ ХАРАКТЕРИСТИКИ МЕЛКОДИСПЕРСНЫХ ЧАСТИЦ Zn_2SiO_4-Mn, ОСАЖДЁННЫХ ИЗ ВОДНОГО РАСТВОРА НА ПОДЛОЖКУ В ЭЛЕКТРИЧЕСКОМ ИЛИ МАГНИТНОМ ПОЛЕ
В.И. Тютюнников

Приазовский Государственный Технический Университет
г. Мариуполь, ул. Университетская, 7, 87500, Украина

Исследовались спектральные параметры ультрадисперсных частиц Zn_2SiO_4-Mn, осаждённых на подложку в магнитном или в электрическом поле. Для получения мелкодисперсных частиц использовали промышленный люминофор К-60 (Zn_2SiO_4-Mn). Спектры люминесценции получали при воздействии на образец ультрафиолетом или пучком заряженных ионов кислорода. При возбуждении ультрафиолетом спектральные характеристики отличались для образцов с различной размерностью кристаллов. Так для промышленного образца спектр люминесценции имел полосу с λ_{max}=521 нм, а для ультрадисперсных кристаллов виллемита спектральная полоса имела λ_{max}=550 нм. Анализ спектров ионолюминесценции показал, что уменьшение размеров кристаллов Zn_2SiO_4-Mn не влияет на спектральные характеристики при возбуждении пучком ионов кислорода низких энергий. Спектр люминесценции при воздействии ионами низких энергий (1-3 кэВ) имеет полосу с λ_{max}=521 нм и полушириной $\Delta\lambda$=41 нм. При измерении ширины запрещённой зоны была установлена зависимость ширины запрещённой зоны от размеров кристаллов люминофора. Ширина запрещённой зоны увеличивается при уменьшении размеров кристаллов до наноразмерных величин. Значительный эффект был получен при осаждении на подложку наноразмерных кристаллов в магнитном или электрическом поле. Так для промышленного образца ширина запрещённой зоны составила 4,16 эВ, а для осаждённых в магнитном и электрическом поле 4,27, 4,29 эВ соответственно.

Исследования оптическими методами структур с пониженной размерностью интенсивно развиваются в последние десятилетия. Наночастицы, как отмечается в литературе, обладают огромным потенциалом в области приложений фотоники [1]. Исследование оптических свойств ионов переходных металлов и наночастиц, а также изучение динамики возбуждённого состояния ионов переходных металлов в ультрадисперсных средах имеет важное научное и практическое значение. Цинксиликаты, допированные ионами марганца, показывают хорошие люминесцентные свойства, что даёт возможность использовать их в качестве люминофоров при производстве плазменных дисплеев, дисплеев с полевой эмиссией, люминесцентных ламп и катодо-лучевых трубок [2,3]. Эти материалы, также, обладают хорошими механическими свойствами, химической и термической стабильностью. Но в связи с постоянным возрастанием требований к используемым материалам проводятся усовершенствования данных люминофоров, что открывает новые области для их применения [4]. Актуальными остаются поиски стабильных зелёных кристаллофосфоров для применения и в других областях, таких как дозиметрия, радары и др. Для повышения яркости и разрешения этих дисплеев важно синтезировать люминофоры с высокой квантовой эффективностью [5]. Однако ещё не получен зелёный люминофор на основе виллемита, эффективно излучающий при возбуждении в области ВУФ и имеющий длительность послесвечения менее 10мс. В зависимости от кристаллической модификации силиката цинка, природы и концентрации примесных ионов, энергии возбуждения, эти материалы приобретают фотолюминесцентные свойства с излучением в зеленой или жёлтой области видимого света [6-11]. Наибольшее применение получили материалы на основе термодинамически стабильной и высококристаллической α-модификации силиката цинка, допированные ионами марганца и излучающие зелёный свет. Сложнее получение материалов на основе β-модификации Zn$_2$SiO$_4$-Mn, излучающих жёлтый свет, что связано с превращением β - Zn$_2$SiO$_4$ в α - Zn$_2$SiO$_4$ при ~900°C [10,11]. Силикат цинка получают твердофазным методом [12], золь-гель методом [13,14] с использованием полимер-ных прекурсоров [15] и мезопористых кремнеземных матриц [16,17], спрей-пиролизом [18,19], гидротермаль-ным методом [20] и др. Как правило наноматериалы наносяться на специально подготовленную подложку.

Целью данной работы является исследование спектральных характеристик материалов, полученных при осаждении мелкодисперсных кристаллов Zn$_2$SiO$_4$-Mn на подложку не требующую специальной подготовки в элек-трическом и магнитном поле. Процесс выполняется в открытой атмосфере, что даёт возможность использовать большую гибкость для производства материалов на основе виллемита.

ЭКСПЕРИМЕНТ

Спектральные характеристики исследовались на высоковакуумной установке, технические параметры которой представлены в работе [21]. Экспериментальная установка позволяет изучать спектры ионолюминесценции (ИЛ) и фотолюминесценции (ФЛ). Микрофотографии образцов были получены на электронном микроскопе - JSM-6390LV. Коэффициент пропускания измеряли на спектрофотометре СФ-46, затем полученные данные использовали для определения ширины запрещённой зоны. Методика определения ширины запрещённой зоны полупроводников представлена в работах [22,23]. Мелкодисперсные кристаллы Zn$_2$SiO$_4$-Mn получали путём разделения на фракции в коллоидном водном растворе промышленного люминофора К-60. Коллоидный раствор выдерживался в пробирке примерно три недели. После этого для исследований использовалась 1/3 раствора из верхней части пробирки. Образцы для исследования наносились на подложку из нержавеющей стали, или пластинки из кварцевого стекла, в виде эмульсии Zn$_2$SiO$_4$-Mn водного раствора, затем вода удалялась путём выпаривания. Температура подложки, при удалении воды, поддерживалась в пределах 65°C. Такой режим испарения даёт возможность эффективнее удалить воду из образца и, в то же время, не способствует образованию конвективных потоков, которые не позволяют зафиксировать частицы в определённом положении. Процесс нанесения эмульсии производился 5-6 раз до образования матового налёта на подложке. Исследовались образцы Zn$_2$SiO$_4$-Mn, нанесенные на подложку, как при обычных условиях, так и в магнитном и в электрическом поле. Осаждение ультрадисперсных частиц проводили в магнитном поле с индукцией магнитного поля: 0,30Тл. При осаждении частиц в электрическом поле напряжённость электрического поля составляла 10^5 В/м. Спектры получали с помощью монохроматора ЗМР-3 (обратная дисперсия в синей области спектра 0,5 нм/мм). В качестве регистрирующего устройства использовали фотоэлектронный усилитель (ФЭУ 84-3). Сигнал с ФЭУ усиливался усилителем У-5-11 и записывался на диаграмную ленту самописца (КСП-4). Для возбуждения ФЛ применялась ртутная лампа ДРШ-250 со светофильтром УФС-2 (область пропускания света hv=3,35-5,00 эВ). Для возбуждения ИЛ служила плазменная ионная пушка (кислород) с энергией ионов 0,5-3,0 кэВ, ионный ток от 0,004 до 3,5 μA. Индукция магнитного поля измерялась "измерителем магнитной индукции Ш1-8". Запись спектров производилась при комнатной температуре. Для сравнения записывались спектры ФЛ и спектры ионолюминесценции, полученные при воздействии ионами кислорода на образец ИЛ.

РЕЗУЛЬТАТЫ И ИХ ОБСУЖДЕНИЕ

В данной работе были использованы фотолюминесценция и низкоэнергетическая ионолюминесценция, ко-

торые являются весьма информативными и широко применяются для изучения ультрадисперсных систем. На (рис.1) представлены спектры ФЛ образцов промышленного люминофора К-60 (линия-a) и образцов полученных при осаждении частиц ультрадисперсных кристаллов (УДК) при обычных условиях (линия-b), при осаждении в магнитном поле (линия-c), при осаждении в электрическом поле (линия- d). Полученный в данной работе спектр ФЛ (рис.1a) промышленного люминофора Zn_2SiO_4-Mn (К-60) представлен полосой с длиной волны в максимуме: (λ_{max} =521 нм) и с полушириной $\Delta\lambda$=41 нм и охватывающей диапазон от 460 до 610 нм. Анализ микрофотографии промышленного люминофора (рис.1б) показывает, что размеры кристаллов находятся в пределах 500-20нм. Спектр ФЛ для образца, полученного путём осаждения мелкодисперсных кристаллов Zn_2SiO_4-Mn при обычных условиях на подложку представлен линией (рис.1b) с λ_{max}=550 нм и с полушириной $\Delta\lambda$=40 нм и охватывающей диапазон от 490 до 620 нм. Спектры ФЛ для образцов, полученных путём осаждения УДК виллемита на подложку в магнитном поле (рис.1c) имеют параметры с λ_{max}=546 нм и с полушириной $\Delta\lambda$=40 нм охватывающей диапазон от 480 до 620 нм. Спектры ФЛ для образцов, полученных путём осаждения УДК Zn_2SiO_4-Mn в электрическом поле (рис.1d) на подложку имеют параметры с λ_{max}=551 нм и с полушириной $\Delta\lambda$=38 нм и имеют диапазон от 490 до 620 нм.
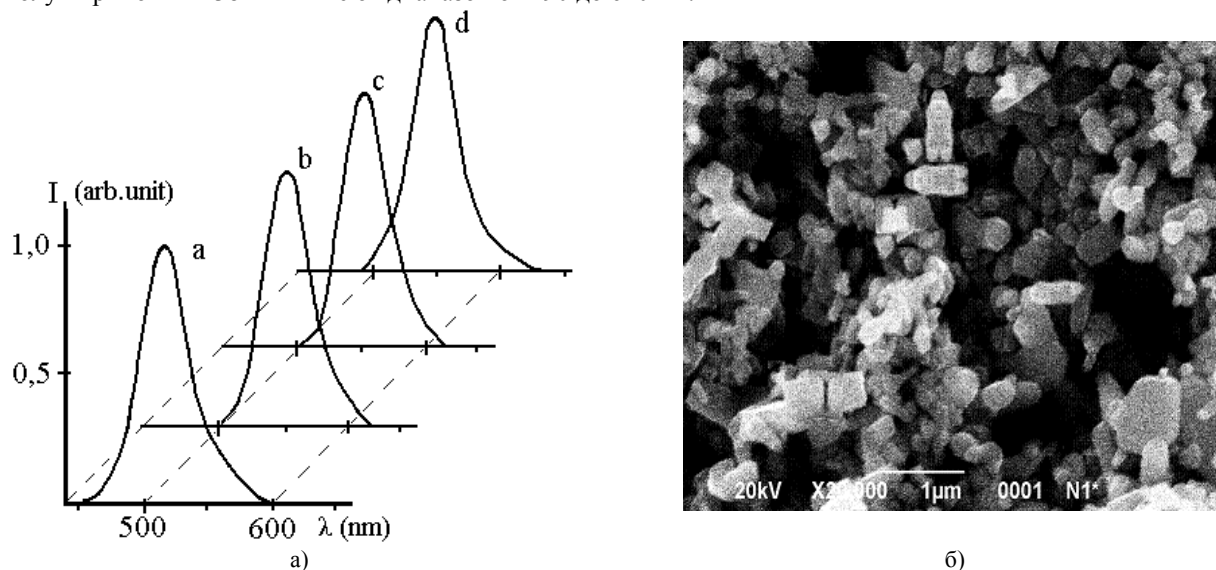
Рис.1. Спектры ФЛ для образцов Zn_2SiO_4-Mn и микрофотография исходного образца
а) a-промышленный люминофор (К-60) Zn_2SiO_4-Mn, b- микрочастицы, осаждённые при обычных условиях, c-микрочастицы, осаждённые в магнитном поле, d- микрочастицы, осаждённые в электрическом поле, б) микрофотография промышленного образца К-60 (Zn_2SiO_4-Mn)

Анализ спектров (рис.1a) показывает различие между спектрами ФЛ для исходного образца, нанесённого на подложку обычным способом и спектрами УДК, нанесённых на подложку в электрическом и магнитном поле. Видно, что исходный образец имеет спектр присущий кристаллической структуре α-Zn_2SiO_4-Mn (решётка ромбоэдрическая R^V). Этой структуре присуще излучение в видимой области с λ_{max}=510-530 нм и хорошо известно в литературе [24-26]. В данной работе спектры ФЛ УДК (рис.1b,c,d) имеют спектральные характеристики с λ_{max}=546-551 нм. Есть работы в которых люминофоры с подобными спектрами относят к α-Zn_2SiO_4 кристаллической структуре [27,28]. В большинстве работ отмечается, что виллемит со структурой β-Zn_2SiO_4-Mn имеет спектр с λ_{max}=570-580 нм [13,17,26,29,30]. Это объясняется тем, что люминесценция иона Mn^{2+} в кристалле Zn_2SiO_4:Mn^{2+} (переход $^4T_{1g}(^4G)\rightarrow^6A_{1g}(^6S)$) наблюдается в зелёной области (490-540 нм) для соединений с координационными числами к.ч. 4 и 8 и в оранжево-красной (570-640 нм) для соединений с к.ч. 6 [25]. Если принять то, что спектры (рис.1b,c,d) получены от смеси виллемита со структурами α- и β-Zn_2SiO_4 , то полуширина этих спектров должна быть в пределах $\Delta\lambda$=70-80нм. В данной работе получены спектры с полушириной $\Delta\lambda$=38-40нм. Уменьшение полуширины полос свидетельствует о структурированности спектральных линий, что в свою очередь указывает на улучшение люминесцентных характеристик кристалла. Этому, видимо, способствует направленная определённым образом ориентация кристаллов в магнитном или электрическом поле. Виллемит является диамагнетиком, что способствует его поляризации в магнитном поле. При попадании УДК Zn_2SiO_4 –Mn в сильное электрическое поле (10^5 В/м) частицы приобретают электрический дипольный момент, что так же способствует их определённой ориентации. Уровень поляризации ультрадисперсных кристаллов в данном случае выше, чем кристаллов исходного образца так, как согласно микрофотографии размеры УДК находятся в пределах 10-40 нм (рис.2в). На поляризацию наночастиц в электрическом и магнитном поле указывается и в работах [21,31-33].

При воздействии на исходный люминофор К-60 и УДК Zn_2SiO_4 –Mn ионами кислорода (энергия 1-3 кэВ) были получены спектры ИЛ (рис. 2a), по внешнему виду напоминающие спектры ФЛ (рис. 1a). В отличие от спектров ФЛ, которые отличались и λ_{max} и полушириной $\Delta\lambda$, спектры ИЛ для всех образцов имеют схожие

параметры λ_{max}=520-522 нм и $\Delta\lambda$=41 нм.

а)   б)
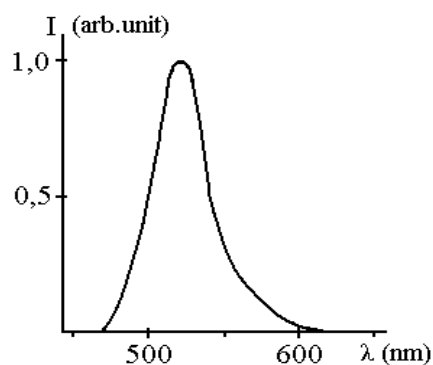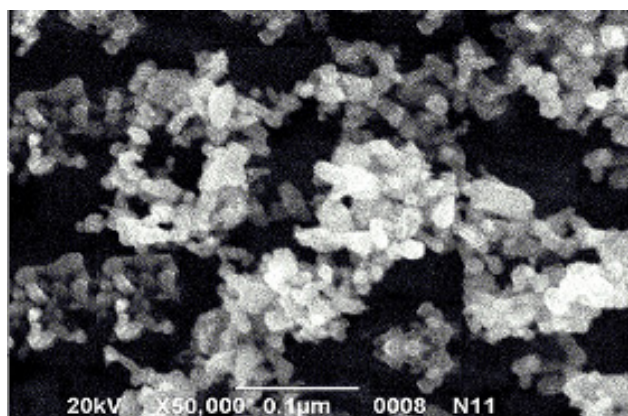
Рис.2. Спектр ионолюминесценции и микрофотография мелкодисперсных частиц виллемита
а) спектральные характеристики ИЛ образцов Zn₂SiO₄-Mn,   б) микрофотография УДК Zn₂SiO₄-Mn.

Отличие спектров ФЛ и ИЛ можно объяснить тем, что ФЛ это объёмная люминесценция кристалла, а люминесценция вызванная ионами низких энергий (до 3кэВ) – поверхностная люминесценция. Ионы низких энергий ~1 КэВ рассеиваются почти полностью на поверхностном слое и широко используются для исследования "первого монослоя" атомов кристалла [34]. Глубина воздействия ультрафиолетового излучения на кристаллические материалы до нескольких микрон. Схожие параметры спектров при ионолюминесценции указывают на то, что кристаллическое окружение активатора (иона марганца) в приповерхностном слое остаётся неизменным при измельчении виллемита. Также необходимо учитывать, что механизм взаимодействия ионов с кристаллической решёткой твёрдого тела отличается от механизма взаимодействия электро-магнитного поля УФ излучения с веществом. По данным УФ-спектроскопии ультрадисперсные кристаллы Zn₂SiO₄ -Mn прозрачны в видимом диапазоне длин волн. Для того чтобы определить ширину запрещённой зоны УДК Zn₂SiO₄ -Mn на спектрофотометре СФ-46 были определены коэффициенты пропускания в необходимой области длин волн. Затем по известной методике определили коэффициенты поглощения и построили графики в координатах $(\alpha h v)^2$ -hv [22, 23]. Значение ширины запрещённой зоны (Eg) получили путём линейной интерполяции прямолинейного участка графика на ось абсцисс.
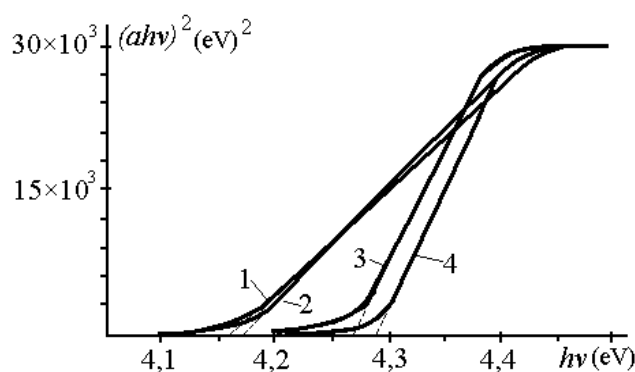
Рис.3. Спектры поглощения образцов Zn₂SiO₄ –Mn
Определение ширины запрещённой зоны образцов в координатах $(\alpha h v)^2$ –hv; 1-промышленный люминофор (К-60), 2-УДК, осаждённые при обычных условиях, 3- УДК, осаждённые в магнитном поле напряжённостью 0,3 Тл, 4- УДК, осаждённые в электрическом поле напряжённостью 10^5 В/м

На рис.3. показаны графики промышленного и УДК Zn₂SiO₄ -Mn. Значение ширины запрещённой зоны образца К-60 равно 4,16 эВ, для УДК Zn₂SiO₄ -Mn (при осаждении в обычных условиях) 4,17эВ, для УДК Zn₂SiO₄-Mn (при осаждении в магнитном поле напряжённостью 0,3 Тл) 4,27 эВ и для УДК Zn₂SiO₄ -Mn. (при осаждении в электрическом поле, напряжённостью 10^5 В/м) 4,29 эВ. Данные значения ширины запрещённой зоны получены при комнатной температуре. Наблюдается зависимость значения ширины запрещённой зоны Eg от размеров кристаллов и способа осаждения. В литературе отмечается, что уменьшение размеров нанокристаллов приводит и к изменению их спектров свечения. Влияние размеров наночастиц на их спектральные характеристики наиболее ярко проявляется при размерах наночастиц в области 10 нм. Сдвиг спектральных линий в данном случае можно объяснить размерным эффектом. Размерным эффектом

объясняется сдвиг полос в работах [35-39].

Таким образом, уменьшение размеров наночастиц позволяет кардинальным образом изменять спектральные характеристики материала. Ширина запрещённой зоны виллемита значительно увеличивается при осаждении УДК Zn_2SiO_4-Mn в магнитном или электрическом поле. В данной работе было установлено, что осаждённые в магнитном или электрическом поле кристаллы Zn_2SiO_4-Mn ультрадисперсных размеров улучшают свои спектральные свойства. Причём в настоящей работе для этого использовалась не специально подготовленная подложка. Результаты работы показывают, что на неориентированной подложке, при осаждении УДК в магнитном или в электрическом поле тоже можно получать образцы с высокими спектральными параметрами близкими к параметрам для кристаллов высокой чистоты и идеальной кристаллической решёткой.

ЗАКЛЮЧЕНИЕ

Получены спектральные характеристики при возбуждении Zn_2SiO_4-Mn ультрафиолетом и пучком ионов кислорода. Анализ спектров показал, что уменьшение размеров кристаллов Zn_2SiO_4-Mn не влияет на спектральные характеристики при возбуждении пучком ионов кислорода низких энергий. Спектр люминесценции при воздействии ионами низких энергий (1-3 кэВ) имеет полосу с λ_{max}=521 нм и полушириной $\Delta\lambda$=41 нм. При возбуждении ультрафиолетом спектральные характеристики имели отличие для образцов с различной размерностью кристаллов. Так для промышленного образца спектр люминесценции имел полосу с λ_{max}=521 нм, а для ультрадисперсных кристаллов виллемита спектральная полоса имела λ_{max}=550 нм. Это указывает на то, что размерность кристаллов люминофора влияет на спектральные характеристики фотолюминесценции. При измерении ширины запрещённой зоны была установлена зависимость ширины запрещённой зоны от размеров кристаллов люминофора. Ширина запрещённой зоны увеличивается при уменьшении размеров кристаллов до наноразмерных величин. Значительный эффект был получен при осаждении на подложку наноразмерных кристаллов в магнитном или электрическом поле. Так для промышленного образца ширина запрещённой зоны составила 4,16 эВ, а для осаждённых в магнитном и электрическом поле 4,27 и 4,29 эВ соответственно.

СПИСОК ЛИТЕРАТУРЫ
1. Bhargava R.N., Gallaghar D., Hong X., Nurmikko A. Optical properties of manganese-doped nanocrystals of ZnS //J. Phys. Rev. Lett.- 1994.- Vol. 72.- P. 416-419.
2. Ronda C.R. Recent achievements in research on phosphors for lamps and displays // J. Luminescence. - 1997. - Vol. 72-74. - P. 49-54.
3. Ozel E., Yurdakul H., Turan S., Ardit M., Cruciani G., Dondi M. Co-doped willemite ceramic pigments: Technological behaviour, crystal structure and optical properties // J. Europ.Ceram.Soc. -2010. - Vol. 30. - P. 3319-3329.
4. Van der Kolk E. VUV phosphors for lamp and display application. -Amsterdam: Elsevier, 2001. -198 p.
5. Chandra Babu B., Buddhudu S. Dielectric properties of willemite α - Zn_2SiO_4 nano powders by sol-gel method//Physics Procedia.-2013.-Vol.49.-P.128-136.
6. Podbrscek P., Drazic G., Anzlovar A., Orel Z.C. The preparation of zinc silicate/ZnO particles and their use as an efficient UV absorber // Mater. Res.Bul. -2011. -Vol. 46. -P. 2105-2111.
7. El Mir L., Omri K. Photoconversion from UV-to-yellow in Mn doped zinc silicate nanophosphor material // Superlat. Microstruc. -2014. -Vol. 75. -P. 89-98.
8. Chandrappa G.T., Ghosh S., Patil K.C. Synthesis and Properties of Willemite, Zn_2SiO_4 and M2+: Zn_2SiO_4 M = Co and Ni) // J,Mater.Synt.Proc. -1999. - Vol. 7, No 5. -P. 273-279.
9. Pozas R., Orera V.M., Ocuna M. Hydrothermal synthesis of Co-doped willemite powders with controlled particle size and shape // J.Europ.Ceram.Soc. -2005. -Vol. 25. -P. 3165-3172.
10. Jiang Y., Chen J., Xie Z., Zheng L. Syntheses and optical properties of α - and β- Zn_2SiO_4: Mn nanoparticles by solvothermal method in ethylene glycol–water system // Mater.Chem.Phys. -2010. -Vol. 120. -P. 313-318.
11. El Mir L., Omri K., El Ghoul J., Al-Hobaib A.S., Dahman H., Barthou C. Yellow emission of SiO2/ Zn_2SiO_4:Mn nanocomposite synthesized by sol–gel method // Superlat.Microstruc. -2014. -Vol. 65. -P. 248-255.
12. Babu K.S., Reddy A.R., Reddy K.V., Mallika A.N. High thermal annealing effect on structural and optical properties of ZnO– SiO2 nanocomposite // Mater.Sci. Semicond. Proc. -2014. -Vol. 27. -P. 643-648.
13. Omri K, El Mir L. Effect of manganese concentration on photoluminescence properties of Zn2SiO4:Mn nanophosphor material // Superlattices and Microstructures. -2014.-Vol.70.-P. 24-32.
14. Kong D.Y., YU M., Lin C.R., Liu X.M., Lin J., Fang J. Sol-gel synthesis and characterization of Zn_2SiO_4 :Mn@SiO_2 Spherical core-shell particles//Journal of The Electrochemical Society.-2005.-Vol.152, No. 9.-P146-151.
15. Dacanin L., Lukic S.R., Petrovic D.M., Antic Z., Krsmanovic R., Marinovic-Cincovic M., Dramicanin M.D. PMMA Zn_2SiO_4 :Eu3+(Mn2+) Composites: Preparation, Optical, and Thermal Properties // J.Mater.Eng.Perform. -2012. -Vol. 21, No. 7. - P.1509-1513.
16. Lu Q., Wang P., Li J. Structure and luminescence properties of Mn-dope Zn_2SiO_4 doprepared with extracted mesoporous silica // Mater.Res.Bul. -2011. -Vol. 46. -P. 791-795.
17. Li X., Chen F. Structure and luminescence properties of Zn_2SiO_4-Mn phosphor prepared with MCM-48 // Mater.Res.Bul. - 2013. -Vol. 48. - P. 2304-2307.
18. Sang-Hun Nam, Myoung-Hwa Kim, Jun-Yong Lee, Sang Duck Lee, Jin-Hyo Boo. Spray pyrolysis of manganese doped zinc silicate phosphor particles //Functional Materials Letters.-2010.-Vol.3, No2.- H.97-100.
19. Sivakumar V., Lakshmanan A. Pyrolysis synthesis of Zn_2SiO_4:Mn2+ phosphors -effect offuel, flux and co-dopants // J.Lumin. -

2014. -Vol. 145. -P. 420-424.

20. Li Q. H., Komarneni S., Roy R. Control of morphology of Zn2Si04 by hydrothermal Preparation // J.Mater.Sci. -1995. -Vol. 30. -P. 2358-2363.

21. Tyutyunnikov V.I. Spectra of ZnO Superdispersed Paticles Polaized in an Electric Field // East European Journal of Physics.- 2015.-Vol.2, No 3.-P.64-69.

22. Kulak A.I., Streltsov E.A., Rabchynski S.M. Band gap determination of semiconductor electrodes from photopotential spectrum // Sviridov Readings.- Iss.7.-Minsk.-2011.-P.1-10.

23. Troshin A.V., Kovalenko A.A., Dorofeev S.H., BaranovA.N. Sensitization ZnO nanorods CdSe quantum dots // Inorganic materials.-2012.-Vol.48, No7.-P.1-8. (in Russian).

24. Bhatkar V.B., Omanwar S.K.,Moharil S.V. Combustion synthesis of the Zn_2SiO_4 :Mn Phosphor //Phys. Stat. Sol.-2002.-Vol.191, No.1.-P.272-276.

25. Shamshurin A.V., Efryushina N.P.,Malinka E.V. Kinetika zatuhaniy lyuminescencii ionov marganca (II) in krisnallofosforah na osnove Zn_2SiO_4 and CaF_2 // Transactions of the Odessa Polytechnic universiteta.- 2003.-Issue.2(20).-C.1-5.

26. Kang Z.T., Liu Y., Wagner B.K., Gilstrap R., Liu M., Summers C.J. Luminescence properties of Mn^{2+} doped Zn_2SiO_4 phosphor films synthesized by combustion CVD // Journal of luminescence.-2006.-Vol.121.- P.595-600.

27. Dubey V., Tiwari R., Pradhan M.K., Rathore G. S., Sharma C., Tamrakar R.K. Photoluminescece and thermoluminescence behavior of Zn_2SiO_4 :Mn^{2+} , Eu^{2+} phosphor // Journal of luminescence and applications. – 2014. – Vol.1. – No.1. – P.30-39.

28. Alexanderovskiy A.S. Gudim I.A. Krylov A.S., Temerov V.L. Luminescence single crystals of yttrium aluminum borate, activated manganese // Solid State Physics.-2007.-Vol.49, No. 9.-P.1618-1621.

29. Omri K., El Mir L. Dahman H., Barthou C. Synthesis and luminescence properties of yellow-emitting SiO_2 $_-$ Zn_2SiO_4 : Mn nanocomposite // Sensors&Transducers.-2014.-Vol.27, Special Issue May.-P.295-298.

30. Bertail C., Maron S., Buissette V., Le Mercier T., Gacoin T., Boilot J.P. Structural and Photoluminescent properties of Zn_2SiO_4 :Mn^{2+} nanoparticles prepared by a protected annealing process // Chemistry of materials.-2011.-Vol.23.-P.2961-2967.

31. Malyshev K.V. The polarization of the nanoparticles in the tunneling microscope // Science and education. - 2011.- No.10. - P.1-13(in Russian). http://technomag.edu.ru/pdf/out/228079.pdf

32. Shirokov V.P., Biryukov S.V., Mukhortov V.M., Yuzyuk Y.I. The polarization of thin films of barium strontium titanate under the influence of an external electric field // Technical Physics. - 2011.-Vol.81. - Vyp.8.-P.115-121. (in Russian).

33. Tyutyunnikov V.I. Spectra of ZnO Superdispersed Paticles Polaized in an Magnetic Field // East European Journal of Physics.- 2016.-Vol.3, No.1.-P.61-66.

34. Oura K., Lifshiz V.H., Saranin A.A. et al. Introduction to the physics of surfacee. - M.: Nauka, 2006 - 490 p. (in Russian).

35. Gusev A.I. Nanomaterials technology structure.- M: FIZMATLIT.- 2005.- 416p. (in Russian).

36. Ivanov M.S, Kastryulina T.G, Soloviev V.G, Filippov V.A, Gerbreder V.I, Ogurcov A.S. Physical properties of nitrite and sodium nitrate in the nanoparticle matrices zeolites NaA and NaX // Vestnik PskovGU Series «Natural, physical and mathematical sciences».- 2014.-Vol.4.-P.153-161. (in Russian).

37. Agekyan V.F., Akai I.V, Karasawa T. Morphology and optical spectra of microcrystals metal iodates in porous matrices // Solid State Physics. - 2003. - Vol. 45, No 6.-P.1115-1121.

38. Ekimov A.I., Efros AL., Onushchenko A.A. Quantum size effect in semiconductor microcrystals. // Solid State Communication.-1995. -Vol.56, No. 11. - P.921- 924.

39. Feofilov S.P. Spectroscopy of dielectric nanocrystals doped with rare earth and transition metals // Solid State Physics.-2002.-Vol. 44, No. 8.-P.1348-1355.

THE THERMODYNAMIC FUNCTIONS OF MONOBORIDES XB (X=Ti, Mn, Fe, Co)

N. Yu. Filonenko

Dnipropetrovsk Medical Academy, Ministry of Public Health of Ukraine
49044, Ukraine, Dnipro, Vladimir Vernadsky, 9
E-mail: natph@mail.ru
Received December 1, 2016

In the paper the physical properties and thermodynamic functions of monoborides XB (X=Ti, Mn, Fe, Co) are studied with accounting for fluctuation processes. The research was performed for alloys with boron content of 9,0-15,0 % (wt.), the rest is metal X (X=Ti, Mn, Fe, Co). We use the microstructure analysis, the X-ray structural and the durometric analyses to determine the physical properties of alloys. In the paper it is determined the phase composition of Ti-B, Mn-B, Fe-B and Co-B alloys and physical properties of monoborides. In this paper for the first time it is determined the thermodynamic functions of monoborides using the Hillert and Staffansson model with accounting for the first degree approximation of high-temperature expansion for the free energy potential of binary alloys. We obtain the temperature dependences for such thermodynamic functions as Gibbs free energy, entropy, enthalpy and heat capacity C_p along with their values at the formation temperature for XB monoborides (X=Ti, Mn, Fe, Co). The approach under consideration enables to give more thorough from the thermodynamic point of view description of monoborides formed from the liquid. The outcomes of the thermodynamic function calculation for TiB, MnB, CoB та FeB monoborides are in good agreement with experimental data and results of other authors.
KEY WORDS: monoborides, Gibbs energy, entropy, enthalpy, heat capacity, fluctuation process

ТЕРМОДИНАМІЧНІ ФУНКЦІЇ МОНОБОРИДІВ XB (XB (X=Ti, Mn, Fe, Co)
Н.Ю. Філоненко
Державний заклад «Дніпропетровська медична академія МОЗ України»
м. Дніпро, вул. Володимира Вернадського, 9, 49044, Україна

У роботі досліджено фізичні властивості та термодинамічні функції моноборидів XB (X=Ti, Mn, Fe, Co) з урахуванням флуктуаційних процесів. Дослідження проводили на сплавах з вмістом бору 9,0-15,0 % (мас.), інше – метал X (X=Ti, Mn, Fe, Co). Для визначення фізичних властивостей сплавів використовували мікроструктурний, рентгеноструктурний та дюрометричний аналізи. В роботі було визначено фазовий склад сплавів Ti-B, Mn-B, Fe-B та Co-B і фізичні властивості моноборидів. Вперше визначено термодинамічні функції моноборидів з використанням моделі Хіллерта і Стеффансона та з урахуванням першого ступеня наближення високотемпературного розвинення термодинамічного потенціалу бінарних сплавів. Для моноборидів XB (X=Ti, Mn, Fe, Co) отримано залежності від температури таких термодинамічних функцій, як енергія Гіббса, ентропія, ентальпія й теплоємність Cp, а також визначено їх значення при температурі утворення. Використаний у даній роботі підхід дає можливість надати найбільш повний з термодинамічної точки зору опис моноборидів, що утворюються з рідини. Отримані результати розрахунків термодинамічних функцій моноборидів TiB, MnB, CoB та FeB добре узгоджуються з експериментальними даними та даними інших авторів.
КЛЮЧОВІ СЛОВА: монобориди, енергія Гіббса, ентропія, ентальпія, теплоємність, флуктуаційний процес

ТЕРМОДИНАМИЧЕСКИЕ ФУНКЦИИ МОНОБОРИДОВ XB (X=Ti, Mn, Fe, Co)
Н.Ю. Филоненко
ГУ «Днепропетровская государственная медицинская академия МОЗ Украины»
49044, Украина, г. Днепро, ул. Владимира Вернадского, 9

В работе исследованы физические свойства и термодинамические функции моноборидов XB (X=Ti, Mn, Fe, Co) с учетом флуктуационных процессов. Исследования проводились на сплавах с содержанием бора 9,0-15,0 % (масс.), остальное – металл X (X=Ti, Mn, Fe, Co). Для определения физических свойств сплавов использовались микроструктурный, рентгеноструктурный и дюрометрический анализы. В работе были определены фазовый состав сплавов Ti-B, Mn-B, Fe-B и Co-B и физические свойства моноборидов. Экспериментальное определение термодинамических характеристик моноборидов является достаточно сложным. Поэтому в данной работе впервые определены термодинамические функции моноборидов при использовании модели Хиллерта и Стеффансона и с учетом первой степени приближения высокотемпературного разложения термодинамического потенциала бинарных сплавов. Для моноборидов XB (X=Ti, Mn, Fe, Co) получены зависимости от температуры таких термодинамических функций, как энергия Гиббса, энтропия, энтальпия и теплоемкость Cp, а также определены их значения при температуре образования. Использованный в данной работе подход позволяет предоставить наиболее полное с термодинамической точки зрения описание моноборидов, образующихся из жидкости. Полученные результаты расчетов термодинамических функций моноборидов TiB, MnB, CoB и FeB хорошо согласуются с экспериментальными данными и данными других авторов.
КЛЮЧЕВЫЕ СЛОВА: монобориды, энергия Гиббса, энтропия, энтальпия, теплоёмкость, флуктуационный процесс

Сплави, що містять бор мають практичне застосування, через комплекс унікальних властивостей, таких як тугоплавкість, висока твердість, хімічна стійкість в різних агресивних середовищах та інші [1-2]. Так, наприклад, бориди та сплави, що містять бор, застосовують в атомній енергетиці завдяки їх спеціальним властивостям [3], а також, при створенні нових композиційних матеріалів, де в якості зміцнюючи фаз використовують монобориди [1-2].

Дослідження фізичних властивостей та термодинамічних функцій сплавів, що містять бор має теоретичне та практичне значення, тому, що монобориди утворюються не тільки в сплавах на основі металів з вмістом бору 9,0-16,0 % (мас.), а також в результаті процесу насичення поверхні сплавів бором і впливають на фізичні властивості борованого шару. Крім того, це дозволить розробити металеві сплави, що містять бориди, композиційні матеріали та покриття з прогнозованими фізичні властивостями та фазовим складом.

Як відомо, у сплавах, що містять 50 % (ат.) бору відбувається утворення монобориду з рідини [1-2]. Монобориди TiB, MnB, CoB та FeB мають ромбічну елементарну комірку з 4 атомами в елементарній комірці та відносяться до просторової групи [4].

В роботах [5-10] автори наводять результати розрахунку енергії Гіббса фаз TiB, MnB, CoB та FeB з застосуванням моделей, які можуть бути використані тільки за рівноважних умов та не враховують флуктуаційні процеси.

Метою даної роботи було дослідження фізичних властивостей та термодинамічних функцій моноборидів, їх залежності від температури з урахуванням першого ступеня наближення високотемпературного розвинення термодинамічного потенціалу бінарних сплавів, що дозволить визначити значення термодинамічних функцій моноборидів, у високотемпературній області та врахувати внесок флуктуаційних процесів.

МАТЕРІАЛИ ТА МЕТОДИКА ДОСЛІДЖЕНЬ

Дослідження проводили на зразках із вмістом бору 9,0-15,0 % (мас.), інше – метал (титан, марганець, кобальт та залізо), для отримання яких використовували шихту такого складу: метал з вмістом 99,99 %, аморфний бор (з вмістом бору 97,5 % (мас.). Виплавку зразків проводили в печі Тамана з графітовим нагрівачем в алундових тиглях в атмосфері аргону. Швидкість охолодження сплавів складала 10 К/с. Для визначення хімічного складу сплаву використовували хімічний та спектральний аналіз [11]. Мікротвердість фаз вимірювали на приборі ПМТ-3.

Фазовий склад сплавів визначали методом мікрорентгеноспектрального аналізу на мікроскопі JSM–6490, а також за допомогою оптичного мікроскопу «Неофот-21». Локальний рентгеноспектральний аналіз проведено з використанням внутрішніх еталонів. Рентгеноструктурний аналіз здійснювали на дифрактометрі ДРОН-3 в монохроматизованному Fe-Kα випромінюванні.

РЕЗУЛЬТАТИ ТА ЇХ ОБГОВОРЕННЯ

Мікроструктура сплавів Mn-B, Fe-B та Co-B в литому стані, з вмістом бору в інтервалі 9,0-15,0 % (мас.), містить округлі дендрити моноборидів, розташованих у твердому розчині на основі бориду металу (рис. 1).

Відомо, що бор має малу розчинність в титані, тому при легуванні бором титану в кількості, навіть більшій ніж 0,2 % (мас.), по границях β-зерен спостерігали утворення монобориду TiB, який мав морфологію первинних волокон (рис. 1a).

Результати визначення параметра гратки фаз TiB, MnB, FeB та CoB рентгеноструктурним методом корелюють з даними, наведеними іншими авторами (табл. 1).

Таблиця 1

Параметри кристалічної гратки моноборидів

Моно-борид	Вміст бору, % (мас.)	Параметри кристалічної гратки (експ.)			Параметри кристалічної гратки (табл.)			Джерело
		a, Å	b, Å	c, Å	a, Å	b, Å	c, Å	
TiB	0,3	4,563	3,065	6,115	4,56	3,06	6,112	[1]
MnB	12,0	4,145	2,979	5,5562	4,144	2,977	5,556	[12]
FeB	12,0	4,0569	3,027	5,0683	4.061	2,295	5,502	[4]
CoB	12,1	3,952	3,021	5,254	3,956	3,043	5,253	[13]

Для моноборидів TiB та MnB спостерігали незначне збільшення ступеня мікронапружень та густини дислокацій (табл. 2) у порівнянні з іншими моноборидами.

Таблиця 2

Розмір кристалітів, густина дислокацій, ступень мікронапружень у моноборидах

Моноборид	Вміст бору, % (мас.)	Розмір кристалітів L, Å	Ступень мікронапружень	Густина дислокацій $\rho \times 1010$, см-2
TiB	0,3	1022	$7{,}81 \cdot 10$-3	8,64
MnB	12,0	984	$7{,}12 \cdot 10$-3	6,79
FeB	12,0	920	$5{,}26 \cdot 10$-4	5,1
CoB	12,1	856	$2{,}85 \cdot 10$-3	4,92
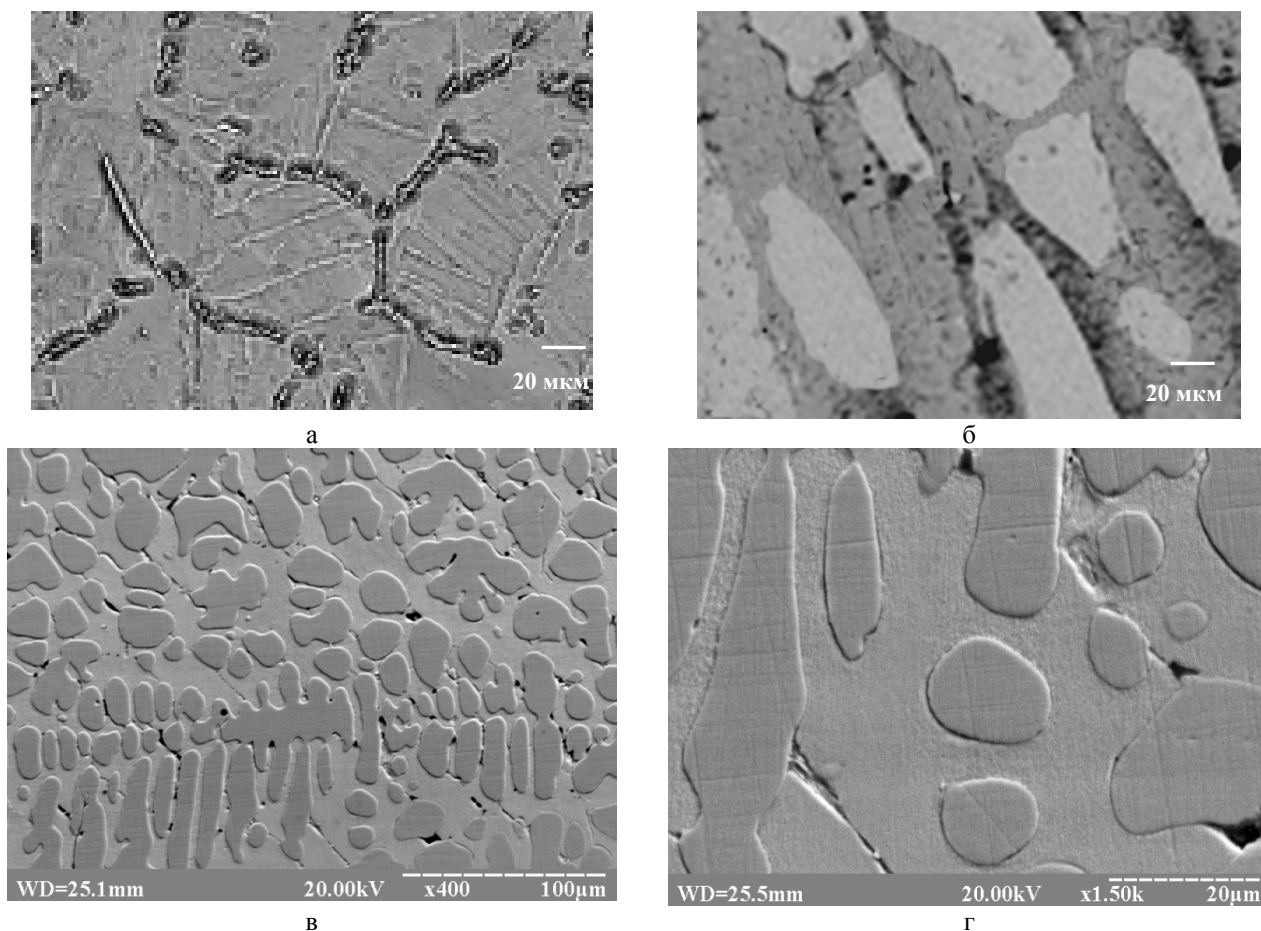
Рис. 1. Мікроструктура сплавів з вмістом бору 13 % (мас.) Ti-B (а), Mn-B (б), Fe-B (в) та Co-B (г)

Крім того, відомо, що на фазові перетворення у сплавах на основі металів, що містять бор мають вплив домішки карбону та інших елементів [14-15]. Результати спектрального аналізу сплавів Ti-B, Mn-B, Fe-B та Co-B показали, що у сплаві, крім металів та бору, присутні: домішки карбону з вмістом 0,05 %(мас.), кремнію – 0,004 % (мас.). Відомо, що розчинність карбону в боридах мала, але більша за значенням, ніж у сплавах, які досліджували в даній роботі [16]. Незважаючи на присутність карбону у сплавах, що досліджували можна стверджувати, що його вплив на фазові перетворення незначний.

Отримання на підставі експериментальних досліджень значень термодинамічних функцій моноборидів TiB, MnB, FeB та CoB містить певні труднощі. Тому врахування внеску першого ступеню наближення високотемпературного розвинення термодинамічного потенціалу у моделі Хіллерта й Стеффансона дає змогу теоретично визначити термодинамічні функції моноборидів та їх залежність від температури.

Енергія Гіббса моноборидів TiB, MnB, FeB та CoB. Енергія Гіббса фази, як відомо, є функцією незалежних змінних $G = G(p, T, y)$, де p – тиск, T – температура, y – масовий вміст елементів. Для мольних часток компонентів в сполуці чи сплаві виконується умова $\sum_{i=1}^{2} y_i = 1$.

За підгратковою моделлю Хіллерта й Стеффансона [17] було розраховано енергію Гіббса моноборидів:

$$G_m^{MeB} = y_{Me}{}^0 G_{Me} + y_B{}^0 G_B + RT\left(y_{Me}\ln y_{Me} + y_B\ln y_B\right) + y_{Me}y_B L_{Me:B}. \qquad (1)$$

Використовуючи дані для енергії чистих компонент ${}^0 G_{Me}$, ${}^0 G_B$ [18-19], дані енергії взаємодії між компонентами в фазі $L_{Me:B}$ з робіт [5, 7, 8, 20], отримано наступну залежність енергії Гіббса моноборидів від температури (табл. 3).

Модель Хіллерта й Стеффансона можна застосувати для рівноважного стану. У потенціалах моделі Хіллерта й Стеффансона не враховано внесок першого ступеня наближення високотемпературного розвинення термодинамічного потенціалу бінарного сплаву, який необхідно враховувати при знаходженні енергії Гіббса фаз, що утворюються з рідини, та включенні до розгляду флуктуаційних процесів.

Залежність енергії Гіббса моноборидів від температури

Моноборид	G_m^{MB}, (Дж/моль)	Джерело
TiB	$-83553 + 2,1\,T$	У даній роботі
	$-83020 + 1,62\,T$	[20]
	$-142942 + 28,03\,T$	[21]
MnB	$-49296,3 + 1,8\,T$	У даній роботі
	$-35800 - 9,9995\,T$	[9]
	$-36225 + 0,439\,T$	[12]
FeB	$-41500 + 9,8\,T$	У даній роботі
	$-73410 + 6,5\,T$	[22]
	$-34300 + 3,25\,T$	[23]
CoB	$-35786,5 + 1,3\,T$	У даній роботі
	$-34500,0 + 0,24\,T$	[10]
	$-28564 + 5,07\,T$	[24]

Як відомо з теорії бінарних сплавів, статистична сума такої системи не може бути обчислена точно, але згідно з методом Кірквуда може бути записана у вигляді нескінченного ряду за ступенями $1/T$ [25-26]. Таким чином, енергію Гіббса з урахуванням першого ступеня наближення для моноборидів визначимо як:

$$G_m^{MeB} = y_{Me}\,^0G_{Me} + y_B\,^0G_B + RT\left(y_{Me}\ln y_{Me} + y_B \ln y_B\right) + y_{Me}y_B L_{Me:B} - \frac{L^2_{Me;B}y^2_{Me}y^2_B}{2ZRT}. \tag{1}$$

де Z – координаційне число, яке для монобориду дорівнює $Z = 4$.

За результатами розрахунку за формулою (1) були отримані математичні залежності енергії Гіббса моноборидів TiB, MnB, CoB та FeB від температури та значення енергії Гіббса моноборидів при температурі утворення (табл. 4).

Залежності енергії Гіббса моноборидів від температури та її числове значення при температурі утворення

Моно-борид	G_m^{MeB}, Дж/моль	G_m^{MeB} при температурі утворення, Дж/моль	G_m^{MeB}, (Дж/моль)
TiB	$G_m^{TiB} = -89553,32 + 2,1\,T - 9,8\cdot10^5 T^{-1}$	-82821,29	-81633,7 [21]
MnB	$G_m^{MnB} = -49296,3 + 1,8\,T - 5,1\cdot10^6 T^{-1}$	-47731,88	-56029 [9]
FeB	$G_m^{FeB} = -41500 + 7,8\,T - 7\cdot10^5 T^{-1}$	-27264,3	-28203 [23]
CoB	$G_m^{CoB} = -35786 + 1,3\,T - 2,8\cdot10^6 T^{-1}$	-35171,2	-34086,5 [13]

Як видно з табл. 4, отримані значення енергії Гіббса моноборидів корелюють зі значеннями інших авторів.

Таким чином, отримана залежність енергії Гіббса моноборидів від температури дозволяє визначити їх значення в високотемпературній області та врахувати внесок флуктуаційних процесів.

Ентропія, ентальпія та теплоємність Ср моноборидів TiB, MnB, FeB та CoB. Однією з найважливіших термодинамічних характеристик фази є ентропія. Ентропію моноборидів можна визначити за формулою

$$S = -\left(\frac{\partial G}{\partial T}\right)_p = -R\left(y_{Me}\ln y_{Me} + y_B \ln y_B\right) - \frac{L_{Me:B}^2}{2ZRT^2}y^2_{Me}y^2_B.$$

Врахування внеску першого ступеня наближення високотемпературного розвинення термодинамічного потенціалу в енергії Гіббса дозволило визначити ентальпію моноборидів. Для обчислення ентальпії моноборидів використаємо співвідношення [27]: $\Delta H = \Delta G + T\Delta S$.

Залежність ентальпії фаз TiB, MnB, CoB та FeB від температури має наступний вигляд:

$$H^{TiB} = -82369 + 0,7\,T - 3,2\cdot10^5\,T^{-1} \quad H^{MnB} = -49253 + 0,5\,T - 4,25\cdot10^5\,T^{-1},$$

$$H^{FeB} = -38852 + 1,2\,T - 3\cdot10^5\,T^{-1}, \quad H^{CoB} = -36534 + 0,7\,T - 4,2\cdot10^5\,T^{-1}.$$

Таким чином, результати розрахунку чисельних значень ентальпії при температурі утворення, отримані в даній роботі, узгоджуються з результатами інших авторів [9, 13, 21, 7,28, 29].

Для фаз TiB, MnB, CoB та FeB було визначено теплоємність з застосуванням співвідношення

$$C_p = T\left(\frac{\partial S}{\partial T}\right)_p = \frac{L_{Fe:B}^2}{RZT^2}\,y_{Fe}^2 y_B^2.$$
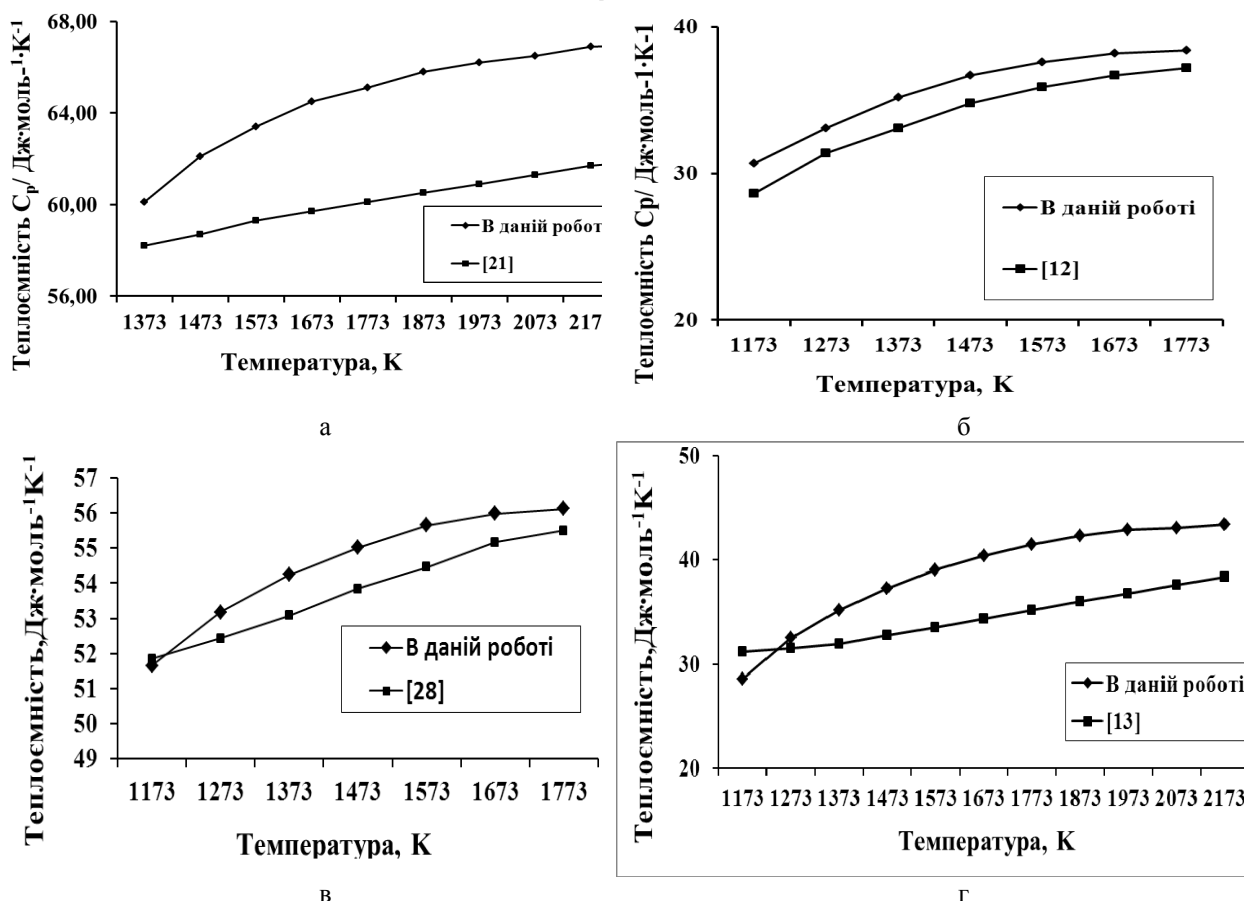
Рис. 2. Залежність теплоємності Cp моноборидів TiB (а), MnB (б), FeB (в) та CoB (г) від температури

Отримані результати − залежність теплоємності Cp моноборидів TiB, MnB, FeB та CoB від температури (рис. 2) − корелюють з результатами наведеними в роботах [8, 12, 21, 28, 30].

Аналіз отриманих результатів дозволяє зробити висновок про те, що врахування у моделі Хіллерта й Стеффансона внеску першого ступеня наближення високотемпературного розвинення термодинамічного потенціалу бінарних сплавів дозволяє виконати розрахунки таких термодинамічних величин моноборидів, як ентропія, ентальпія, теплоємність та їх залежність від температури. Крім того, це дає змогу найбільш повно з термодинамічної точки зору надати опис моноборидів, що утворюються з рідини.

ВИСНОВКИ

У роботі досліджено структурні та фізичні властивості моноборидів TiB, MnB, CoB та FeB в бінарних сплавах з масовим вмістом бору 9,0-15,0 % (мас.), інше − метал.

Слід зазначити, що термодинамічні функції фаз дають змогу прогнозувати фізичні та хімічні властивості сплавів за змінних зовнішніх умов, таких як температура, тиск тощо. Достатньо відомі методи розрахунку термодинамічних функцій фаз можуть бути використані тільки за рівноважних умов і не враховують флуктуаційні процеси. Тому в роботі за моделлю Хіллерта й Стеффансона з урахуванням внеску першого ступеня наближення високотемпературного розвинення термодинамічного потенціалу моноборидів TiB, MnB, CoB та FeB були отримані залежності від температури таких термодинамічних функцій, як енергія Гіббса, ентропія, ентальпія і теплоємність Cp.

Отримані результати розрахунків термодинамічних функцій моноборидів TiB, MnB, CoB та FeB добре узгоджуються з експериментальними даними.

СПИСОК ЛІТЕРАТУРИ

1. Samsonov G.V., Serebryakova T.I., Neronov V.A. Boridy [Borides]. – Moscow: Atomizdat, 1999. – 220 p. (In Russian)
2. Lyakishev N.P., Pliner Yu.L., Lappo S.I. Borsoderzhaschiye stali i splavy [Boron containing steels and alloys.]. – Moscow: Metallurgiya, 1986. – 191 p. (In Russian)
3. Smirnov A.V. Rust-resisting steel Boron 304 with boron, meant for divided cask making for storage and transportation of nuclear waste // Iron and steel industry news bulletin abroad. Alerting service. - 1981, issue 63-И. - P. 1-4.
4. Kuzma Yu.B. Kristallokhimiya boridov [Crystal chemistry of borides]. – Kyiv: Vyscha shkola, 1983. – 159 p. (In Russian)
5. Halemans B., Wollemans P., Roos J.R. Thermodynamic Reassessment and Calculationofthe Fe-B Phase Diagram // Metallkd.– 1994. – 85(10). – P. 676-682.
6. Li Yan-feng, Xu Hui, Xia Qing-lin, LIU Xiao-liang J. First-principles calculation of structural and Thermodynamic properties of titanium boride // Cent. SouthUniv. Technol. – 2011. – Vol.18. – P. 1773−1779.
7. Bing Wang, Xiang Li,Yuan Xu Wang, Yu Fei Tu Phase Stability and Physical Properties of Manganese Borides: A First-Principles Study // J. Phys. Chem. C. – 2011. – Vol.115 (43). – P. 21429–21435.
8. Mikhajlovskij B.V., Goryacheva V.I., Kutsenok I.B. Calculation of self-consistentt hermodynamic data and phase equilibria for the cobalt-boron system // Zhurnal Fizicheskoj Khimii. – 1999. –Vol. 73(4). – P. 763-765.
9. Weihua Sun, Yong Du, Shuhong Liu, Baiyun Huang, Chao Jiang Terodynamic Assessment of the Mn-B System // Journal of Phase Equilibria and Diffusion. – 2010. – Vol. 31. – No. 4. – P. 357–364.
10. Witusiewicz V.T. Thermodynamics of binary and ternary melts of the 3d transition metals (Cr, Mn, Fe, Co and Ni) with boron // Thermochimica Acta. – 1995. – Vol. 264. – P. 41-58.
11. Tverdokhlebova S.V. Spektrometriya borsoderzhaschikh splavov [Spectrometry of boron alloys] // Visnyk Dnipropetrovskogo universytety. Seria «Fizyka. Radioelektronika». – 2007. – Issue 14. – No. 12/1. – P. 100-104. (In Russian)
12. Liao P.K., Spear K.E. The B-Mn (Boron-Manganese) System // Bulletin of Alloy Phase Diagrams. – 1986. – Vol. 7. – No. 6. – P. 543-549.
13. Liao P.K., Spear K.E. The B-Co (Boron-Cobalt) System // Bulletin of Alloy Phase Diagrams. – 1988. – Vol. 9. – No.4. – P. 452-457.
14. Portnoy K.I., Levinskaya M. Kh., Romashov V.M. State diagram of iron-boron system // Metal powder industry. – 1969. – No.8(80). – P. 66-69.
15. Filonenko N.Yu., Beryoza O.Yu., Bezrukava O.G. The effect of carbon on phase composition and phase transformations in Fe-B system alloys // Promblems of atomic science and technology. − 2013. – No.5. – P. 168-172.
16. Filonenko N.Yu., Galdina O.M. Effect of carbon on physical and structural properties of FeB iron monoboride // East Eur. J. Phys. – 2016. – Vol.3. – No.2. – P. 49-53.
17. Hillert M., Staffonsson L. The Regular Model for Stoichiometric Phases and Ionic Melts // Acta Chemica Scand. – 1970. – Vol.24(10). – P. 3618-3626.
18. Richard A. Roble and David R. Waldbaum Thermodynamic Properties of Minerals and Related Substances at 298.15°K (25.0°C) and One Atmosphere (1.013 Bars) Pressure and at Higher Temperatures. – Orton memorial library the OHIO State University 155 S. Oval Drive, 1970. – P. 262.
19. SGTE data for pure elements A T Dinsdale NPL Materials Centre, Division of Industry and Innovation, National Physical Laboratory, Teddington, Middlesex, TW11 0LW, UK. – P. 174.
20. Nakama Yu., Ohtani Hiroshi, Hasebe Mitsuhiro Thermodynamic Analysis of the Nb–Ti–B Ternary Phase Diagram // Materials Transactions. – 2009. – Vol. 50. – No. 5. – P. 984-993.
21. Murray J.L., Liao P.K. The B-Ti (Boron-Titanium) System // Bulletin, of Alloy Phase Diagrams. –1986. – Vol. 7. – No. 6. – P. 550-555.
22. Keita Yoshimoti,Yu Nakama, Hiroshi Ohtani, Mitsuhiro Haseb Thermodynamic Analysis of the Fe–Nb–B Terrnary System // ISIJ International. – 2008. – No.48(6). – P. 835-844.
23. Hiroshi Ohtani, Mitsuhiro Hasebe, Taiji Nishzawa Calculation of Fe-C-B // Ternary Phase Diagram. Transactions ISIJ. – 1988. –Vol. 28. – P. 1043-1050.
24. Liu Y.Q., Zhao X.S., Yang J., Shen J.Y. Thermodynamic optimization of the boron–cobalt–iron system // J. of Alloys and Compounds. – 2011. – Vol.509. - P. 4805-4810.
25. Shakhparonov M.I. Introduction to the molecular theory of solutions. – Moscow: Gosud. izd-vo tekhniko-teorit. lit, 1956. – 507 p. (In Russian)
26. Ghirifalko L. Statistical physics of a solid body. – Moscow: Mir, 1975 – 386 p. (In Russian)
27. Bazarov I.P. Thermodynamics. – Moscow: Vysshaja shkola, 1991– 376 p. (In Russian)
28. Van T. Rompaey et al. Thermodynamic. Optimization of the B-Fe System // Journal of Alloys and Compounds – 2002. – No. 334. – P. 173–181.
29. Mihalkovic M., Widom M. Initio Calculations of Cohesive Energies of Fe-based Glass-forming Alloys // Physical Review. – 2004. – Vol. B70. – No. 14. – P. 144107–144112.
30. Voitovieh R.F., Shakhanova N.P. Calculation of the capacities of refractory compounds // Translated from Poroshkovaya Metallurgiya.– 1967. – No. 3(51). – P. 75-79.

THE STRUCTURE OF MONOATOMIC LAYER ON GRAPHITE SURFACE

V.G. Kirichenko, A.A. Yampolskiy
V.N. Karazin Kharkiv National University
4 Svobody Sq., Kharkiv, 61022, Ukraine
E-mail: val_kir48@mail.ru
Received September 5, 2016

Monatomic surface layers of graphite were simulated on the basis of experimental data, which was obtained by scanning tunneling electron microscopy of atomically smooth surface of graphite. Values of relative deviation of the electron density were defined in the direction perpendicular to the plane of the layer. Increase in the degree of waviness layer to 2 nm are observed by increasing of linear dimensions under review graphite surface area of up to 25 nm. These results are confirmed by the data available for the graphene layers, which is caused by waviness defect. Indeed, defects such as vacancies and interstitial carbon atom are formed by increasing the number of cells to the surface layer up to 20.
KEY WORDS: graphite, surface, structure, graphene, electron density, defects

СТРУКТУРА МОНОАТОМНОГО ШАРУ НА ПОВЕРХНІ ГРАФІТУ
В.Г. Кіріченко, О.О. Ямпольський
Харківський національний університет імені В.Н. Каразіна
61022, Харків, м. Свободи, 4
На основі експериментальних даних, отриманих за допомогою скануючої тунельної мікроскопії атомарно гладкої поверхні графіту, промодельовано моноатомні поверхневі шари графіту. Визначені значення відносних відхилень електронної густини в напрямі перпендикулярному площині шару. При збільшенні лінійних розмірів ділянки поверхні графіту до 25 нм спостерігається збільшення ступеня хвилястості шару до 2 нм. Ці результати підтверджуються даними для вільних графенових шарів, хвилястість яких обумовлена дефектами. Дійсно, при збільшенні числа осередків поверхневого шару до 20 формуються дефекти типу вакансія і впроваджений атом вуглецю.
КЛЮЧЕВІ СЛОВА: графіт, поверхня, структура, графен, електронна густина, дефекти

СТРУКТУРА МОНОАТОМНОГО СЛОЯ НА ПОВЕРХНОСТИ ГРАФИТА
В.Г. Кириченко, А.А. Ямпольский
Харьковский национальный университет имени В.Н. Каразина
61022, г. Харьков, пл. Свободы, 4
На основе экспериментальных данных, полученных с помощью сканирующей туннельной микроскопии атомарно гладкой поверхности графита, промоделированы моноатомные поверхностные слои графита. Определены значения относительных отклонений электронной плотности в направлении перпендикулярном плоскости слоя. При увеличении линейных размеров обозреваемого участка поверхности графита до 25 нм наблюдается увеличение степени волнистости слоя до 2 нм. Эти результаты подтверждаются данными для свободных графеновых слоев, волнистость которых обусловлена дефектами. Действительно, при увеличении числа ячеек поверхностного слоя до 20 формируются дефекты типа вакансия и внедренный атом углерода.
КЛЮЧЕВЫЕ СЛОВА: графит, поверхность, структура, графен, электронная плотность, дефекты

Interest in monatomic hexagonal layers of graphite has appeared in the mid 40's, last century [1]. In this work we calculated the monoatomic graphite layer in the strong-coupling approximation. In graphite, each C-atom is sp^3-hybridized [2 - 6], orbital symmetry s-, p_x- и p_y located on the plane of the monatomic layer (σ-orbital); such orbitals are fully occupied and do not participate in the conduction. The fourth electron has a wave function p_z-symmetry; these orbitals are perpendicular to the atomic layer (π- orbital). These π-electrons are responsible for conductivity, and it will be further shown that energy band has both electrons and holes. π-electron interaction is considered and representation of the energy bands of the graphite is obtained in [1] and it predicts the most important properties. The main conclusion is the presence of degeneracy between filled and empty π - band, that follows from the symmetry of the monolayer. The bottom π - band must be filled and the top - must be empty at absolute zero. Also the energy gap between the bands must be absent. Progress in the preparation of thin film methods allowed synthesizing a monolayer of graphite monolayer on the surface of nickel [7], the lanthanum hexaboride crystals [8], platinum [9], iridium and rhenium [10,11], titanium carbide [12].

The first monolayer of graphite in a free state is graphene. It was obtained by Geim and Novoselov [13, 14]. Graphene is allotropic form of carbon, that consisting of a monolayer of graphite, which has a number of non-conventional properties - good electrical conductivity, transparency, good mechanical properties, high mobility of charge carriers at room temperature, the possibility of quantum conductivity and the epitaxial layer deposition. It is interesting to note that the basic approximation of Solid State Physics - Born-Oppenheimer approximation (adiabatic approximation) is broken down in graphene. So, fluctuations in the ion cores of the lattice must be included as a disturbance in the form of phonons in the lattice in the construction zone theory of graphene [15].

The aim of this work is the research of the structure of monoatomic layer on the real atomic surface of highly oriented graphite, obtained using scanning tunneling microscopy and computer modeling monoatomic layer on the graphite surface.

METHODS OF EXPERIMENTAL RESEARCH

Highly oriented graphite crystal served as the object of research. The purification of the graphite surface and the formation of a real atomic surface of a layered type of crystal was produced by cleaving the top layer of crystal before measurement. The research of the graphite surface was produced by scanning tunneling electron microscopy in normal conditions by the scanning tunneling microscope STM – 1. The experimental data were used to construct three-dimensional charts monoatomic graphite layer with a program Harvard Chart XL 2.0, that shows the structure of the first surface layer of graphite and its connection with the second surface layer.

RESULTS AND DISCUSSION

Topographical image of the nanostructure surface of graphite unit cells is shown in Fig.1: ordered rows of hexagonal graphite structure are observed in the area of highly oriented graphite, that obtained by scanning tunneling current mode of stabilization with maximizing. The unit cell has the shape of a hexagon and consists of atoms with different levels of the local electronic density of states. Partitioning according to the scheme of the experimental data (Fig. 2) was carried out in all possible directions a = 0.14 nm, b = 0.24 nm. The top surface of the monatomic layer of graphite was selected with Harvard Chart XL 2,0 program. Flat hexagonal grid was used to represent experimental data (Fig.3).
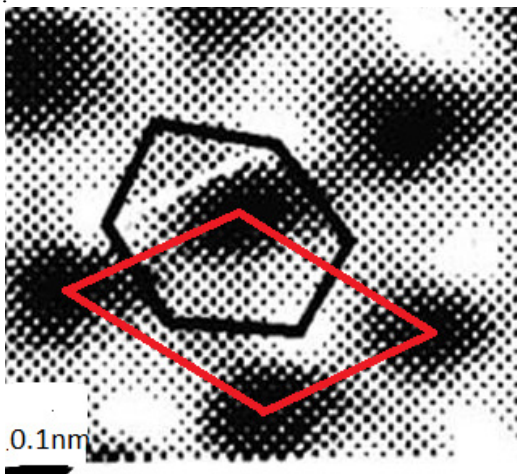
Fig. 1. The topographical image of the surface of graphite. Unit cell (hexagon) and a primitive (60 ° - rhombus) are show
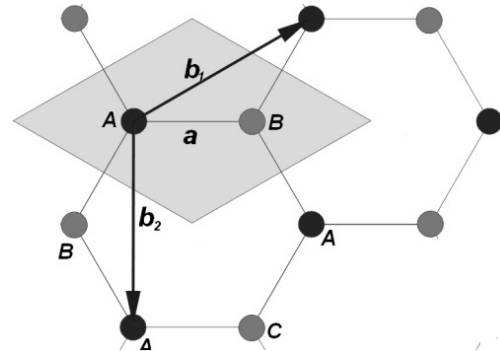
Fig. 2. Partitioning scheme of the experimental data concerning the node (A). The first neighbors B, the second - marked (A), the third as C.

The fact of the modulation of the vertical component, the ribs (a) of the unit cell and the ribs (b) of the primitive structure of the cell, is important in the experimental data obtained by the electron density on the graphite surface (Fig.3). That displays the modulation of electron density of atoms on a graphite surface. Significant periodic deviations is noted at the height of the image of two neighboring atoms (to be exact - the provisions of the local electron density maxima).
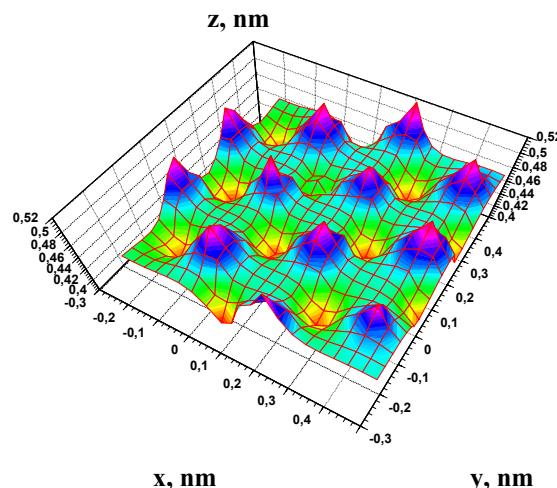
Fig 3. The electron density distribution of 7 unit cells

STM allows us to observe the spatial distribution of the atoms around the electron density, expressed in the values of the coordinates z. Neutral carbon atom in the ground state is divalent and has $1s^2 2s^2 2p^2$ configuration. The radius of the atom is 0.62 Å. Tetravalent state of carbon is formed at 2s electron switches to the 2p – state, that corresponds to the configuration $1s^2 2s 2p_x 2p_v 2p_z$. The hexagonal graphite lattice belongs to the space group C6 / mmc - D 4 6h with four atoms per unit cell. The parameter b primitive cell is 0.246 nm, the parameter d = 0.671nm, the theoretical density of this crystal is equal to 2.267 g / sm^3. Carbon atoms form a regular grid of hexagons with the distance between atoms 1.42Å in each plane. Connections inside the layers, which are covalent, are trigonal hybrids (2s, 2p$_x$, 2p$_v$) [5, 6]. The unit cell parameters are consistent with the data presented by other authors (see table).

Table

Graphite structure parameters

Structure	Parameter of Unit cell a, nm	Parameter of primitive cell b, nm	The distance between adjacent layers c, nm	The height of the primitive cell d, nm	Links
Graphite	0.146		0.3343		[16]
	0.142	0.246	0.337		[1]
	0.142	0.2464	0.335	0.6701	[6]
	0.141	0.246		0.67	[5]
	0.1418	0.246	0.335		[4]
	0.1418	0.24612		0.67079	[19]
	0.14	0.24			[18]
Graphene	0.142	0.246			[17]
Grafan	0.142	0.242			[17]
Grafan, theory	≈ 0.153 (disagreement with the theory)	≈ 0.242 Å with the theory of consent			[17]

Real monoatomic layer of graphite crystal atoms are observed deviations from the equilibrium electron density, which is represented relative to a weighted average plane and the three nearest neighbors of the central carbon atoms are deflected in the opposite direction. This is confirmed by the data on the values of the electron density variations within the unit and primitive cells.

These absolute values Δr deviation from the median plane depend on the distance r along the length of the ribs and primitive elementary cells (Fig. 4, 5). It should be noted that the size of the ribs in the graphene hexagon grid somewhat larger (0.246 nm), than on the graphite surface (0.24 nm), which is possible due to the interaction interlayer carbon atoms in graphite.
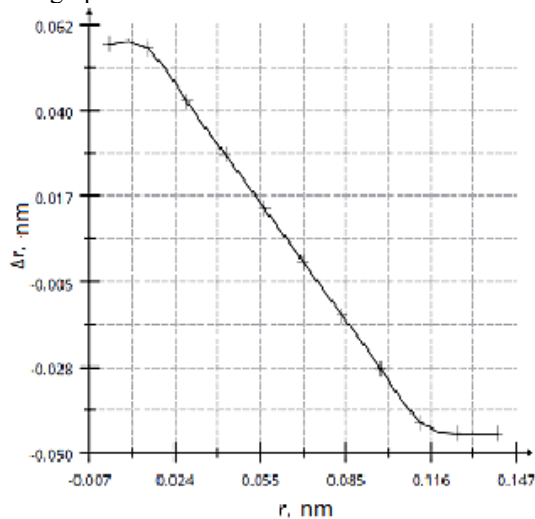
Fig. 4. The dependence of the deviations from the median plane depending on the distance r along the length of the unit cell edges
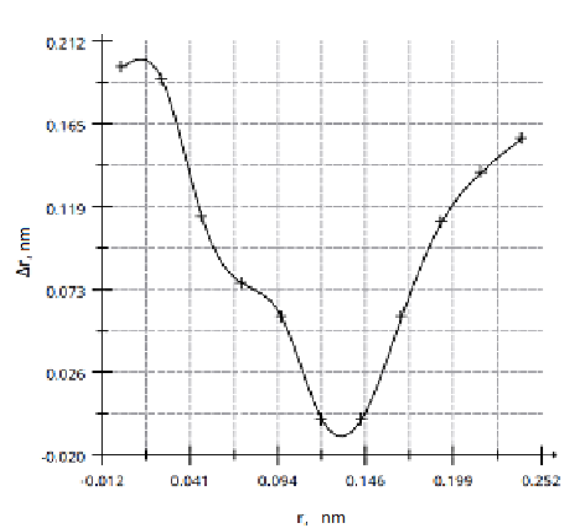
Fig. 5. The dependence of the deviations from the median plane depending on the distance r along the length of the unit cell edges.

Mismatch scale grating period in planes tangential to the surface of each of the crystal layers, leads to a normal to the surface of the crystal near the boundary stresses. These forces acting in both the vertical and horizontal directions can realize a state of equilibrium at a relatively low level fluctuations [22 – 24]. Such equilibrium state must have a certain vertical depth of modulation of the crystal surface to align the scale on the surface and in the bulk. Formation of the spatial modulation of the surface layer takes place under the action of the physical mechanism of formation of defects, therefore the role of defects, that accompany this process, may be significant

Increasing the degree of undulation of the layer to 2 nm is observed with an increase in the area under review graphite surface of the linear dimensions of 25 nm (Fig.6). These results are confirmed by the data available for the graphene layers, which undulation due to defects.

Ideal two-dimensional film in the free state can not be obtained due to its thermodynamic instability. But if the film has the defects or it will be deformed in the space (a third dimension), such a "non-ideal" film can exist without contact with the substrate [20]. In [21] it was shown that there are free graphene film surface and form a complex undulating shape, with lateral dimensions spatial inhomogeneities about 5-10 nm and a height of 1 nm. The results obtained in this paper waviness parameters are in good agreement with data reported for graphene.

Indeed, in this case, defects such as vacancies and interstitial carbon atom are formed by increasing the number of cells of the surface layer to 20. Fig. 7 shows a topographic image of the electron density distribution in the surface layer of monoatomic 20 unit cells. Defect (vacancy) occurs in tandem with embedded carbon in bottom right of the image.
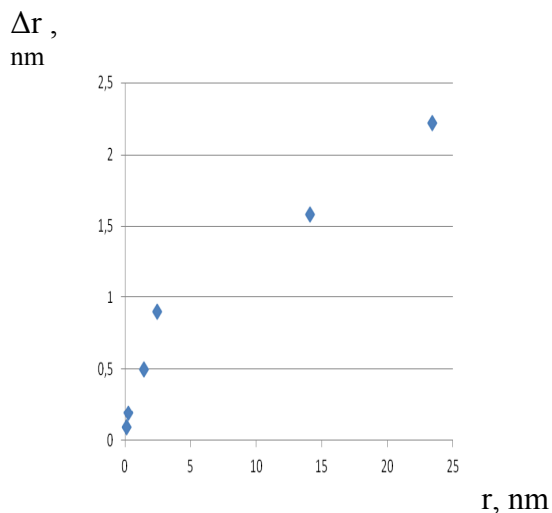
Fig. 6. Dependence waviness monatomic layer by scaling the length of the graphite surface
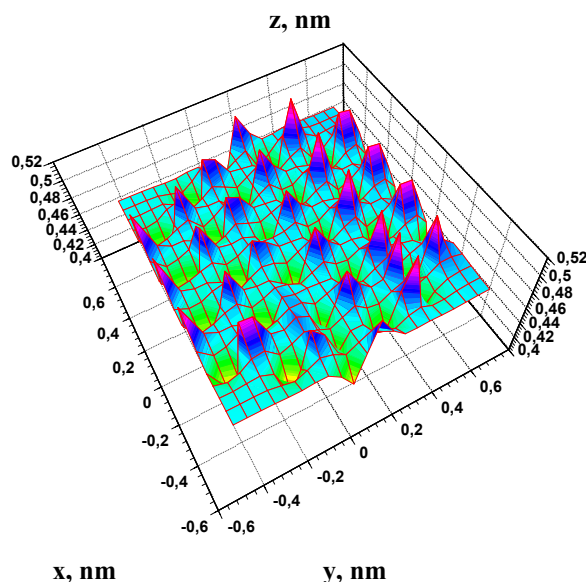
Рис. 7. The distribution of electron density in the unit cells 20. Defects (vacancies) with the embedded-atom is located at bottom right

The simplest defects that break down the translational symmetry of graphene are isolated 5- and 7-gons. But the formation of such defects is energetically unfavorable because it requires quite a strong distortion of the hexagonal structure. Much more likely a combination thereof. [25] On the other hand, stable ordering of carbon atoms is formed as part of Graphene in their zig-zag stacking, as in the case of carbyne [26].
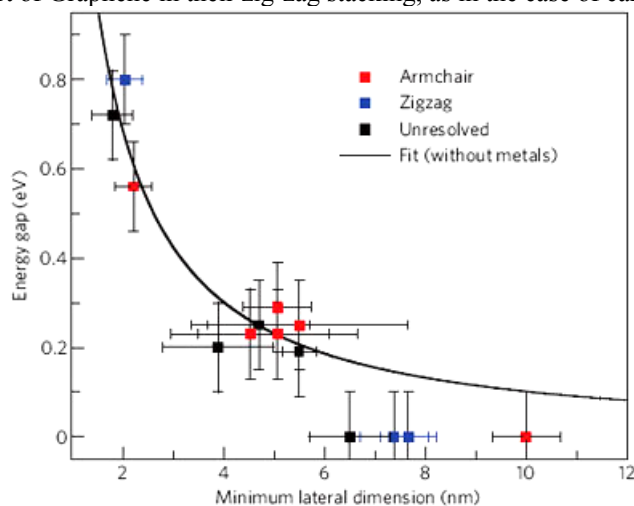
Fig. 8. The dependence of the band gap of the lateral size of graphene quantum dot structure with different edges [27]

As it turns out, most of the particles whose size is less than 10 nm, has a "zigzag" metal edges and exhibits electrical properties rather than semiconductor [27]. On the other hand, in the semiconductor quantum dot in the band gap E_g graphene zone depends on the size of the minimum cross-by law L $E_g = (1.57 \pm 0.21)/L^{1.19 \pm 0.15}$ (where E_g is measured in eV, and L – nm) - in full compliance with the theoretical dependence $E_g = 1.68/L$ (Fig. 8). The nanoribbons width of 2-3 nm and a length of 20-30 nm, in which the edges of a specific proportion of the zigzag sections more than the "chair", the value of E_g less than nanoribbons is the same width, but with a "chairlifts" edges [27]. In connection with the results is an important analysis and control of lateral heterogeneities on the surface of monatomic layers of graphite.

CONCLUSIONS

Modeling monoatomic layers of graphite based on the data scanning tunneling electron microscopy of graphite surface shows a periodic modulation of the electron density at the surface of the monatomic layer at modeling 7×7 – type cells. Computer modeling of the structure of mononuclear cells of the surface layers was carried out on the basis of technology developed by the partitioning of the experimental values of the surface electron density.

The monoatomic surface layers of graphite, the values of the absolute deviations of the electron density in the

direction perpendicular to the plane of the layer. By increasing the area under review the linear dimensions of the graphite surface to 25 nm, an increase in the degree of undulation of the layer to 2 nm. These results are confirmed by the data available for the graphene layers, which is caused by waviness defect. Indeed, when increasing the number of cells of the surface layer 20 to form defects such as vacancies and interstitial carbon atom. These scaling properties of monatomic layer on atomically clean surfaces of graphite must be considered in the analysis of the formation of graphene and graphane.

REFERENCES

1. Wallace P.R. The Band Theory of Graphite // Phys. Rev. – 1947. - Vol.71. – No.1. – P.622 – 634.
2. Joseph Callaway. Teoriya energeticheskoy zonnoy struktury [Energy band theory]. – M.: Mir, 1969. – 360p.
3. Dyadin Yu.A. Grafit i ego soyedineniya vklyucheniya [Graphite and its inclusion compounds] // Sorosovskiy zhurnal [Soros journal]. – 2000. – Vol. 6. – No.10. – P.43 – 49.
4. Podgornyy D.A. Uglerod vo vsem svoyem mnogoobrazii [Carbon in all its diversity] // Chelyabinsk, 2014. – 31p. (in Russion)
5. Zhmurikov E.I., Bubnenkov I.A., Dryomov V.V. i dr. Grafit v nauke i yadernoy tekhnike [Graphite in science and nuclear engineering] // Novosibirsk, 2013. – 193 p.
6. Knunyants I. L. (gl. red.) Khimicheskaya entsiklopediya: v 5 tomakh [Chemical Encyclopedia: in 5 volumes]. Vol. 1. – Ablyatsionnyye materialy [Ablative materials]. – M.: Sov. Enc. [Soviet encyclopedia]. – 1988. – 623 p. (in Russion)
7. Shelton J.C., Patil H.R., Blakely J.M. Equilibrium segregation of carbon to a nickel (111) surface: A surface phase transition // Surf. Sci. – 1974. - Vol.43. – No.1. – P.493-520.
8. Oshima C., Bannai E., Tanaka T., Kawai S. Carbon layer on lanthanum hexaboride (100) surface // Jpn. J. Appl. Phys. – 1977. – Vol. 16. - P.965.
9. Zi-Pu H., Ogletree D., Hove M. V., Somorjai G. Leed theory for incommensurate overlayers: Application to graphite on Pt(111) // Surf. Sci. – 1 987. – Vol. 180. – P. 433.
10. Kholin N., Rut'kov E., Tontegode A. The nature of the adsorption bond between graphite islands and iridium surface // Surf. Sci. – 1984. – Vol. 139. – P.155.
11. Gall N.R., Mihailov C.N., Rutkov E.V., Tontegode A.Ya. Harakter adsorbcionnoi svyazi mejdu monosloem grafita i poverhnostyu reniya [Character absorption connection between the graphite and the rhenium surface monolayer] // FTT. – 1985. – Vol. 27. – P. 2351. (in Russion)
12. Nagashima A., Nuka K., Itoh H., Ichinokawa T., Oshima C. et al. Electronic states of monolayer graphite formed on TiC(111) surface // Surf. Sci. – 1993. – P. 291.
13. Novoselov K.S., Geim A.K., Morozov S.V., Jiang D., Zhang Y. et al. Electric field effect in atomically thin carbon films // Science. – 2004. – Vol.306. – P. 666.
14. Novoselov K. S., Jiang D., Schedin F., Booth T. J., Khotkevich V. V. et al. Two-dimensional atomic crystals // Proc. Nat. Acad. Sci. USA. – 2005. – Vol. 102. – P. 10451.
15. Pisana S. et. Al. .Breakdown of the adiabatic Born-Oppenheimer approximation in graphene // Nature Materials. – 2007. – Vol. 6. – P. 198. DOI:10.1038/nmat1846.
16. Goncharov V.V. Grafit v reaktorostroyenii [The graphite in reactor]. // AE. – 1957. – Vol.2. – P. 398-409.
17. D.C. Elias, R. R. Nair, T. M. G. Mohiuddin, S. V. Morozov, P. Blake, M. P. Halsall, A. C. Ferrari, D. W. Boukhvalov, M.I. Katsnelson, A.K. Geim, K. S. Novoselov. Control of Graphene's Properties by Reversible Hydrogenation: Evidence for Graphane // Science. – 2009. – Vol.323. – P.610–613.
18. Kirichenko V.G., Melnikova E.S. The features of structure of nanomettric surface layers of graphite // The Journal of Kharkiv National University, physical series: "Nuclei, Particles, Fields". – 2009. – No.880. – Iss.4(44). - P.103-108.
19. iznedr.ru/books/item/f00/s00/z0000019/st035.shtm
20. Bunch J. S. et al. Coulomb Oscillations and Hall Effect in Quasi-2D Graphite Quantum Dots Nano Lett. 5, 287 (2005) DOI:10.1021/nl048111+
21. Boehm's 1961 isolation of graphene. Graphene
22. Kirichenko Valeriy G., Kuklin Vladimir M. The Formation of the Multiscale Structures on the Crystal Surfaces and Conversion of Crystals Under Phase Transformations // Electron Microscopy and Multiscale Materials Modelling. – 2007. – P.177.
23. Ramstad A., Brocks G., Kelly P.J. Theoretical study of Si (100) surface reconstruction // Phys. Rev. – 1995. – Vol.51. – No.20. – P.1450-1457.
24. Alekperov S.D.. Vasilyev S.I.. Leonov V.B.. Panov V.I.. Semenov A.E. Issledovaniye asimmetrii atomnogo izobrazheniya poverkhnostnoy reshetki grafita metodom STM [The study of the atomic image of the surface of the graphite lattice asymmetry by STM] // Doklady AN SSSR. Fizika. . – 1989. – Vol.307. – No.5. – P.1104-1109. (in Russion)
25. Kirichenko V.G. The formation of topological defects on graphite's surface // East Eur. J. Phys. – 2015. – Vol.2. – P.80-84.
26. Kirichenko V.G., Yampolskiy A.A. The formation of one dimensional structure in monoatomic layer on graphite surface// East Eur. J. Phys. – 2015. – Vol. 2. – No.3. – P.70-73.
27. Ritter K.A., Lyding J.W. // Nature Mater. – 2009. – Vol.8. – P. 235.

Алла Таньшина

Посвящается светлой памяти В. Т. Толока

В 1960-м Игорь Васильевич Курчатов поручил молодому харьковскому физику Владимиру Тарасовичу Толоку руководство научной программой по разработке основ управляемого термоядерного реактора стеллараторного типа.

По этой программе в Харьковском физико-техническом институте была создана единственная в Украине мощная экспериментальная база для актуальных исследований термоядерной энергетики и сформирована харьковская школа плазмистов-термоядерщиков.

В 70-х гг. по инициативе и непосредственном участии В. Т. Толока получили широкое развитие исследования в области неравновесной плазмохимии высоких энергий, которые привели к созданию нового прогрессивного направления в плазменной технологии – получение новых материалов на атомно-ионном уровне в установках «Булат».

К 90-й годовщине со времени рождения
члена-корреспондента НАН Украины В. Т. Толока

ХАРЬКОВ: «УРАГАН-3»
(крупнейшая в мире термоядерная установка)

<…> академик Курчатов,
по рекомендации директора института Синельникова,
предложил мне возглавить работы по сооружению в институте
крупнейшей в мире термоядерной установки <…>
Из воспоминаний В. Т. Толока[*]

Владимир Тарасович Толок родился 25 декабря 1926 года в городе Умань Черкасской области. «Отца, Тараса Владимировича, со своего сознательного возраста и до его пенсионного помню только в военной форме. Мама говорила, что у него чрезвычайно важная и опасная работа. Он перевозил большие ценности: деньги и всякие секретные бумаги. С самого раннего детства запомнил и мудреные слова: фельдсвязь и фельдъегерь. Со временем мне пояснили, что отец работал в отделе инкассации и перевозки ценностей…

Читать научился неожиданно. Сам. Все буквы знал уже давно. Но из них ничего не получалось. У нас дома была толстая подшивка великолепного журнала "Всемирный следопыт" с интересными рассказами и картинками. Эти журналы я рассматривал очень часто, изучил каждую страницу. А прочесть ничего не мог! И вдруг меня осенило! Оказывается, если буквы произносить "неправильно": не так, как в азбуке, и не по одной, то получаться могут знакомые слова. Вот это было открытие! С тех самых пор я полюбил чтение. Более того – оно стало моей настоящей страстью».

1941 год… Эвакуация… Оренбургская область…

Володя Толок – помимо учёбы – также старается *по-мужски* и помогать: наравне со взрослыми работать. «Начали мы трудиться в колхозе украинско-казахского села Айдерля. Женщины работали на току, а я был определён на "лобогрейку" (?). Когда впервые услышал это слово, то не мог понять, что ОНО такое. Ассоциации возникали разные. Когда же увидел этот "агрегат" – сенокосилку, то и тогда не сразу постиг смысл меткого народного названия. Объяснение пришло после первого трудового дня: лоб нагревался в процессе тяжёлого физического труда. Всё оказалось просто».

А в ноябре 1943 года, проучившись всего два месяца в 10-м классе (г. Махачкала), он добровольно, в неполные 17 лет, ушел на фронт… «Зашёл в школу. На перемене попрощался с классом…

Вечером же нас, новобранцев, на вокзале провожали родители. Сцена была тяжёлой. Впервые расставался с мамой, впереди была война. Уже на ходу поезда, с подножки крикнул: "Мама, я скоро вернусь!"».

И действительно, в конце мая 45-го воздушный стрелок-радист Владимир Толок по состоянию здоровья был демобилизован. (Кстати, именно 9 мая 1945 года он был выписан из главного военно-морского госпиталя, где находился на излечении после аварии самолёта.)

«Положение моё стало неопределённым. Как жить дальше? Что делать? Образование – всего девять классов. Не доучился, хотя и не по своей вине. Дома решили: только учиться дальше».

Сдав экстерном экзамены за 10-й класс, Володя Толок поступил на физико-математический факультет Днепропетровского государственного университета.

«На физмате впервые почувствовал, как, оказывается, трудно может быть учиться. Особенно на первом курсе. Одно время меня даже посещала мысль: а не пойти ли мне в другой вуз, где легче учиться. Но выдержал год, потом освоился. Невольно вспоминался тогда курс молодого краснофлотца с его первоначальной закалкой новичков.

---

[*] Исторические и биографические факты – со слов Владимира Тарасовича Толока – впервые обнародованы автором статьи в кандидатской диссертации.

В Днепропетровском университете началась и моя спортивная "карьера". Я серьёзно увлёкся волейболом. Много тренировался. Был капитаном факультетской команды – чемпиона ДГУ 1949 года».

В конце 40-х гг. по специальному постановлению правительства из ряда вузов СССР начали отбор лучших студентов на спецфакультет Харьковского государственного университета (далее – ХГУ). В марте 1950 г. и Владимир Толок был переведен на 4-й курс ядерного отделения этого факультета.

«Учились мы тогда, – уточняет Владимир Тарасович, – отдельно от студентов ХГУ в небольшом здании во дворе университета. Вход в это помещение был только по пропускам. Лекции читали нам ведущие сотрудники УФТИ: Кирилл Дмитриевич Синельников, Антон Карлович Вальтер, Александр Ильич Ахиезер, Яков Борисович Файнберг и другие известные учёные.

Лекции полагалось записывать в специальные тетради, где страницы были пронумерованы, прошнурованы и скреплены сургучной печатью. Эти тетради выносить за пределы корпуса не разрешалось.

Учились увлечённо и очень напряжённо. Да и стипендия у нас была почти втрое больше чем у студентов других факультетов ХГУ.

Дипломную работу я выполнял в УФТИ, в лаборатории Якова Борисовича Фогеля. Он, мой первый настоящий учитель, привил мне не только любовь к эксперименту и поиску, но и научил скрупулёзно вести записи в лабораторных журналах, что не раз помогало в дальнейшей моей научной работе правильно интерпретировать результаты.

Защита дипломной работы проходила в кабинете директора УФТИ К. Д. Синельникова. Нас по одному вызывали в этот кабинет для защиты своей дипломной работы. Это было обусловлено секретностью наших работ.

А 25 декабря 1951 года, как раз в день моего 25-летия, я получил диплом об окончании Харьковского государственного университета».

В Харьковском физико-техническом институте Владимир Тарасович Толок прошёл путь от младшего научного сотрудника до первого заместителя директора по научной работе.

Его первыми экспериментальными работами были исследования в области физики и техники линейных ускорителей протонов и электронов.

В 1956 году в результате самопроизвольного включения ускорителя во время проведения эксперимента произошёл несчастный случай: Владимир Тарасович получил лучевое поражение кистей рук (при замене мишени, облучаемой электронным пучком). Далее с его слов: «Санчасть института "командировала" меня в Москву, в Институт биофизики Академии наук СССР. Клиника Института, куда я попал, была секретным учреждением. В ней изучалось влияние радиации на людей и животных, возможности их лечения.

В те годы полным ходом шли испытания атомного оружия, в этой клинике постоянно находились люди, работающие с атомным оружием и реакторами. Например, мне запомнился Лёша Галкин. Он находился в клинике уже не первый год. Лёша был лаборантом Института атомной энергии и стал "знаменит" тем, что вместе с одним инженером в аварийной ситуации вынужден был разобрать руками[*sic*] экспериментальный реактор, который готов уже был готов пойти в "разнос". Тяжело было смотреть на этого парня: правой руки у него не было вовсе, а на левой, от которой остались кости, обтянутые прозрачной кожей, было два скрученных пальца. Передвигался он на костылях, ноги были покрыты незаживающими язвами…

Итог моего двухлетнего лечения был таков: ампутированы поражённые фаланги пальцев и нормализован состав крови.

"Приобрёл" я и необычные особенности: резкое сужение цветного поля зрения, полное отсутствие реакции на горькое и мгновенно возникающую головную боль при малейшей дозе рентгеновского облучения. Последняя особенность однажды сработала в США.

В начале 80-х годов, когда я часто бывал там в составе делегаций советских учёных-специалистов по управляемым термоядерным реакциям, произошёл любопытный случай. В Ливерморской лаборатории *(Lawrence Livermore National Laboratory. – Прим. А.Т.*) нашу делегацию в составе пяти человек провели через небольшое строение. Именно провели, потому что мы вошли и тут же вышли, ничего не осмотрев. На этот эпизод никто из наших не обратил внимания. Но не я…

Выйдя оттуда, я сразу почувствовал резкую головную боль. Сказал об этом главе делегации академику Е.П. Велихову: "Женя, нас прилично облучили". Пришлось коротко на ходу объяснять, в чём дело. Конечно, говорить об этом не имело смысла американцам, скандал был не нужен, да и как докажешь? Однако за обедом, как бы "невзначай", рассказал гостеприимным хозяевам историю моего *свойства*. Они люди умные, думаю, дошло. Мы и раньше знали, что в этой лаборатории занимаются не только мирными делами, но со временем стало известно, что тогда создавали там нейтронную бомбу. Похоже, нас "обработали", на всякий случай».

Кстати, врачи категорически запретили Владимиру Тарасовичу работать с любым ионизирующим излучением.

В это же время в Харьковском физико-техническом институте начались исследования в новой области науки – физики плазмы.

Директором института Кириллом Дмитриевичем Синельниковым был создан научный отдел «Р» из пяти экспериментальных и двух теоретических лабораторий. Руководителем одной из лабораторий был назначен Владимир Тарасович Толок.

«О плазме, – как вспоминает Владимир Тарасович, – мы имели весьма смутное представление. Предстояла

интенсивная учеба. Приходилось много читать периодической литературы. Всем пришлось серьезно заняться английским языком. Вскоре под руководством Кирилла Дмитриевича Синельникова на относительно простых установках начали появляться наши первые результаты работы с "живой" плазмой.

СОВЕТСКИЕ УЧЕНЫЕ В ПРИНСТОНСКОЙ ЛАБОРАТОРИИ. СЛЕВА НАПРАВО: 2.Б.Б.КАДОМЦЕВ 4.В.Т.ТОЛОК, 5.С.СТРЕЛКОВ. США. 70-е ГОДЫ.

В январе 1960-го приехал в ХФТИ Игорь Васильевич Курчатов. Он привез в институт новое, очень интересное и важное спецзадание – начать на термоядерных установках-стеллараторах исследования по глобальной проблеме человечества – управляемому термоядерному синтезу (УТС).

Тогда академик Курчатов, по рекомендации директора института Синельникова, предложил мне возглавить работы по сооружению в институте крупнейшей в мире термоядерной установки – стелларатора, которому он дал название "Украина". Я был озадачен. Кто-то, конечно, должен был это делать, но я себя в такой роли не представлял.

К тому времени мой стаж работы в ХФТИ был около 8 лет. Я "дал жизнь" двум ускорителям – протонному и уникальному электронному с током в 10 ампер, что еще долго было мировым рекордом для резонансных ускорителей, а в физике плазмы успел "добыть" циклотронный резонанс на протонах в плотной плазме.

Наверное, об этом и был ранее разговор Синельникова с Курчатовым. Когда зашла речь о моём научном опыте, Курчатов весело заметил, что нужно добавить к этому опыту мои 33 года и смело начинать большую работу.

Как известно, у Игоря Васильевича Курчатова была привычка давать прозвища тем, с кем он работал. Меня он стал называть стрелком-радистом – после расспросов о моей жизни».

Вскоре Владимир Тарасович Толок был командирован в Москву в распоряжение академика И. В. Курчатова для подготовки постановления правительства о развитии работ по УТС в Харьковском физико-техническом институте.

Все дни Владимира Тарасовича были расписаны по часам: в 9.00 – постановка задач на день в рабочем кабинете И. В. Курчатова, вечером – доклад Курчатову у него дома о проведенной за день работе. В субботу – ночной поезд в Харьков. Утром в воскресенье – доклад Синельникову. Подготовка новых техзаданий. Вечером – поезд в Москву. Понедельник: 9.00 – рабочий кабинет И. В. Курчатова…

7 февраля 1960 года неожиданно умер Игорь Васильевич Курчатов.

Из воспоминаний Владимира Тарасовича Толока: «В пятницу вечером, 5 февраля, я пришёл к Курчатову просить отпустить меня в Харьков в тот же вечер, а не в субботу, как обычно.

Игорь Васильевич был в превосходном настроении. Напевал что-то, шутил. Домой, правда, меня не отпустил, т. к. намечалось на субботу ещё какое-то дело. Тут же позвонил по прямому спецтелефону в Харьков Синельникову и перенёс намеченную мою встречу с ним с субботы на воскресенье. В конце этого телефонного разговора сказал, что собирается ехать с женой (сестрой Синельникова) в консерваторию слушать "Реквием" Моцарта.

То был роковой реквием.

В воскресенье 7-го февраля, когда я был уже дома в Харькове, позвонил мне Синельников. Говорил он медленно, с трудом подбирая слова: "Володя, мне сейчас позвонили из Москвы. Игорю Васильевичу очень плохо. Боюсь, что это серьёзно".

Вскоре по радио было объявлено о внезапной кончине академика Курчатова. Ему было только 57 лет. Это было горе для всей страны.

Так уж совпало, что именно в день внезапной кончины Курчатова в газете "Правда" была опубликована

его статья "Развитие атомной физики на Украине"[*]. Игорь Васильевич писал о том, что недавно побывал в Харькове в институте своего друга К. Д. Синельникова и что там начаты работы над главной проблемой современной науки – проблемой управления термоядерными реакциями.

В настоящее время в области исследования ядерных реакций при энергиях сталкивающихся частиц от одного до ста миллионов электроновольт Украина благодаря работам Физико-технического института Академии наук УССР в Харькове и Института Физики АН УССР в Киеве вышла на первое место в ряду братских республик нашей великой Родины…

Наконец, в настоящее время в Харьковском физико-техническом институте начаты работы над главной проблемой современной науки – проблемой управления термоядерными реакциями. Успешное решение этой задачи откроет поистине невиданные перспективы.

В Харьковском физико-техническом институте работы по управляемым термоядерным реакциям под общим научным руководством К.Д. Синельникова начаты всего полтора - два года назад. Но за это короткое время выполнены важные теоретические и экспериментальные исследования свойств ионизованной плазмы… Все это позволяет уже сейчас перейти на Украине к проектированию и строительству крупных установок для проведения исследований по термоядерным реакциям» [«Правда» от 7 февраля 1960 года].

Кончина И. В. Курчатова серьёзнейшим образом отразилась на судьбе стеллараторной программы ХФТИ. В итоге только через семь лет (вместо одного года, намеченного Курчатовым) была сооружена установка значительно меньших размеров, чем он намечал. Да и к тому же имя "Украина", совсем не напрасно данное Курчатовым, было заменено на "Ураган"».

Стоит подчеркнуть и тот факт, что термоядерные исследования в СССР, США и Англии начали проводить почти одновременно в начале 50-х. Эти работы велись под грифом "секретно".

Перед учеными была поставлена сложнейшая задача – перейти от неуправляемого взрыва водородной бомбы, где термоядерная реакция уже была осуществлена, к управляемому процессу получения энергии. Необходимо было найти способы нагреть вещество до 100 миллионов градусов и удержать в изоляции от окружающей среды (NB: температура самого тугоплавкого металла – вольфрама – всего 3 500 ° С).

Начало широкому международному сотрудничеству в этой области положил доклад И. В. Курчатова в Харуэльской Лаборатории (Англия, 1956 год) о результатах работ по управляемым термоядерным реакциям в СССР.

И это была сенсация (!).

Американцы и англичане решили «в долгу» не остаться и вскоре выпустили «Nature», в котором все статьи были посвящены только управляемому термоядерному синтезу.

Затем на международном уровне было принято решение о создании совместной советско-американской координационной комиссии (далее – СКК) по управляемому термоядерному синтезу. В эту комиссию входили руководители ведущих термоядерных лабораторий СССР и США.

Постоянным членом этой комиссии от ХФТИ был назначен Владимир Тарасович Толок. Об этом этапе своей жизни он рассказал следующее: «Работа комиссии заключалась в ежегодном ознакомлении ее членов с работами советских и американских термоядерных лабораторий. За 14 лет совместной работы мы хорошо узнали друг друга.

В США днём мы обычно напряженно работали в лаборатории, а вечером были обязательные приемы в домах руководителей этих лабораторий. Открытое деловое обсуждение результатов работ способствовало выравниванию их научного уровня до международного.

Термоядерные лаборатории США были разбросаны по всей стране от Атлантического океана до Тихого.

Однажды случилось так, что по дороге в Лос-Аламос (где были созданы первые атомные бомбы) мы оказались в самолете-такси без сопровождающих нас американцев. Во время полета пилот нам вдруг заявил: "А мій батько з Києва". Правда, на "мові*" своїх предков он больше ничего сказать не мог, но контакт между нами возник. И он решил гостеприимно показать нам окрестности Лос-Аламоса (самой закрытой территории США). Мы тогда сверху увидели не только индейские резервации, но и отдельные сооружения, которые располагались в глубоких ущельях. Наш полет в этом районе несколько затянулся, что вызвало немалое беспокойство американцев, прилетевших на место раньше нас.

В музее Лос-Аламоса нам показали макеты первых атомных бомб – "Малыша" и "Толстяка". Предложили поработать с манипулятором – механической "рукой" для работы с радиоактивными материалами – и попросили что-нибудь написать на память. Я оставил им на память свою подпись, но было искушение написать традиционно-родное "Здесь был Вова". В общем, за время моих туров по Америке накопилось много впечатлений, поводов для раздумий и сравнений».

Следует особо отметить тот факт, что именно с 1960 года Харьковский физико-технический институт активно сотрудничает со многими термоядерными центрами мира.

Например, Владимир Тарасович Толок как руководитель термоядерных исследований ХФТИ посетил – с 1960-го по 1985 год – следующие страны:

---

[*] Развитие атомной физики на Украине" – и. в. Курчатов: «В январе нынешнего года я, как в старое время, провел в этом институте несколько дней, доставивших мне много радости…

США (ознакомление с работами научных центров в области физики плазмы и УТС; 1960),
Австрия (международная конференция МАГАТЭ в области физики плазмы и УТС; 1961, Зальцбург),
Англия (совещание по устойчивости плазмы в магнитном поле; 1962, Кембридж),
США (ежегодная конференция американского физического общества; 1962, Атлантик-Сити),
США (ознакомление с работами термоядерных центров; 1964),
Англия (международная конференция по физике плазмы и УТС; Лондон, 1965),
Италия (ознакомление с работами по физике плазмы; Фраскати, 1966),
Швеция (2-я европейская конференция по физике плазмы и УТС; Стокгольм, 1967),
ФРГ (ознакомление с работами по физике плазмы; Бохум, Гархинг,1972),
США (член постоянной советско-американской комиссии по термоядерной энергетике, ознакомление с работами плазменных лабораторий в Принстоне, Ок-Ридже, Лос-Аламосе, Ливерпуле, Беркли, Бостоне (МТИ); 1973-1987),
США (ознакомление с работами термоядерных центров в рамках СКК; 1973,1975,1977),
Чехословакия (8-я европейская конференция по физике плазмы и УТС; Прага, 1977),
Франция (ознакомление с работами термоядерных центров; 1978),
США (ознакомление с работами термоядерных центров в рамках СКК; 1979),
США (9-я международная конференция МАГАТЭ по физике плазмы; ознакомление с работами научных центров в рамках СКК; 1982),
США (ознакомление с работами термоядерных центров в рамках СКК; 1985),
Иран (чтение лекций в Тегеранском университете; 1994).

В 1966 году Владимир Тарасович Толок возглавил отделение физики плазмы Харьковского физико-технического института. Отделение состояло из пяти научных отделов, инженерно-технического сектора и специализированной лаборатории плазменной технологии.

Работы в отделении были развёрнуты по долгосрочным программам «Ураган», «Юпитер», «Пучок» и «Булат».

Стеллараторная программа «Ураган» – самая большая – включала в себя разработку научных и технологических вопросов, связанных с сооружением крупных термоядерных установок. В частности, в рамках этой программы была сооружена серия уникальных замкнутых магнитных ловушек стеллараторного типа: «Сириус», «Ураган-1», «Ураган-2», «Ураган-2м».

По этой же программе были построены первые в мире, разработанные в ХФТИ, усовершенствованные новые модификации стелларатора – торсатроны «Сатурн», «Винт» и не имеющий аналогов в мире «Ураган-3».

И вот что по этому поводу рапортовала года газета «Правда» от 29 августа 1982 года:

«Новый шаг на пути к созданию управляемого термоядерного синтеза сделали ученые Харькова. В Физико-техническом институте Академии наук УССР начала действовать одна из крупнейших в мире стеллараторных установок – "Ураган-3". Широкая программа исследований предусматривает изучение закономерностей поведения плазмы, нагретой до нескольких десятков миллионов градусов…

Первый стелларатор этого типа был создан в нашем институте в 1970 году. С тех пор в рамках общесоюзной термоядерной программы в Харькове сконструировано несколько подобных систем. Ученых привлекает их способность работать в постоянном режиме, необходимом для функционирования будущих промышленных реакторов. "Ураган-3" – базовая установка, которую предполагается непрерывно совершенствовать, наращивая ее мощность» [*Цитирование по*: «Заработал "Ураган"»].

Также успешно разрабатывалась и научная программа «Юпитер», которая была направлена на изучение удержания горячей плазмы в электромагнитных ловушках, предложенных О. А. Лаврентьевым.

Основной же задачей программы «Пучок» было изучение эффектов взаимодействия плазмы с электронными и ионными пучками, а также исследование процессов ускорения заряженных частиц и генерации излучения в широком диапазоне частот (научный руководитель Я. Б. Файнберг).

Во всех программах были получены фундаментальные научные результаты. В частности, на стеллараторах были изучены закономерности удержания плотной водородной плазмы с температурой в десятки миллионов градусов.

«Программа "Булат" – моё "детище", важная и теперь уже последняя часть моей научной жизни, – не без заслуженной гордости подчёркивает Владимир Тарасович Толок. – Появление научной программы "Булат" – пример "закономерной случайности", когда в ходе решения "стратегической" задачи удалось не пропустить побочный эффект, правильно оценить его значение и развить его в целое новое направление в технологии, т.е. удалось "по дороге в Индию заметить Америку".

Основой этой технологии является способ, названный нами "КИБ" – Конденсация с Ионной Бомбардировкой.

Он родился при разработке сверхмощных высоковакуумных безмасляных насосов для наших стеллараторов. В этих насосах использовался эффект интенсивного поглощения газов слоями распылённого титана. Было обращено внимание на то, что при распылении титана с помощью электрической дуги образуется плазма, более чем на ¾ состоящая из ионов титана.

После этого нетрудно было прийти к мысли, что с помощью дополнительного электрического поля, ускоряющего ионы "бомбардирующие" поверхность, можно внедрить в неё титан.

И уже в первых экспериментах были получены прочные плёнки металлов. Изготовленные по этой программе установки мы назвали "Булатами"».

Технологии и установки "Булат" впоследствии были широко внедрены в промышленность нашей страны и за рубежом. Например, была продана лицензия американской фирме «Малти арс» с правом создания дочерних фирм в 47 странах мира.

Также Владимир Тарасович Толок – автор и соавтор более 200 научных работ, 18 изобретений и патентов.

Сердце члена-корреспондента НАН Украины Владимира Тарасовича Толока перестало биться 11 декабря 2012 года.

Но… "Они жили! " – так говорят римляне о мертвых, не желая произносить зловещих слов[*].

---

[*] Цитирование по: *Плутарх*. Сравнительные жизнеописания в двух томах, М.: Издательство «Наука», 1994. Издание второе, исправленное и дополненное. Т. II.

blank line)
(blank line)
PACS: Here you must specify PACS codes
(blank line)

INSTRUCTIONS FOR PREPARING MANUSCRIPT (TITLE)

(blank line)

N.N. Author[1], N.N. Co-author(s)[2]

[1] *Affiliation*
[2] *Affiliation (if different from Authors affiliation)*
e-mail: corresponding_authors@mail.com
Received January 14, 2016

(blank line)

Each paper must begin with an abstract. The abstract should be typed in the same manner as the body text (see below). Please note that these Instructions are typed just like the manuscripts should be. The abstract must have at least 1000 phonetic symbols, supplying general information about the achievements, and objectives of the paper, experimental technique, methods applied, significant results and conclusions. Page layout: the text should be printed on the paper A4 format, at least 3 pages, with margins of: Top - 3, Bottom, Left and Right - 2 cm. The abstract should be presented in English (only for foreign authors), Ukraine and Russian.
KEYWORDS: there, must, be, at least, 5 keywords

(blank line)
This is introduction section. This paper contains instructions for preparing the manuscripts. The text should be prepared in .doc format (using MS Word).
(blank line)

INSTRUCTIONS

The text should be typed as follows:
• title: Times New Roman, 12 pt, ALL CAPS, bold, 1 spacing, centered;
• authors: name, initials and family names; Times New Roman, 12 pt, bold, 1 spacing, centered;
• affiliation(s): Times New Roman, 9 pt, italic, 1 spacing, centered;
• abstract: Times New Roman, 9 pt, 1 spacing, justified;
• body text: Times New Roman, 10 pt, 1 spacing, justified; paragraphs in sections should be indented right (tabulated) for 0.75 cm;
• section titles: Times New Roman, 10 pt, bold, 1 spacing, centered, without numbering, one line should be left, blank above section title;
• subsection titles: Times New Roman, 10 pt, bold, 1 spacing, centered, without numbering in accordance to the section (see below), one line should be left blank above subsection title;
• figure captions: width of the figure should be 85 or 170 mm, figures should be numbered (Fig. 1) and titled below figures using sentence format, Times New Roman, 9 pt, 1 spacing, centered (if one line) or justified (if more than one line); one line should be left blank below figure captions;
• table captions: width of the table should be 85 or 170 mm, tables should be numbered (Table 1.) and titled above tables using sentence format, Times New Roman, 10 pt, 1 spacing, centered (if one line) or justified (if more than one line), tables should be formatted with a single-line box around the outside border and single ruling lines between rows and columns; one line should be left blank below tables;
• equations: place equations centered, numbered in Arabic (1), flush right, equations should be specially prepared in MathType; one line should be left blank below and above equation.
(blank line)

Additional instructions

Numerated figures and tables should be embedded in your text and placed after they are cited. Only black and white drawings and sharp photographs are acceptable. Letters in the figures should be 3 mm high. The figures should be presented in one of the following graphic formats: jpg, gif, pcx, bmp, tif.
(blank line)

REFERENCES

Titles of journals, articles and author names in references should be given in Roman script. References should be numbered in the order of referring in the text, e.g. [1], [2-5], etc. Do not superscript your reference numbers. Cite references as in journal format. The full references should be listed in numerical order of citation in the text at the end of the paper (justified), Times New Roman, 9 pt, 1 spacing.
References should be given in the following form:

Journals
1. Holzwarth G., Eckart G. Fluid-dynamical approximation for finite Fermi systems // Nucl. Phys. - 1979. - Vol. A325. - P.1-30.
Books
2. Bertsch G.F., Broglia R.A. Oscillations in finite quantum systems. Ch. 6. - Cambridge: Cambridge University, 1994. - 150 p.
Chapters
3. Van der Woude A. The electric giant resonances // Electric and magnetic giant resonances in nuclei / Ed. by J. Speth. - Singapure: World Scientific P.C., 1991. - P. 99-232.
Conference or symposium proceedings
4. Smolanzuk R., Skalski J., Sobiczewski A. Masses and half-life of superheavy elements // Proc. of the International Workshop 24 on Gross Properties of Nuclei and Nuclear Excitations / Ed. by H. Feldmeier et al. - GSI, Darmstadt, 1996. - P.35-42.

Special Notes
1. Use International System of Units (SI system). 2. It is undesirable to use acronyms in the titles. Please define the acronym on its first use in the paper. 3. Refer to isotopes as ^{14}C, ^{3}H, ^{60}Co, etc.